AL/CF-TR-1994-0151

ARMSTRONG LABORATORY
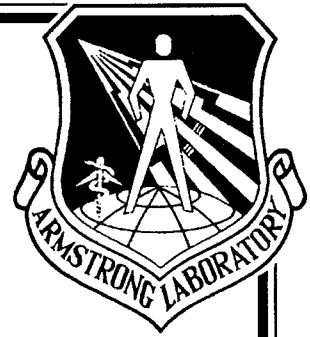
ERECT, NEUTRAL AND SLUMP SITTING POSTURES: A STUDY OF THE TORSO LINKAGE SYSTEM FROM SHOULDER TO HIP JOINT

Herbert M. Reynolds

SYSTEMS ANTHROPOMETRY LABORATORY
DEPARTMENT OF BIOMECHANICS
MICHIGAN STATE UNIVERSITY
EAST LANSING MI 48824-1316

DTIC
SELECTED
APR 12 1995
B

19950410 088

OCTOBER 1994

FINAL REPORT FOR THE PERIOD DECEMBER 1983 TO DECEMBER 1985

**AIR FORCE MATERIEL COMMAND
WRIGHT-PATTERSON AIR FORCE BASE, OHIO 45433-7604**

TECHNICAL REVIEW AND APPROVAL

AL/CF-TR-1994- 0151

This report has been reviewed by the Office of Public Affairs
(PA) and is releasable to the National Technical Information
Service (NTIS). At NTIS, it will be available to the general
public, including foreign nations.

This technical report has been reviewed and is approved for
publication.

FOR THE DIRECTOR

THOMAS J. MOORE, Chief
Biodynamics and Biocommunications Division
Armstrong Laboratory

REPORT DOCUMENTATION PAGE	Form Approved OMB No. 0704-0188

Public reporting burden for this collection of information is estimated to average 1 hour per response, including the time for reviewing instructions, searching existing data sources, gathering and maintaining the data needed, and completing and reviewing the collection of information. Send comments regarding this burden estimate or any other aspect of this collection of information, including suggestions for reducing this burden, to Washington Headquarters Services, Directorate for Information Operations and Reports, 1215 Jefferson Davis Highway, Suite 1204, Arlington, VA 22202-4302, and to the Office of Management and Budget, Paperwork Reduction Project (0704-0188), Washington, DC 20503.

1. AGENCY USE ONLY (Leave blank)	2. REPORT DATE October 1994	3. REPORT TYPE AND DATES COVERED Final – December 1983 – December 1985

4. TITLE AND SUBTITLE
Erect, Neutral and Slump Sitting Postures: A study of the torso linkage system from shoulder to hip joint

6. AUTHOR(S)

Herbert M. Reynolds

5. FUNDING NUMBERS
C – F33615-84-C-0507
PE – 61101F
PR – 7231
TA – 23
WU – 10

7. PERFORMING ORGANIZATION NAME(S) AND ADDRESS(ES)
Systems Anthropometry Laboratory
Department of Biomechanics
Michigan State University
East Lansing MI 48824-1316

8. PERFORMING ORGANIZATION REPORT NUMBER

9. SPONSORING/MONITORING AGENCY NAME(S) AND ADDRESS(ES)
Armstrong Laboratory, Crew Systems Directorate
Biodynamics and Biocommunications Division
Human Systems Center
Air Force Materiel Command
Wright-Patterson AFB OH 45433-7022

10. SPONSORING/MONITORING AGENCY REPORT NUMBER

AL/CF-TR-1994- 0151

11. SUPPLEMENTARY NOTES

12a. DISTRIBUTION/AVAILABILITY STATEMENT

Approved for public release; distribution is unlimited

12b. DISTRIBUTION CODE

13. ABSTRACT (Maximum 200 words)
Sitting postures representative of a maximum erect, neutral and maximum slumped spinal curvature were defined by comparable anatomical pointmarks in three dimensional space. Nine, male, unembalmed cadavers were measured with a roentgen stereophotogrammetric system. The results describe thoracic and lumbar curvatures in three postures and the locations of specific landmarks representing the shoulder joint, spinal column, and hip joint in a three dimensional seat reference system. In addition to the three dimensional analysis of sitting posture, the range of motion for each motion segment measured in the spine was calculated. These data were used to evaluate the contribution of specific lumbar motion segments in the change of sitting posture from maximum erect to maximum slump. To evaluate the condition of each subject's musculoskeletal system, osteological, morphological and physiological procedures were used to describe the sample.

14. SUBJECT TERMS
Spinal column, Three dimensional anthropometry, Range of Motion, Posture, Roentgen stereophotogrammetry

15. NUMBER OF PAGES
173

16. PRICE CODE

17. SECURITY CLASSIFICATION OF REPORT	18. SECURITY CLASSIFICATION OF THIS PAGE	19. SECURITY CLASSIFICATION OF ABSTRACT	20. LIMITATION OF ABSTRACT
UNCLASSIFIED	UNCLASSIFIED	UNCLASSIFIED	UL

NSN 7540-01-280-5500

Standard Form 298 (Rev. 2-89)
Prescribed by ANSI Std. Z39-18
298-102

i

THIS PAGE LEFT BLANK INTENTIONALLY

ACKNOWLEDGMENTS

and the Chair of the Department of Biomechanics, Dr. Robert Soutas-Little, built the laboratory and supported the research through many hard financial times. In addition, Robert Ward, Myron Beal, and Paul Moga, physicians in the College of Osteopathic Medicine, graciously examined the cadavers and recorded their findings for the project.

James Freeman, Laurie Batzer, and Vance Kincaid, II contributed to the daily laboratory work. Collecting the data, digitizing the films, and maintaining the enormous files of data were a difficult job that required discipline and patience.

As with all University research, much of the progress is due to student assistants. Jeff Marcus, David Van Buren, Paul Panzl, and Steven J. Bologna contributed their invaluable skills in computer programming. In particular, Jeff Marcus developed many of the algorithms and programs used in the laboratory. William McMillan contributed his skill in the osteological studies. Recently, Ray Brodeur contributed to the development of the concept of a torso angle that describes the relative positions between thorax and pelvis for analyzing lumbar motion segment displacements.

I owe a very large debt of gratitude to Brenda Robinson. She has worked diligently in typing and copying the many reports submitted by this project. With her help, I made a few deadlines.

In conclusion, I would like to extend my appreciation to all those people who contributed to this research. Their questions, suggestions, time, and labor provided the impetus to maintain the needed level of scientific intensity for this research.

TABLE OF CONTENTS

v

vi

LIST OF FIGURES

LIST OF TABLES

THIS PAGE LEFT BLANK INTENTIONALLY

The Torso Linkage System from Hip to Shoulder Joint: Erect, Neutral and Slump Sitting Postures

INTRODUCTION

Seated posture has been a subject of scientific study for many years, beginning with the works of Staffel (Ref 60, 61) and followed by Strasser (Ref 63) and Åkerblom (Ref 2). Initially, the design of school and office seats was the goal of investigations into the physical support needed for good posture. In the middle of the twentieth century, this goal was also desired in seats used in civilian and military transport vehicles. At approximately the same time, Wilfred Taylor Dempster at The University of Michigan began a study of the human linkage system for the United States Air Force (Ref 18). Research in postural biomechanics, thus, became associated with investigations of the safety and health of the human operator in military and industrial equipment.

Dempster investigated the use of mechanical linkage systems to the study of the human appendicular linkage system. Dempster, however, did not define a linkage system from shoulder to hip and subsequent studies have worked on this problem. A torso linkage investigation by Snyder et al (Ref 59) developed a model of torso mobility. This model used elbow position and traditional anthropometry to estimate vertebral position in standing and sitting postures but it did not define geometric relationships between the pelvis and spinal column. Jiro Kohara (Ref 31), Gunnar Andersson, et al (Ref 5), R. Rebiffe (Ref 47) and Tom Bendix (Ref 10) have subsequently investigated the torso linkage system.

With the growth of biomechanical studies of the seated operator, knowledge of the geometric relationships in the torso linkage system that determine seated posture increased. For example, Keegan (Ref 29) pointed out that the orientation of the pelvis controlled lumbar curvature. In 1969, Mohr et al (Ref 37)

1

measured spinal column variation in the sagittal plane. _In vivo_ investigations of spinal mobility have measured the shape of the back (Ref 4) or angular displacements of surface landmarks (Ref 68). Previous investigations of spinal mobility have utilized _in vitro_ vertebral motion segments (Ref 44, 41).

In the past four decades, retrospective studies of emergency egress from military aircraft have demonstrated that the most severe injuries occur in the vertebral column of the seated pilot (Ref 16, 25, 27). Theories to explain these injuries use the position of the seated pilot as their starting point. Since loads in the body pass through the skeletal system, the skeletal position in the seat determines the path of load transmission. Given the complexities of load transmission paths through the skeletal linkage system, mathematical models of the torso are essential tools for investigating possible injury mechanisms (Ref 9, 43). All the models, however, lacked detailed anatomical geometry that accurately described seated posture.

Throughout the literature, data are lacking on quantitative geometry of the spinal column for different seated postures. Traditional anthropometric investigations measure geometry of the body in standardized postures. In ergonomics and biomechanics, anthropometric dimensions estimate the geometric size and shape of body segments that define seated posture. A more accurate measure of the linkage system was developed by Dempster et al (Ref 18a). He developed equations to estimate the appendicular link lengths from anthropometric lengths of long bones in the skeleton. The most poorly defined linkage system lies within the torso. The torso linkage geometry uses primarily the results of Bakke et al (Ref 8) and Snyder et al (Ref 59).

The appendicular and torso linkage systems connect at the shoulder and hip joints through a complex spinal column geometry. Anthropometric linkage studies, however, have not defined the spinal column geometry of the torso between these two joints for representative seated or standing postures. To improve upon our knowledge of the spinal linkage system in seated postures, the

2

present research measured the position of the spinal column in a variety of erect and slumped seated postures. The results identified comparable seated postures and located the three-dimensional positions of the shoulder and hip joints in these postures.

The subjects were nine unembalmed male cadavers. A roentgen stereophotogrammetric system (Ref 42, 61, 55), developed for this investigation, measured the three-dimensional positions of vertebrae and pelvis. This radiographic technique measured the _in situ_ skeleton with high accuracy. To obtain comparable data between subjects, a unique and complex experimental procedure was developed to measure bone position _in situ_ and _in vitro_. The _in situ_ measured pointmarks established a mathematical map that an algorithm used to mathematically transform anatomical landmarks into the _in situ_ measured positions. Thus, inter-subject pointmark data were comparable because the same anatomical structures on different subjects defined the similar frames of reference for all analyses.

From all of the three-dimensional position and mobility data, three positions defined seated geometry in representative ERECT, NEUTRAL, and SLUMP postures. In addition to three-dimensional coordinates in an external axis system describing fixed postures, the linear and angular displacements for each vertebra in the sagittal plane were calculated and reported. These biometric results included anthropometric data, a palpatory examination of the musculo-skeletal system, osteological data, and observations of intervertebral disk degeneration. Thus, this investigation studied the position and motion of the torso linkage system and sitting postures.

EXPERIMENTAL PROTOCOL

Subjects came from the Willed Body Program, Department of Anatomy, Michigan State University. The Department of Anatomy carefully screened all subjects. Thus, subjects with serious musculo-skeletal problems did not enter the study.

Subjects were usually available for study within 12 hours after death. Upon receipt at Michigan State University, the Department of Anatomy stored the body at 36°F. Systems Anthropometry Laboratory (SAL) made standard radiographs to evaluate degeneration and pathology in the musculo-skeletal system. If there was no significant joint degeneration or other skeletal pathology, the roentgen stereophotogrammetric investigation began.

The joints were initially moved through their ranges of motion to eliminate resistance caused by rigor mortis. For example, with the subject lying supine, a technician raised the cadaver's head and shoulders until he completely flexed the torso. The body remained in this position for approximately 5 minutes. This procedure removed as much rigor mortis as possible in the erector spinae and deeper muscles between the vertebrae. Then, the technician moved the subject into a prone position. He lifted the head and shoulders from the table to stretch the tissues in the abdomen, pelvis and thighs that resist torso extension. Likewise, the major upper and lower limb joints were moved through their primary ranges of motion to remove the effects of rigor mortis.

An osteopathic physician then conducted a palpatory examination of the musculo-skeletal system of each subject in both prone and supine positions. All conclusions of the physician depended upon his visual and palpable observations of the size, shape and relative function of the musculo-skeletal system (Section 4.1). The examination assessed leg length inequalities, joint motion quality, lumbar vertebrae position and tissue texture abnormalities.

4

Leg length inequality is the difference in the length between the medial maleoli of the right and left legs. The change from supine to prone positions produced a visually estimated difference.

The physician assessed joint motion quality and the position of lumbar vertebrae by palpation. He moved the cadaver through normal motions to palpate restrictions in the joint. The relative prominence of the transverse processes served to indicate vertebra position. For example, if the right transverse process was more prominent than the left, the physician interpreted this observation as a vertebral rotation to the left.

For tissue texture abnormalities, if the physician felt that the soft tissues were stiff, he recorded an abnormality at the anatomical location by reference to the skeletal structure. These observations assumed that the physician could palpate post-mortem rigor effects and distinguish them from the tissue textures he felt in living patients.

Standard anthropometric protocols (Ref 15) were followed to measure dimensions that described body size (Appendix A). The dimensions measured on each subject were:

1. Stature (vertex to right and left heels)
2. Trochanteric height (vertex to right and left trochanters)
3. Symphysion height (vertex to symphysion)
4. Suprasternale height (vertex to suprasternale)
5. Bispinous breadth (right to left anterior superior iliac spines)
6. Acromion-radiale length
7. Radiale-stylion length

The roentgen stereophotogrammetry investigation began by first implanting radiographic targets in the skeleton. The three-dimensional positions of these targets defined the location of each bone. The implanted targets were tungsten carbide balls. These balls were implanted according to a standard protocol

5

Table 1. SAL protocol for targeting subject's skeleton.

BONE	TARGET SIZE*	TARGET NUMBER	ANATOMICAL LOCATIONS	CADAVER TARGETS
Innominate R & L	Large*	6	ASIS, PSIS Pubic Tubercle Iliac Crest Iliac blade	HIP001L-6
Sacrum	Small*	6	2 Lateral (R/L) 2 Medial (R/L) S1 Body S5 Spine	SAC001-6
L5	Large	6	2 Trans. Proc. L. 2 Trans. Proc. R. Dorsal Spine Sup./Inf.	L05001-6
L4	Small	6	Same as L5	L04001-6
L3	Large	6	Same as L5	L03001-6
L2	Small	6	Same as L5	L02001-6
L1	Large	6	Same as L5	L01001-6
T12	Small	6	2 Lamina R. 2 Lamina L. Dorsal Spine Sup./Inf.	T12001-6
T11	Small	1	Dorsal Spine Midpt.	T11001
T10	Small	1	Same as T11	T10001
T9	Small	1	Same as T11	T09001
T8	Small	6	Same as T12	T08001-6
T7	Small	1	Same as T11	T07001
T6	Small	1	Same as T11	T06001
T5	Small	1	Same as T11	T05001
T4	Small	6	Same as T12	T04001-6
T3	Small	1	Same as T11	T03001
T2	Small	1	Same as T11	T02001
T1	Small	6	Same as T12	T01001-6
C7	Small	6	Same as T12	C07001-6
Scapula R.	Large/Small	6	Inferior angle (S) Superior angle (S) Medial border (S) Acromion (L) Coracoid Process (L) Glenoid Fossa (L)	SCA001R-6
Clavicle R.	Large	5	Sternoclavicular Jt. Acromioclavicular Jt. Anterior Midpoint 2 Medial	CLA001R-5
Sternum	Large	6	2 Lateral L/R 2 Medial L/R Inferior (3/4 Rib) Suprasternale	STE001-6
Humerus Right	Large	5	Lateral Epicondyle Medial Epicondyle Shaft, Neck, Head	HUM001R-6

*Large = 1.2 mm; Small = 0.8 mm

described in Table 1. Each bone was identified in Table 1 and the corresponding size of targets was indicated as Large (1.2 mm) or small (0.8 mm). These ball sizes alternated in successive bones so that the ball and corresponding bone were easily identified targets on each radiograph for digitizing. In general, six targets were implanted in each bone but in some cases, T11 for example, there was only one target. The number of targets per bone is indicated in Table 1 under the column heading, Target Number. The approximate anatomical location of each target is identified under the column heading, Anatomical Locations, and the codes used in the database are given under the column heading, Cadaver Targets.

To assist the implantation, a drill was used to make a small hole in the bone. A spring-loaded syringe (Aronson et al, 1978) pressed the ball into the hole. There were usually six balls implanted in each bone with this technique. Pre-drilling the holes and using the spring-loaded syringe assured that the ball was through the periosteum and firmly implanted in bone. The targets that were implanted before measurements of the different seated positions were called cadaver targets.

Anatomical structures on each bone defined the location of each target. The anterior superior iliac spines (ASIS), posterior superior iliac spines (PSIS), pubic tubercles and ilium (Crest and blade) represented the innominate (i.e., hip) bone. The fifth lumbar vertebra described the pattern used for all lumbar vertebrae and T12 described the pattern for the thoracic and cervical vertebrae.

A radiographic double exposure on a single film was used to define initial calibration geometry for the roentgen stereophoto-grammetric system. The body was then seated and the roentgen stereophoto-grammetric measurements made. After the completion of measurements, another double exposure was performed.

Three sets of measurements were used to investigate 1) erect and slumped (i.e., lumbar extension and flexion) torso postures in the sagittal plane, 2) sidebent torso postures in the frontal

7

in the sagittal plane, 2) sidebent torso postures in the frontal plane, and 3) arm and shoulder positions in the frontal and horizontal planes.

The wooden chair had 105° seat back and 6° seat pan angles from the horizontal (Figure 1). The chair back had an adjustable Plexiglas semi-circular bar that controlled the amount of lumbar lordosis. The 38.1 mm diameter bar extended across the seat back. Two screws adjusted the distance of the bar from the seat back. To measure the relative location of these physical structures in the radiographic system, the bar and chair back had tungsten balls implanted in them.

Cotton straps (25.4 mm wide) held the head, thorax and pelvis in position. The head was in the Frankfort plane parallel to the floor. A rubber block supported the head and neck against the seat back. A strap passed around the chest and seat back at nipple level. Similarly, a strap passed under the anterior superior iliac spines around the pelvis and seat back. These three straps remained in place for the ERECT positions.
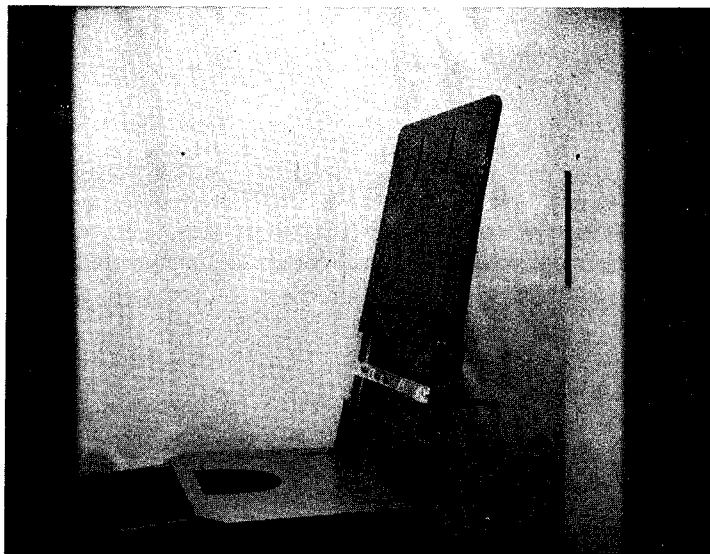
Figure 1. The wooden seat with Plexiglas bar attached for measuring postures with lumbar support.

The Plexiglas bar pushed the lumbar vertebrae into the first ERECT position, ERECT07, a maximum lordotic position (Figure 2). Since the bar was adjusted for each subject based upon their spinal flexibility, the average maximum distance of the bar for all subjects, perpendicular from the seat back, was 64.5 ±0.8 mm. Likewise, the average height of the bar from the seat pan for all subjects, parallel to the seat back, was 240.5 ±0.7 mm. To move each subject from a maximum lordotic position to the unsupported ERECT00 position, the bar was incrementally moved towards the seat. The average increment for all subjects that the bar moved towards the seat back between seated positions was 6.2 ±0.2 mm.
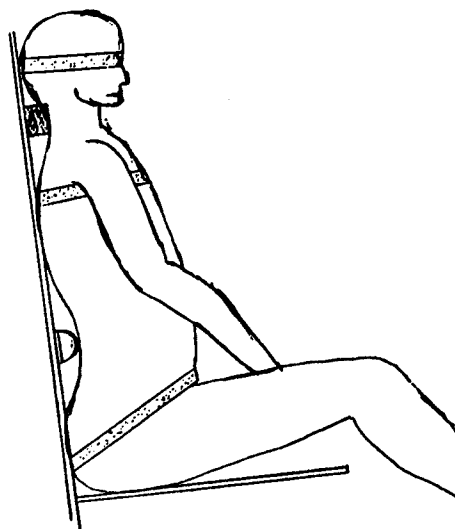
Figure 2. Position of subject seated in an ERECT posture.

The supporting structure was modified to improve data collection after the third subject resulting in lowering the bar 20 mm. This change in bar location necessitated an investigation of the possible effect on comparable positions between subjects.

In the NEUTRAL position, the subject sat erect without lumbar support (Figure 3). To maintain a vertically erect posture, the cotton straps remained around the head, chest and pelvis. The SLUMP10 position was the same as ERECT00. The

subject sat upright without any external lumbar support or straps around the chest.
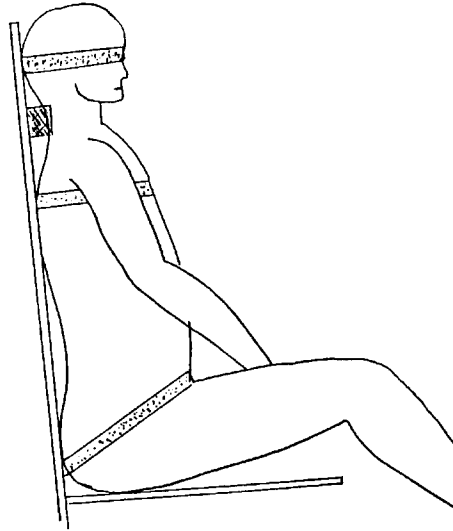
Figure 3. Position of subject seated in a NEUTRAL posture.

In the SLUMP positions, the pelvis was moved forward, SLUMP11 to SLUMP17, by pulling the knees forward in approximately 25 mm increments (Figure 4).

The SHOULDER positions were measured after the ERECT and SLUMP positions (Ref 51). Rigid arm cuffs were used to control the positions of the arms. In the first position measured, SHOULDER40, the subject sat erect as in the NEUTRAL position, described above.

The right arm was measured in 12 positions, SHOULDER40-45 and SHOULDER52-53, 55-56, 58-59. The bones measured in these SHOULDER positions were the humerus, scapula, clavicle, sternum, C07, T01, T04, T08, T12, L01, L02, and L03 (Appendix B).

The arms were hanging freely by the cadaver's side in SHOULDER40. The arms were measured abducted in the plane of the scapula at 30°, 45°, 90° and 135° (SHOULDER41-45) and horizontally

flexed at 45° and 60° at the 45°, 90°, and 135° abduction positions (SHOULDER52-59). The arm was at maximum abduction when additional movement of the arm elevated the body.
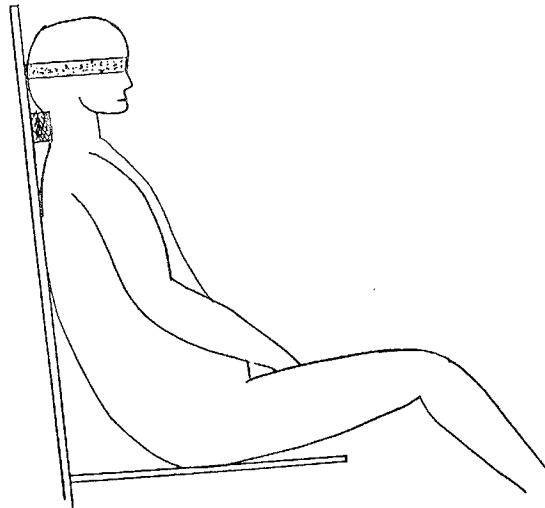
Figure 4. Position of subject seated in a SLUMP posture.

To position the arms in these measurement positions, simple trigonometric relationships between the arm and shoulder were used to calculate the arm locations. A hypotenuse of a right triangle was assumed to be approximated by the line formed by the straight arm from shoulder joint to wrist joint. The height of the right triangle thus formed was the difference between radial styloid height (i.e. wrist joint) and acromion height (i.e. shoulder joint). The length of the hypotenuse (i.e. Arm L in equation 1) of the right triangle was the straight line distance between the acromion landmark and the radial styloid landmark. Thus, to calculate the location of the radial styloid process as a height from the floor and an angle at the shoulder joint (i.e., (θ) in equation 1) a simple equation was used.

$$\text{Radial Styloid Hgt} = \text{Acromion Hgt} - \text{Arm L } (\cos \theta) \qquad (1)$$

where the heights of Radial Styloid and Acromion were from the floor. Arm L was the length from Radial Styloid to Acromion. θ was the angle of shoulder abduction.

For subjects' #4-9, the center of gravity was measured in the horizontal plane (Section 3.2). Three load cells were used in the laboratory axis system.

The results on bone position had variable sample sizes (Table 2). The difference in sample size for individual bones arose from some mis-identification of bone and some missing film image data. The bones per subject by ERECT, SLUMP and SHOULDER were tabulated in Appendix B.

Incorrectly targeting some bones occurred because of mistaking one vertebra for another. For example, targets were implanted in T09 instead of T08. As a result of this mistake, the investigation had data on T03 (n = 1), T09 (n = 2) and T11 (n = 1).

Table 2. Sample for positions measured in ERECT, NEUTRAL, SLUMP and SHOULDER positions.

BONE	ERECT	NEUTRAL	SLUMP	SHOULDER
Sternum	8	8	8	8
R Clavicle	8	8	8	9
R Scapula	7	7	6	9
R Humerus	–	–	–	9
C07	8	8	8	8
T01	8	8	8	9
T03	1	1	1	1
T04	8	8	8	8
T08	6	6	6	7
T09	2	2	2	2
T11	1	1	1	1
T12	8	8	8	8
L01	9	9	9	9
L02	9	9	9	9
L03	9	9	9	9
L04	9	9	9	8
L05	8	8	8	7
Sacrum	9	9	9	6
RInn	9	9	7	5
LInn	9	9	9	6

At least three cadaver targets per bone were necessary for processing data with comparable pointmarks. Thus, complete images of a bone and its targets were necessary on a film pair to obtain the positions of anatomical pointmarks (See Section 3.3). Loss of image data occurred most frequently for the innominate bones in the SLUMP positions because the x-ray tubes were improperly positioned.

After completing the radiographic study of sitting positions, the bones in the shoulder, right arm, spinal column from C4 through L5, and pelvis were excised. The bones were excised carefully so the targets remained undisturbed. Then a film pair of the excised spinal column and pelvis was used to locate the implanted targets.

As much soft tissue as possible was removed from each excised bone. Then, a second set of targets was implanted at anatomical landmarks (Ref 50). If the original cadaver targets were small (0.8 mm in diameter), then large targets were used for the new set (1.2 mm in diameter). After implanting the new targets, films were made. These films were measured to determine the three-dimensional locations of all the targets.

While excising the vertebrae, each intervertebral disk was graded according to Nachemson's (Ref 38) levels of disk degeneration.

After making stereo radiographs of the retargeted bones, all soft tissues were removed. Autoclaving the bones for 30 minutes at 20 lbs pressure softened and removed most of the soft tissue. Then the bones were cooled before manually removing the remaining soft tissue, e.g., periosteum. On clean bones, osteological observations and measurements were performed to describe their pathology and size.

The radiographic film measurements followed a fixed protocol. First, a technician labeled targets on all films following a pattern standardized in the ERECT00 film pair. The

13

same operator digitized a subject's films to minimize variation in data. Accuracy was assumed to be equivalent for different operators. However, due to parallax, operators, consistently differed by 0.2-0.5 mm in their digitizing results.

The initial digitizing results defined two sets of position vectors for each bone. The first set described the location of cadaver targets in each position. The second set measured the three-dimensional locations of the anatomical and cadaver pointmarks in the excised bones. A master file contained all data for each subject. An editing program identified outliers in a subject's data, produced by digitizing or labeling errors, by comparing distances between cadaver targets. For example, the editing program calculated the distances between the same cadaver targets in all positions. The computer program identified any pair of cadaver targets that had a variation greater than ± 0.1 mm from the average. Then, a technician corrected or deleted outliers for further analysis.

After editing the cadaver targets, a computer program computed the three-dimensional coordinates of the anatomical pointmarks in the seated positions. The definition of local three-dimensional axis system used three cadaver targets. A program was written to select the three cadaver pointmarks that had the largest and most comparable perimeters of the triangles formed by these three cadaver targets in the two sets of measurements (Ref 50). A technician selected the most equivalent triad of cadaver targets from these results.

The anatomical targets were transformed into cadaver positions so that anatomical pointmarks (Ref 50) would describe the bone locations comparably between subjects (Ref 50).

Right-handed, orthogonal axes' systems were used to define the laboratory (Section 3.1) seat and body coordinate systems. The origin of the axis system in the seat, SRP, lay in the middle of the intersection between seat back and seat pan. The direction of the positive x axis was eyes forward in the chair. The direction of the positive y-axis was eyes left in the chair.

14

The direction of the positive z-axis was eyes upwards in the chair. The transformation matrix from laboratory to seat axis system typically had no cross-product elements greater than 0.005. Thus, the chair was approximately parallel to the laboratory axis system.

Three pointmarks defined axes' systems (Section 3.3) that corresponded to anatomical directions. The direction of the positive x axis was anterior. The direction of the positive y axis was left lateral. The direction of the positive z axis was superior. Thus, the XZ, YZ, and XY planes were equivalent to the anatomical sagittal, coronal, and transverse planes.

METHODS: EXPERIMENTAL AND ANALYTICAL

Roentgen Stereophotogrammetry

Roentgen stereophotogrammetry was used to measure the position of radiographic targets implanted in the subjects' skeletons in three-dimensional space. Clinical investigations of low back pain (Ref 62, 40), prosthesis implants (Ref 23), growth (Ref 28) and other areas of clinical interest (Ref 42, 32, 69) had also used this technique. In most of these roentgen stereophotogrammetric systems, whether they used orthogonal (Ref 13) or convergent (Ref 56) geometries, the active measurement space was highly constrained. For example, a 356 x 432 x 432 mm space provided enough space to measure the positions of the lumbar vertebrae. Investigations of torso mobility needed a larger measurement space.

Reynolds, Hallgren and Marcus (Ref 48) described the roentgen stereophotogrammetric system initially used in the Systems Anthropometry Laboratory. Significant changes and improvements made since 1982 that defined an analytical film plane greater than the size of the film requires a new description of the measurement system.

Instrumentation and radiographic targets.

Roentgen stereophotogrammetry measured the positions of the targets in the bones of the shoulder, vertebral column, and pelvis. Since stereo images were needed, x-radiation from two x-ray tubes were used to create the radiographic images for measurement. The radiographic focal spots of the Tubes I and II, the stereo base in Figure 5, were 735 mm apart. The focal length, perpendicular distance from film plane to the midpoint of the stereo base, was adjustable from 1200 to 2400 mm. The average focal length used in this investigation was 2063 ± 51 mm.

16

Thus, the angle of convergence between central rays from each x-ray tube was approximately 20°.
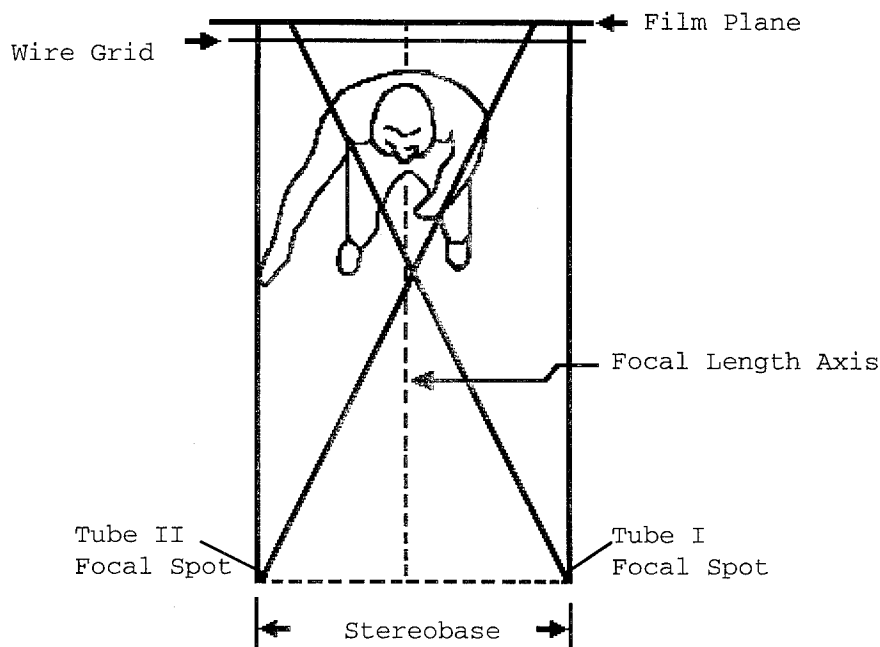
Figure 5. Top view of stereo radiographic system showing subject, film plane, and x-ray tube geometry.

The movement plane of the film cassette holder defined the film plane. A rigid steel structure established a vertical plane in which the film cassette moved. Two steel channels (51 mm x 102 mm x 2648 mm) extended from floor to ceiling with a pair of 13 mm x 76 mm steel plates attached to the side of each channel. These plates interacted with the steel channels through a series of screws forcing the channels into vertical alignment.

Thompson stainless steel shafts, 25 mm in diameter, were mounted in the channels. Two pairs of Thompson pillow blocks containing linear bearings provided vertical movement of the film cassette. A pair of Thompson stainless steel shafts, 25 mm in diameter and 914 mm long, spanned the distance between the

17

vertical channels to provide horizontal movement of the film cassette. These horizontal shafts were 229 mm apart. The film cassette moved on the horizontal shafts with two pairs of Thompson ball bushing pillow blocks. One electrical motor moved the film vertically.

The film cassette rotated about a shaft attached in the middle of the four pillow blocks providing the horizontal movement. The cassette could rotate 360° in the film plane. Magnetic locks held the cassette in place.

The size of the radiographic film was 356 x 914 mm. The two-dimensional displacements of the film cassette defined the analytical film plane of 1500 mm x 2000 mm. Two vertical (z direction) and six horizontal (y direction) tungsten wires formed a wire grid plane that was parallel to the film plane (Figure 6).
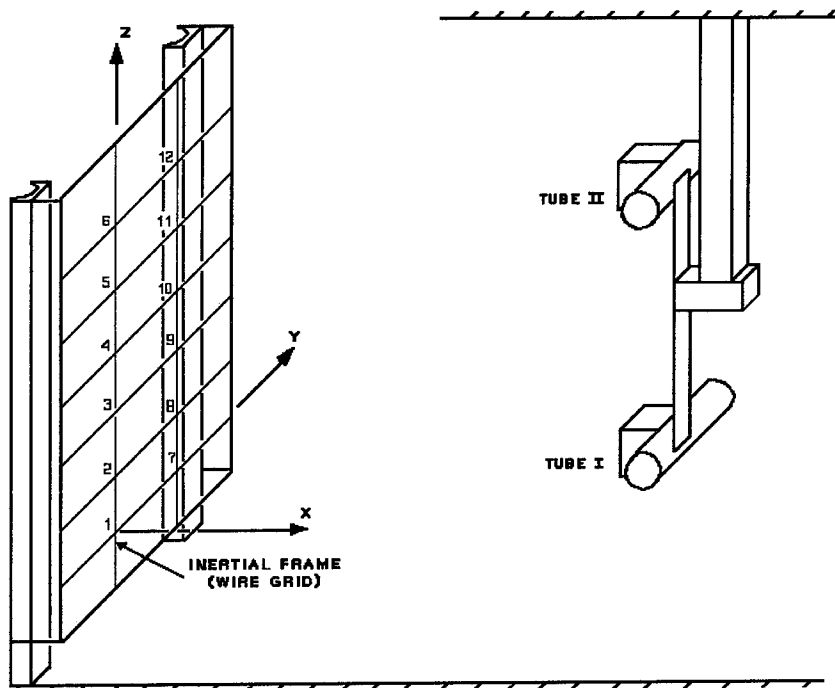
Figure 6. Laboratory axis system, film plane, and x-ray tubes.

The origin of the laboratory axis system was at intersection 1 (Figure 6). The x direction was perpendicular to the wire grid. The film plane was behind the wire grid.

Projected on each film were images of the wire grid and 0.8 mm tungsten-carbide balls. The tungsten-carbide balls were in the seat back, a Plexiglas bar, a glass rod, and a quartz cube. The glass rod had a ball at each end and was perpendicular to the film plane between the subject and x-ray tubes. The quartz glass cube with balls at each corner was near the glass rod. Distances between targets on the glass rod and quartz cube were measured with vernier calipers.

Focal length measurement used a double exposure (two radiographic images on the same film). Two films comprising a stereophotogrammetric film pair recorded each body position. A technician measured the targets on each film on a back-lit, electro-static, Talos digitizer. The digitizer was accurate to ± 0.13 mm. A computer program calculated the three-dimensional coordinates of each target from these measurements.

Stereophotogrammetric algorithm

The following nomenclature was used in the algorithm for analyzing the stereophotogrammetric films.

y_i^I, z_i^I Two-dimensional coordinates of x-ray tube I image targets in the film axis system.

y_i^{II}, z_i^{II} Two-dimensional coordinates of x-ray tube II image targets in the film axis system.

Y_i^I, Z_i^I Two-dimensional coordinates of x-ray tube I image targets in the film axis system after merging films for double exposure geometry.

Y_i^{II}, Z_i^{II} Two-dimensional coordinates of x-ray tube II image targets in the film axis system after merging films for double exposure geometry.

19

$Y_i{}^I$, $z_i{}^I$ — Two-dimensional coordinates of x-ray tube I image targets in the stereo base axis system.

$Y_i{}^{II}$, $z_i{}^{II}$ — Two-dimensional coordinates of x-ray tube II image targets in the stereo base axis system.

X_i', Y_i', Z_i' — 3-dimensional coordinates of the physical target in the stereo base axis system.

Two sets of position vectors in the digitizer axis system represented the target images for a film pair. Images of the same horizontal and vertical wires defined a two-dimensional film axis system unique to each film pair. The analytical algorithm merged the data from the two films as if they were from a double exposure. Position vectors for each target in the merged data were in the film axis system.

Merging the two films in a film pair used:

1) a known, constant geometry, and

2) a constant slope for the stereo base.

Optimally, films recorded the maximum number of targets. Thus, the distance between films in the film plane was variable. The algorithm calculated this variable offset between films to merge the film pair into a double exposure geometry.

The slope of the stereo base was tan θ.

$$\tan\theta = \frac{\left(z_i^{II} - z_i^{I}\right) + t_z}{\left(y_i^{II} - y_i^{I}\right) + t_y} \tag{2}$$

where θ was the angle between the horizontal wire image and a line constructed between the tube I ($y_i{}^I$, $z_i{}^I$) and tube II ($y_i{}^{II}$, $z_i{}^{II}$) image coordinates of the ith target. The two-dimensional offsets between the two films were t_y and t_z.

After rearranging, equation (2) became:

20

$$\begin{bmatrix} \Delta y_1 & 1.0 \\ \Delta y_2 & 1.0 \\ \downarrow & \\ \Delta y_n & 1.0 \end{bmatrix} \begin{bmatrix} \tan\theta \\ K \end{bmatrix} = \begin{bmatrix} \Delta z_1 \\ \Delta z_2 \\ \downarrow \\ \Delta z_n \end{bmatrix} \qquad (3)$$

where Δy_i and Δz_i were the differences in tube I and tube II
images for target i. K equaled t_y (tan θ) - t_z and θ came from
equation (3). Equation (3) calculated t_y and t_z from the known
wire grid and film plane geometries. After adding t_y and t_z to
the digitized data, the image coordinates had the same
relationships as if measured on a double exposure, i.e., (Y_i^I,
Z_i^I) and (Y_i^{II}, Z_i^{II}).

Two physical targets on the glass rod, A and B, lay on a
line perpendicular to the film plane. Targets' A and B located
point O, the midpoint between the focal spots of Tubes I and II.
The locations of O and the focal spots were in the film axis
system (Figure 7). Applying simple trigonometry to the glass rod
target A as shown in the XY plane, established the following
relationships:

$$\frac{FL - X_A'}{(SBY/2) + Y_A'} = \frac{FL}{(SBY/2) + Y_A - TRY} \qquad (4)$$

and, similarly in the XZ plane

$$\frac{FL - X_A'}{(SBZ/2) + Z_A'} = \frac{FL}{(SBZ/2) + Z_A - TRZ} \qquad (5)$$

where FL was the focal length. X_A' was the x coordinate of
target A on the glass rod . SBY/2 was one-half the length of the

21

y component of the stereo base in the film axis system. Y_A' and Z_A' were the coordinates of the physical target A (Figure 7). Y_A and Z_A were the coordinates of the target A image in the film axis system. TRY and TRZ were the y and z distances, respectively, from the origin of the film axis system to point O.
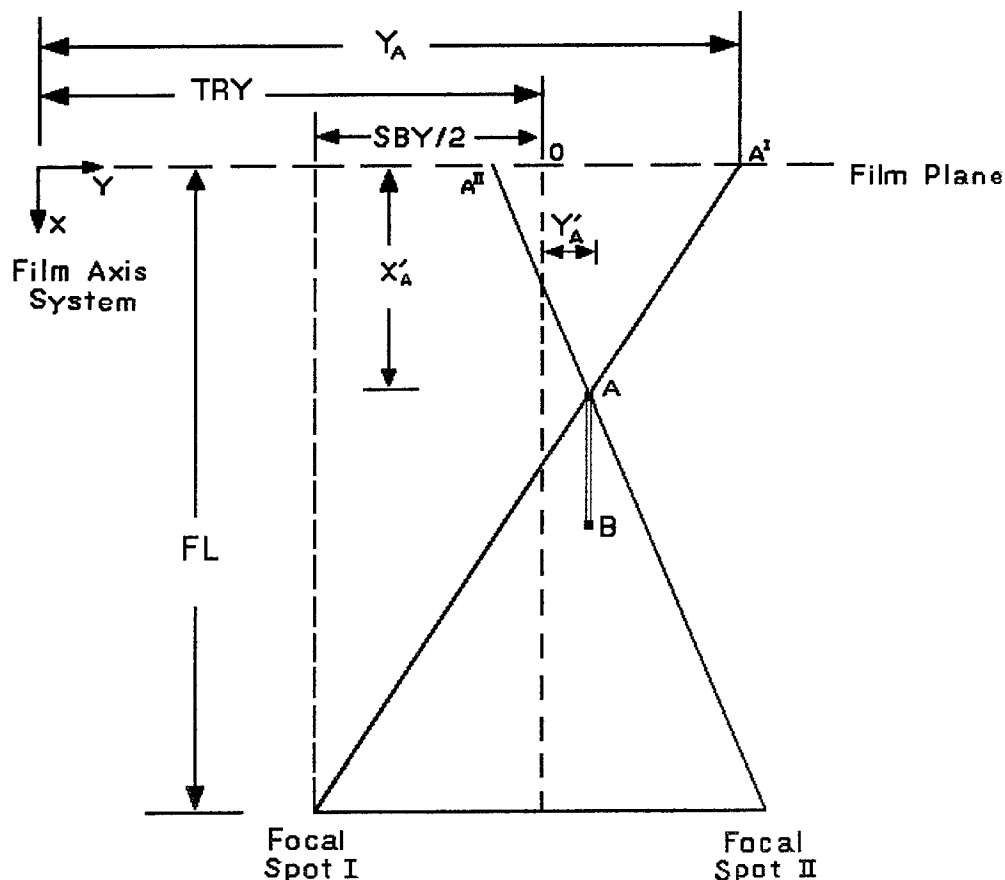
Figure 7. Projection of glass rod targets, A and B, in the xy plane of the film axis system.

Solving for the four unknowns in equations (4) and (5), Y', Z', TRZ and TRZ required two more equations. Like glass rod target A, two equations described glass rod target B.

22

$$\frac{FL - X_B'}{(SBY/2) + Y_B'} = \frac{FL}{(SBY/2) + Y_B - TRY} \tag{6}$$

$$\frac{FL - X_B'}{(SBZ/2) + Z_B'} = \frac{FL}{(SBZ/2) + Z_B - TRZ} \tag{7}$$

There were now six unknowns: Y_A', Z_A', TRY, TRZ, Y_B', and Z_B'. However, the perpendicular glass rod constituted two constraints:

$$Y_A' = Y_B' \tag{8}$$
$$Z_A' = Z_B' \tag{9}$$

Equations 4-9 were therefore used to solve for TRY and TRZ which were used to calculate the coordinates of all physical targets.

The film plane defined a stereo base axis system (Figure 8). The origin of the stereo base axis system was at O. The y-axis paralleled the stereo base, and the z-axis was perpendicular to the y-axis. The next step in the algorithm was to transform all image coordinates from film axis system into the stereo base axis system as (Y_i^I, Z_i^I) and (Y_i^{II}, Z_i^{II}).

The stereo base axis system (Figure 8) depicted the Tube I projection of target i on the film plane. There was an equivalent set of data for the Tube II image of target i.

The transformation of coordinates in the film to stereo base axis system involved a rotation of θ about point O. Using (Y_i^I, Z_i^I) and (Y_i^{II}, Z_i^{II}), the coordinates of the physical target i (X_i', Y_i', Z_i') in the stereo base axis system were calculated from similar triangles in the following equations:

23

$$X_i' = FL\left(1 - \frac{SB}{\left(\mathbf{y_i''} - \mathbf{y_i'}\right) + SB}\right)$$ (10)

$$Y_i' = \left(\frac{FL - X_i'}{FL}\right)\left(\frac{\mathbf{Y_i'} + \mathbf{Y_i''}}{2}\right)$$ (11)

$$Z_i' = \left(\frac{SB}{\mathbf{Y_i''} - \mathbf{Y_i'} + SB}\right)\left(\frac{\mathbf{Z_i'} + \mathbf{Z_i''}}{2}\right)$$ (12)

where ($\mathbf{Y_i^{II}}$ - $\mathbf{Y_i^I}$) was the parallax shift of target i, and SB was the stereo base distance.

Finally, the geometry of the wire grid and film plane defined the data used to transform the coordinates in the stereo base axis system to the laboratory axis system (Figure 8).
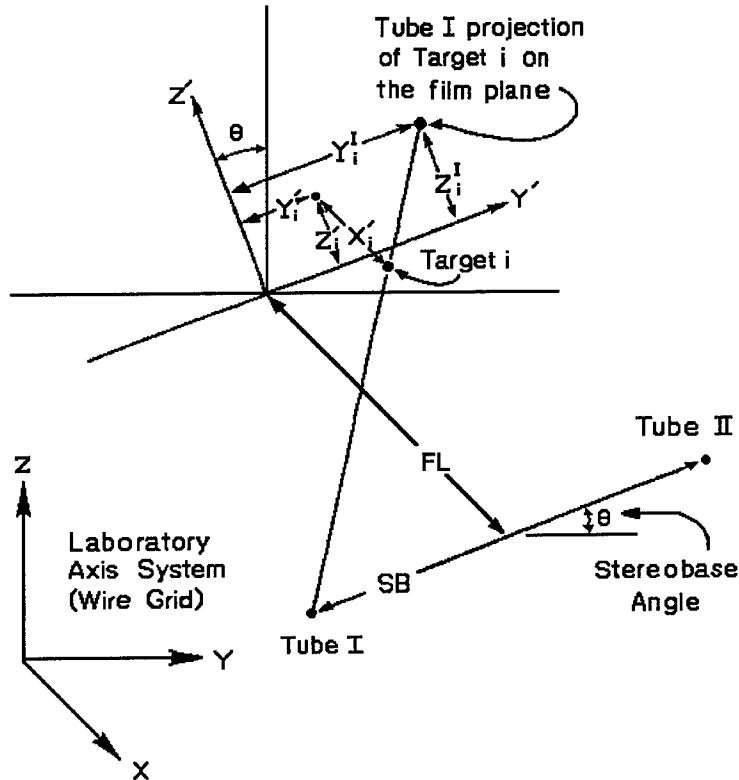
Figure 8. Stereo base axis system showing stereo base angle θ.

Accuracy of stereophotogrammetric system

The following parameters affected accuracy of the roentgen stereophotogrammetry system in the SAL:

1) random error by human operator;
2) variation in cassette thickness and film flatness;
3) non-parallel film and tube-rotation planes;
4) alignment of glass rod.

Two separate experiments investigated the effects of these errors. In both experiments, the same technician digitized each pair of films as many as five times. The standard deviation, describing operator error for repeatedly digitizing the same film targets, was ±0.1 mm. This error lay within the ±0.13 mm digitizer accuracy. Thus, the effect of a trained, experienced operator was considered to be negligible.

Cassette thickness in different commercially available cassettes varied from 0.1-0.4 mm. This distance directly affected the transformation from stereo base axis system to laboratory axis system. Thus, each cassette had a unique film-to-wire grid distance that was a constant in the algorithm.

Forty-two film pairs, taken at seven different angular positions in 30° increments, revealed errors arising from non-parallel film and tube rotation planes. In these data, the stereo base axis rotated 180° from a horizontal position. Initially, tube II had a +y laboratory position and ended in a -y position. The positions of the calibration devices remained fixed during the data collection. Six film pairs, made at each angular position, used different film cassettes.

Distances between targets on the quartz cube were equal to distances calculated from three-dimensional coordinates (Table 3). These 42 film pairs recorded the variation in the data from tube rotation. The sample size for each distance varied according to image quality. For example, targets 1 and 2 were visible on 40 films, and targets 1 and 3 were visible on 27 film

pairs. The average difference between measured and actual distance was 0.1%.

Table 3. The effect of x-ray tube position on measurement of targets distances (mm).

Target		Measured Distance (Tube rotation)		Actual Distance	
Pair	N	Ave	St Dev	Distance	% Diff.
1-2	40	116.4	0.3	116.5	0.1
1-3	27	151.6	0.3	151.6	0.0
1-5	38	92.4	0.1	92.5	0.1
2-4	34	150.6	0.3	151.0	0.3
2-6	36	91.9	0.1	91.8	-0.1
3-4	25	116.8	0.3	116.8	0.0
3-7	28	92.9	0.1	93.0	0.1
4-8	33	93.3	0.1	93.1	-0.2
5-6	36	116.1	0.3	116.4	0.3
6-8	35	150.7	0.3	151.0	0.2
7-8	35	117.7	0.4	117.6	-0.1
Total		117.4	25.4	117.5	0.1

Another source of error in the measurements was the effect of glass rod alignment. With the tubes in a vertical orientation and the quartz calibration cube held fixed, five stereo radiographs recorded the effect of repositioning the glass rod five times. Eleven distances between quartz cube target pairs described the variation produced by repositioning the glass rod. The trials factor for a univariate, repeated measures F-test was the difference between actual and measured distances (Table 4). The average of all six trials was 0.24 ±0.08 mm. Although there were slight differences between trials, an F = 0.824 was not significant at the 0.05 level. Thus, the effect of repositioning

the glass rod contributed a negligible error to variation between subjects.

When the glass rod alignment changed, a slight error in the distances occurred. The standard deviation in five trials of 11 distance measurements with the glass rod realigned for each trial ranged from ±0.29 to 0.65 mm. This variation arose from a more accurate laboratory alignment procedure in the XZ plane than in the YZ plane.

Table 5 reported the locations of two targets on the quartz cube with the stereo base axis oriented 0°, 90°, and 180°. The percentage difference between actual values measured with a cathetometer accurate to ±0.05 mm and with the roentgen stereophotogrammetric system was within 0.4% (Table 5).

Table 4. The effect of glass rod re-positioning on measurements of target distances (mm).

	Trials					
	(1)	(2)	(3)	(4)	(5)	(6)
N	11	11	11	11	11	11
Minimum	-1.05	-0.75	-0.91	-1.07	-0.22	-0.16
Maximum	1.37	1.37	1.36	1.71	0.82	0.83
Average	0.18	0.38	0.31	0.17	0.19	0.26
St Dev	0.65	0.57	0.56	0.83	0.29	0.29

Univariate Repeated Measures F-Test					
Source	SS	DF	MS	F	P
Hypothesis	0.39	5	0.079	0.824	0.540
Error	4.77	50	0.95		

Three-dimensional coordinates were most accurate when the stereo base was vertical. The data were least accurate when the

stereo base was horizontal (Table 5). The accuracy changed because the stereo base axis rotated in a plane that was not parallel to the film. There was a positive systematic error in the three dimensional coordinates. The largest systematic error was in the x direction. The standard deviation for x ranged from ±0.3 to ±0.7. The standard deviation for y and z remained at ±0.1 to ±0.2 with the exception of the Y1 coordinate at 60°.

In summary, the vertical orientation of the tubes in the ERECT, NEUTRAL and SLUMP positions was the most accurate. Tube rotation during shoulder motion and torso side-bending provided a source of random variation in the data. Glass rod alignment produced a systematic error of approximately 0.2 mm. However, the three-dimensional position of the skeletal system in the seat axis system provided an accurate description of skeletal posture.

Table 5. Accuracy of three-dimensional coordinates (mm) in the laboratory axis system.

Stereo base Axis Angle	X1	Y1	Coordinates Z1	X2	Y2	Z2
0°	421.6	69.3	495.5	510.6	143.8	493.6
	(0.5)	(0.1)	(0.0)	(0.4)	(0.1)	(0.1)
30°	421.6	69.2	495.5	511.7	143.7	493.7
	(0.5)	(0.1)	(0.1)	(0.7)	(0.2)	(0.2)
60°	421.7	69.5	495.5	510.8	144.3	493.7
	(0.3)	(0.3)	(0.1)	(0.5)	(0.4)	(0.2)
90°	422.6	69.0	495.5	511.8	143.6	493.7
	(0.4)	(0.1)	(0.1)	(0.5)	(0.2)	(0.1)
120°	422.1	69.5	495.4	511.0	143.9	493.5
	(0.6)	(0.0)	(0.1)	(0.5)	(0.1)	(0.2)
150°	422.8	69.2	495.7	510.8	143.8	493.9
	(0.5)	(0.2)	(0.1)	(0.4)	(0.2)	(0.1)
180°	421.7	69.5	495.6	511.3	144.0	493.8
	(0.3)	(0.2)	(0.0)	(0.3)	(0.2)	(0.1)
Average	421.9	69.3	495.5	511.1	143.9	493.7
St Dev	(0.4)	(0.2)	(0.1)	(0.5)	(0.2)	(0.1)
Actual	423.6	69.5	495.9	512.9	144.0	492.9
% Diff.	0.4%	0.3%	0.1%	0.3%	0.1%	-0.2%

Measurement of center of gravity in the horizontal plane.

The chair sat on a 12.7 mm milled aluminum plate that rested on three Sensotec, SA Series, 113.4 kg capacity load cells. The alignment of the aluminum plate over the load cells was made with four 16 mm steel rods that passed through the plate. These rods absorbed shear forces between the plate and load cells.

A platform, constructed of a 3 mm aluminum plate and 18 mm sheet of plywood, held the load cells in place. The sides of the platform were 50.8 mm x 152.4 pine boards. The center of the platform had a 152 mm square steel plate attached to a screw for leveling and re-enforcement. The screw mounted on a strut that spanned the inner breadth of the platform. At each corner of the platform, a screw adjusted the alignment of the platform in the horizontal plane. A master precision level was used to check the alignment of the aluminum plate within ±0.0127 mm/304.8 mm of horizontal runout.

Three-dimensional coordinates in the laboratory axis system described the location of each load cell (Figure 9). A cathetometer measured the x and y locations of pin holes, directly overlying the center of each load cell. The three measurements of each load cell's location had average standard deviations of ±0.009 and ±0.006 in the x- and y-directions, respectively.

29
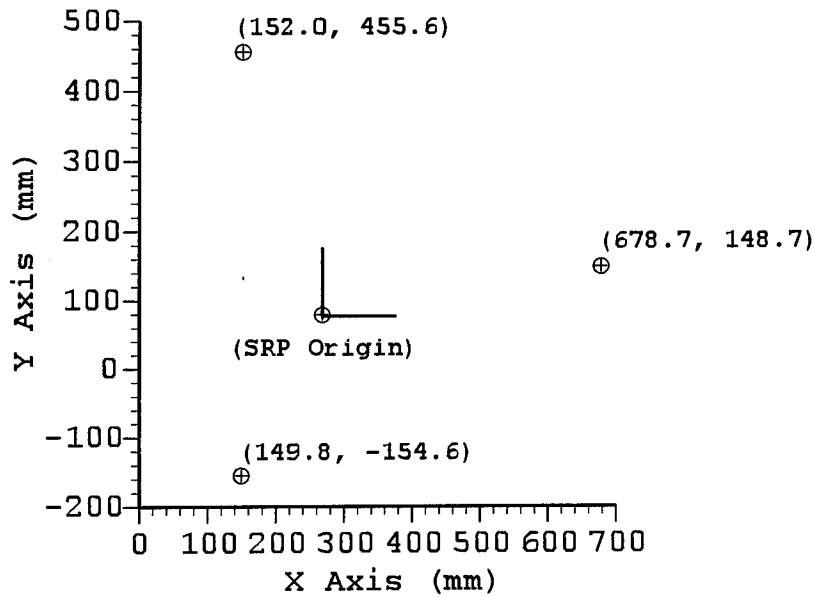
Figure 9. Location of load cells in the laboratory axis system.

Since the locations of the three load cells were in the laboratory axis system, the location of the center of gravity was in the laboratory axis system.

A Zenith Z-100 microcomputer collected the data. A computer program was written to detect any voltage output greater than 0.005 volts (equivalent to 4 oz on a load cell) and any 2% change in voltage. The results were stored on floppy disk. The load cells had a ±5 Vdc output over the 113.4 kp range, and the calibration of each load cell was within the manufacturer's specifications.

The following equations calculated the moments about the x and y axes in the horizontal plane:

$$M_x = \sum_{i=1}^{n=3} \left(x_i F_i \right) \qquad (13)$$

$$M_y = \sum_{i=1}^{n=3} \left(y_i F_i \right) \qquad (14)$$

30

where Mx and My were the sums of total moments about the x- and
y-axes respectively. X_i and y_i were the coordinate locations of
each load cell in the laboratory axis system. F_i was the force
measured at each load cell. To calculate the body's center of
gravity, the empty chair's moments were subtracted from the total
moments of the body and chair. Thus,

$$Mx_t \quad - \quad Mx_c \quad = \quad Mx_b \qquad (15)$$

$$My_t \quad - \quad My_c \quad = \quad My_b \qquad (16)$$

where Mx_t and My_t represented the total moment of body and chair.
Mx_c and My_c represented the empty chair's moments. Mx_b and My_b
were the body's moments around the laboratory x and y-axes. To
compute the location in the laboratory axis system, the following
equations were used to calculate the body's x and y locations:

$$X_b = \frac{M_{xb}}{\sum F - \sum W_{ch}} \qquad (17)$$

$$Y_b = \frac{M_{yb}}{\sum F - \sum W_{ch}} \qquad (18)$$

where Mx_b and My_b were the moments of the body, $\sum F$ was the sum
of the forces, and $\sum W_{ch}$ was the weight of the chair. The
location of the center of gravity in the seat axis system was
calculated by vector subtraction.

31

Definition of a local anatomical axis system.

The locations of anatomical landmarks were in a local three-dimensional axis system for each bone. Three non-collinear anatomical pointmarks were necessary to define an orthogonal coordinate system. A procedure developed by Jeff Marcus (Ref 35) used pointmark position vectors in an external axis system to define an anatomical axis system. By carefully selecting the anatomical pointmarks for axis system definition, the new axis system described the cardinal anatomical planes of the body.

First, three pointmark position vectors in an external axis system were selected. They were **P1**, **P2** and **P3** (Figure 10). Two position vectors, **P1P2** and **P1P3**, defined a fourth point.

$$\mathbf{P1P2} = (P2_x - P1_x)i + (P2_y - P1_y)j + (P2_z - P1_z)k \qquad (19)$$

$$\mathbf{P1P3} = (P3_x - P1_x)i + (P3_y - P1_y)j + (P3_z - P1_z)k \qquad (20)$$

The dot product between **P1P2** and **P1P3** defined Θ:

$$\cos\theta = \frac{\mathbf{P1P2} \cdot \mathbf{P1P3}}{|\mathbf{P1P2}||\mathbf{P1P3}|} \qquad (21)$$
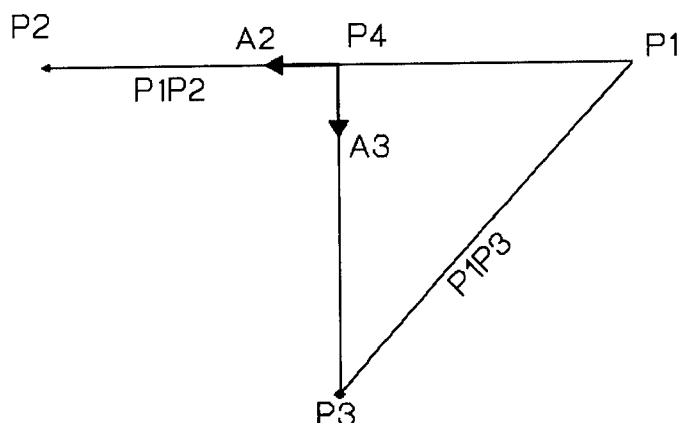
Figure 10. Anatomical pointmarks and local axis system.

The projection of **P1P3** onto **P1P2** located a new position vector, **P4**, on **P1P2**. **P4** was at the intersection between **P1P2** and a perpendicular line passing through **P3**. The distance from **P1** to **P4** on the **P1P2** vector was $|{\bf P1P3}| \cos \Theta$. The coordinates of **P4** were calculated in the external axis system by

$$\mathbf{P4} = \mathbf{P1} + \frac{\mathbf{P1P2}}{|\mathbf{P1P2}|} \; |\mathbf{P1P3}| \; \cos \Theta \tag{22}$$

P4 located the origin for the anatomical coordinate system. The unit anatomical axes' vectors were:

$$\mathbf{A2} = \frac{\mathbf{P2} - \mathbf{P4}}{|\mathbf{P2} - \mathbf{P4}|} \tag{23}$$

and

$$\mathbf{A3} = \frac{\mathbf{P3} - \mathbf{P4}}{|\mathbf{P3} - \mathbf{P4}|} \tag{24}$$

These two unit vectors were orthogonal, and their cross product defined **A1**.

The unit vectors **A1**, **A2** and **A3** were used to define a 3x3 rotational transformation matrix between the external measurement and the anatomical coordinate systems. The superscripts, **e** for the external system and **a** for the anatomical system, denoted the coordinate system in which **r** was measured.

33

$$\mathbf{r}^{(a)} = \mathbf{A}_{ae}\mathbf{r}^{(e)} \qquad (25)$$

The matrix $\mathbf{A}_{ae}$ defined a simple rotational transformation from the external system to the anatomical where:

$$\mathbf{A}_{ae} = \begin{bmatrix} \leftarrow \mathbf{A1}^{(e)} \rightarrow \\ \leftarrow \mathbf{A2}^{(e)} \rightarrow \\ \leftarrow \mathbf{A3}^{(e)} \rightarrow \end{bmatrix} = \begin{bmatrix} A1_x\, A1_y\, A1_z \\ A2_x\, A2_y\, A2_z \\ A3_x\, A3_y\, A3_z \end{bmatrix} \qquad (26)$$

Now, we considered the translation from the origin of the external system to the anatomical origin. The offset vector between the two systems was $\mathbf{P4}^{(e)}$. The combined translation and rotation transformation were in homogeneous form as a 4x4 transformation matrix $\mathbf{T}_{ae}$:

$$\mathbf{T}_{ae} = \begin{bmatrix} & & & \uparrow \\ & \mathbf{A}_{ae} & & -\mathbf{P4}^{(a)} \\ & & & \downarrow \\ 0 & 0 & 0 & 1 \end{bmatrix} \qquad (27)$$

To obtain $\mathbf{P4}^{(a)}$, the offset vector $\mathbf{P4}^{(e)}$ was transformed into the anatomical coordinate system using equation (26), and the resulting vector was inserted into equation (27). The top left-hand corner of the matrix in equation (27) was simply the 3x3 transformation matrix from equation (25).

The transformation matrix $\mathbf{T}_{ae}$ operated on a 4x1 vector where the top three terms were $\mathbf{r}^{(e)}$ as in equation (26) and the bottom

34

term was a 1. Therefore, to transform a vector in the external coordinate system ($\mathbf{r}^{(e)} = [\ r_x^{(e)},\ r_y^{(e)},\ r_z^{(e)}\ ]$), the following transformation equation was used:

$$
\begin{bmatrix} \uparrow \\ \mathbf{r}^{(a)} \\ \downarrow \\ 1 \end{bmatrix}
=
\begin{bmatrix} & & & \uparrow & \\ & \mathbf{A}_{ae} & & -\mathbf{P4}^{(a)} & \\ & & & \downarrow & \\ 0 & 0 & 0 & 1 & \end{bmatrix}
\begin{bmatrix} \uparrow \\ \mathbf{r}^{(e)} \\ \downarrow \\ 1 \end{bmatrix}
\tag{28}
$$

This algorithm defined axes that were consistent with the orientation of the major anatomical axes. Thus, the XZ plane corresponded to the sagittal plane, YZ to the frontal, and XY to the transverse planes. Several applications of this algorithm were necessary. This algorithm defined anatomical axes systems for bones and segments with anatomical pointmarks located on the following axes:

P1	P2	P3	BONE or *SEGMENT*
+x	-x	-z	Innominate, *Thorax*
+y	-y	-z	Scapula, *Pelvis*
+y	-y	+x	Vertebrae, Sacrum
+y	-y	+z	Humerus, Sternum and Clavicle

For example, in the first row, a pointmark lying in the +x direction was **P1**. A second pointmark lying in the -x direction was **P2**. The third pointmark lying in the -z direction was **P3**.

These directions maintained consistent anatomical directions for specific bones. The orientations of the axes define planes

35

that were parallel to the intersection of the cardinal anatomical planes.

Calculation of the location of the shoulder joint center.

Given a spherical model, the loci of all points with a constant radius, r, traced a spherical surface. The location of these points was in three-dimensional space. A radius of this sphere could be calculated inversely, from these points on the surface, if the center was known. If the points of the surface represented the locations of the joint center with the subjacent link, the radius was equal to link length. This model was used to calculate the shoulder joint center.

For each trial a file of the x,y,z, coordinates for each point was created. In solving for the coefficients for the equation of a sphere, the difference between consecutive positions of the same point was used.

For a point $(P_{i,j})$, $i = 1,N$, and $j = 1,3$ where N was the number of points on the sphere. $P(1,1)$ was the x coordinate. $P(1,2)$ was the y coordinate. $P(1,3)$ was the z coordinate. These points lay on a spherical surface with its center at x_o, y_o, z_o.

The initial position of point P was x_i, y_i, z_i. If P moved so radius r was constant from x_o, y_o, z_o, then r was calculated from equation (29).

$$(x_i - x_o)^2 + (y_i - y_o)^2 + (z_i - z_o)^2 = r^2 \qquad (29)$$

Since r was constant, position i + 1 was determined by

$$(x_{i+1} - x_o)^2 + (y_{i+1} - y_o)^2 + (z_{i+1} - z_o)^2 = r^2 \qquad (30)$$

Then, equations 29 and 30 were combined:

$$(x_i - x_o)^2 + (y_i - y_o)^2 + (z_i - z_o)^2 = (x_{i+1} - x_o)^2 + (y_{i+1} - y_o)^2 + (z_{i+1} - z_o)^2$$

The x-terms were squared and collected on the left:

$$x_i^2 - 2x_i x_o + x_o^2 = x_{i+1}^2 - 2x_{i+1} x_o + x_o^2 + x_i^2 - 2x_i x_o + 2x_{i+1} x_o - x_{i+1}^2$$

$$x_i^2 - x_{i+1}^2 - 2(x_i - x_{i+1}) x_o = (y_{i+1} - y_o)^2 + (z_{i+1} - z_o)^2 - (y_i - y_o)^2 - (z_i - z_o)^2 \qquad (31)$$

Similar to equation 31, the y- and z- terms were squared and collected:

$$y_i^2 - y_{i+1}^2 - 2(y_i - y_{i+1}) y_o =$$

$$z_i^2 - z_{i+1}^2 - 2(z_i - z_{o+1}) z_o =$$

Then, x_o, y_o, and z_o were combined on the left:

$$x_o(x_i - x_{i+1}) + y_o(y_i - y_{i+1}) + z_o(z_i - z_{i+1}) = -1/2 \ [x_i^2 - x_{i+1}^2 + y_i^2 - y_{i+1}^2 + z_i^2 - z_{i+1}^2] \qquad (32)$$

From three points on the spherical surface, three equations could be written. Thus, x_o, y_o, z_o were determined. When the centroid was calculated, r could be computed from equation 29.

In the present case, there were more than three points on the surface of the sphere. Consequently there were more equations than unknowns and equation 32 was rewritten as:

$$Ax_o + By_o + Cz_o + D = 0 \qquad (33)$$

$$\text{where} \quad A = x_i - x_{i+1}$$
$$B = y_i - y_{i+1}$$
$$C = z_i - z_{i+1}$$
$$D = -1/2 \ [x_i^2 - x_{i+1}^2 + y_i^2 - y_{i+1}^2 + z_i^2 - z_{i+1}^2]$$

To solve for x_o, y_o, and z_o, all possible permutations of the positions were used. The difference was calculated between the present and next position, e.g., $(x_i - x_{i+1})$ for the A coefficients of x_o. After these equations had been formed, x_o, y_o, and z_o were computed using singular value decomposition.

Each of the coefficients of x_o, y_o, z_o, i.e. A, B, & C, were used in matrix U. This matrix had an M x 3 size where the size of M was determined by the number of points on the spherical surface described with equation (33). Column 1 was composed of the coefficients of x_o. Column 2 contained the coefficients of y_o. Column 3 contained the coefficients of z_o. The matrix X was a 3 x 1 matrix of $[x_o, y_o, z_o]^T$ and T was the M x 1 matrix of the constant D of equation 33, i.e. D_1.

The center of the sphere was found in the following linear equation.

$$[U] \quad [X] = [T] \tag{34}$$

We solved for X by $X = U^{-1}T$. Singular value decomposition was used to find U^{-1}. The methods of Press, et al. (Ref 45) were used to solve for $x = [x_o, y_o, z_o]^T$.

When the location of the center of the sphere (x_o, y_o, z_o) was found, equation 29 was used to solve for the radius. Since multiple points lay on the surface of the sphere, the average radii for the sphere that fits these points was calculated using the same center (x_o, y_o, z_o).

Center and radius of curvature in the spinal column.

The two-dimensional curvature of a spinal region (e.g., lumbar) was modeled as a segmental circle defined by a set of pointmarks representing a planar curve. The most representative

curve was defined by a least squares method to calculate the
center of a circle, $C(x_o, y_o)$, and the radius of the circle, r.

The equation of a circle was

$$(x_i - x_o)^2 + (z_i - z_o)^2 = r^2 \tag{35}$$

The center of curvature lay at x_o, z_o with a radius of r
(Figure 11). Experimentally measured data lay near the curve at
x_i, z_i. The experimentally measured data had an offset which was
used to calculate a least squares solution to equation 35. Thus,
a least squares method was used to minimize the sum of squares
for error, Σf_i^2, where

$$f_i = \left(\sqrt{(x_i - x_o)^2 + (z_i - z_o)^2} \right) - r \tag{36}$$
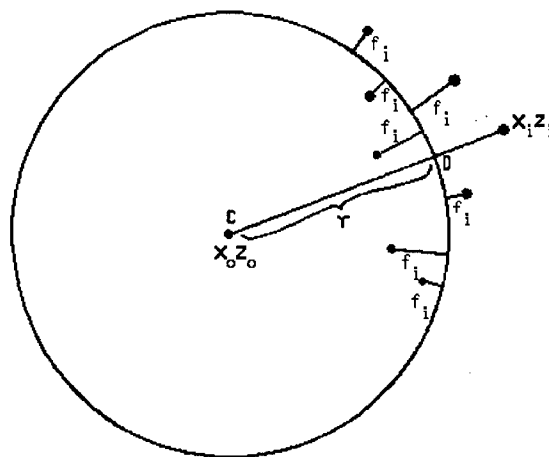
**Figure 11. Geometric model of parameters used to calculate lumbar
curvature from two-dimensional pointmarks.**

which was the shortest distance from experimental data (x_i, z_i) to
a point on the circle that had a center of curvature at (x_o, z_o)
and radius r. Using this method, x_o, z_o, and r of the curve were
calculated to fit the experimentally measured data.

The sum of squares for error, SSE, was

$$SSE=F=\sum_{i=1}^{n} f_i{}^2 = \sum_{i=1}^{n}\left[\sqrt{(x_i-s_o)^2+(z_i-z_o)^2}-\mathbf{r}\right]^2 \qquad (37)$$

A necessary condition to minimize SSE was:

$$\frac{\partial F}{\partial x_o}=0 \qquad (38)$$

$$\frac{\partial F}{\partial y_o}=0 \qquad (39)$$

$$\frac{\partial F}{\partial z_o}=0 \qquad (40)$$

Substituting equation 35 into equations 38, 39, and 40 yielded:

$$\frac{\partial F}{\partial x_o}=0 \Rightarrow \sum_{i=1}^{n}\left[1-\frac{\mathbf{r}}{\sqrt{\Delta}}\right][x_i-x_o]=0 \qquad (41)$$

$$\frac{\partial F}{\partial z_o}=0 \Rightarrow \sum_{i=1}^{n}\left[1-\frac{\mathbf{r}}{\sqrt{\Delta}}\right][z_i-z_o]=0 \qquad (42)$$

$$\frac{\partial F}{\partial \mathbf{r}_o}=0 \Rightarrow \sum_{i=1}^{n}\left[\mathbf{r}-\sqrt{\Delta}\right]=0 \qquad (43)$$

where

$$\Delta = (x_i - x_o)^2 + (z_i - z_o)^2$$

Calculating values with equations 41, 42, and 43, and,

$$\mathbf{r}=\frac{\sum(\sqrt{\Delta})}{n} \qquad (44)$$

$$x_o=\frac{1}{n}\sum_{i=1}^{n}\left[x_i-\frac{\mathbf{r}(x_i-x_o)}{\sqrt{\Delta}}\right] \qquad (45)$$

$$z_o = \frac{1}{n}\sum_{i=1}^{n}\left[z_i - \frac{\mathbf{r}(z_i - z_o)}{\sqrt{\Delta}} \right]$$

(46)

Equations 44, 45, and 46 constituted a set of nonlinear equations without a closed form solution. Consequently, a numerical iteration method was used.

Optimal initial values for x_O, z_O and $\mathbf{r}$, determined by the average of x_i and z_i coordinates of the experimental data, lay within the concavity of the curve. The final solution in the iterative method was a steady state value to which x_O, y_O, and $\mathbf{r}$ converge.

41

SAMPLE DESCRIPTION

The present study described the passive geometry of the musculo-skeletal system in sitting postures. Traditional anthropometric and osteometric measurements described the size and shape of the body and skeleton. Clinical observations were used to assess musculo-skeletal function in each cadaver.

General anthropometric description of sample.

Cause of death and age.

The sample of nine, white adult males (Table 6) ranged in age from 18 to 81 years with an average of 56.4 ±20.5 years. The cause of death was typically due to systemic disorders (subjects #1-8). One trauma-related death was recorded (subject #9).

Table 6. Subject's age and cause of death.

Subject #	Sex	Age	Race	Cause of Death	Days post mortem commencing study
#1	M	33	W	Respiratory failure; brain tumor	19
#2	M	59	W	Metastatic carcinoma of the lung	2
#3	M	56	W	Metastatic carcinoma of the esophagus	1
#4	M	65	W	Arterial thrombosis; arterial sclerosis	1
#5	M	81	W	Lung cancer	5
#6	M	77	W	Pneumonia; cerebral hemorrhage	2
#7	M	49	W	Myocardial infarction	6
#8	M	70	W	Cardiopulmonary arrest; lung cancer	9
#9	M	18	W	Internal head injuries	1

The subjects were typically measured within 1-9 days after death. Subject #1 was the exception. The physical examination was conducted four days after death. However, the radiographic study was delayed for 19 days due to technical problems with the radiographic equipment. A histological examination of selected postural muscles showed typical post-mortem tissues with no additional changes due to the length of storage.

Anthropometry

Anthropometric data on the subjects lying in a supine position were measured (Table 7) according to the techniques developed by Clauser et al (Ref 15). Individual values for each subject are presented in Appendix A.

Table 7. Anthropometric description of sample.

Dimensions	N	Ave	SD	CV*
Body Weight (kg)	9	62.2	±10.1	.17
Vertex-Heel Length (mm)				
Left	9	1750	±57	.03
Right	9	1751	±55	.03
Ave.	9	1751	±55	.03
Vertex-Trochanterion				
Left	7	840	±28	.03
Right	7	838	±26	.03
Ave.	7	840	±27	.03
Vertex-Symphysion	7	854	±23	.03
Vertex-Suprasternale	7	328	±16	.05
Suprasternale-Symphysion	9	531	±18	.03
Bispinous B.	8	236	±20	.09
Acromion-Radiale, R	8	337	±12	.04
Radiale-Stylion, R	6	264	±20	.08
Sitting Height (in AF chair)	6	906	±45	.05

*CV = Coefficient of Variation

43

All measurements of the torso were taken as the
perpendicular distance from a headboard to the landmark with the
cadaver in a supine position. Measurements of the arm and pelvis
followed traditional anthropometric techniques. Sitting height
was measured on subjects #4-9 in the chair. Differences in the
sample size per dimension were due to changes in the protocol.

A comparison of the MSU sample and the USAF Flying Personnel
1967 survey demonstrated considerable differences (Table 8) in
age and body size. The Air Force data were from 2420 adult males
ranging in age from 21-50 years with an average age of 29.53
±6.31 years. The MSU data represented 9 males with an average
age at death of 56.4 ±20.5 years. In addition, the measurement
techniques for stature and seated height differed between the two
studies. For example, cadaver stature was greater than living
stature since additional length resulted from measurements in a
supine position (Ref 66). In both standing and supine positions,
the subject's head was positioned in the Frankfort plane.
However, the muscles and ligaments in the cadaver were relaxed
and the effect of gravity stretched rather than compressed the
body. In Table 8, cadaver stature was the average of head to
heel length from the right and left heels. Also, for seated
height the cadavers leaned against the chair back and the living
sample sat erect.

**Table 8. Anthropometric comparison between MSU and Air Force
1967 survey samples.**

Dimensions	USAF AVE	SD	MSU AVE	SD
Age (yrs)	29.5	± 6.3	56.4	±20.5
Body Weight (kg)	78.7	± 9.7	62.2	±10.5
Stature (mm)	1773	±62	1751	±55
Seated Height (mm)	932	±32	906	±45

44

Physical examination of musculo-skeletal system

Each cadaver was examined by a physician who described the passive functioning of the musculo-skeletal system. The complete description was recorded and transcribed (Appendix C).

Subjects #1, 2, 4, and 7 had musculoskeletal systems that were functionally symmetrical. The other subjects had some unique findings that might have affected their results. Subjects #6 and 8 had a right, thoracolumbar scoliosis with the apex of curvature at T8. Subject #6 had a pacemaker implanted subdermally in the right shoulder region. Subject #8 had a marked kyphosis and a very mobile sacro-iliac joint. Subject #5 had a very kyphotic spine and motions of the right shoulder were restricted. Subject #9, who died from injuries suffered in a car accident, had a fracture in the midline of the fifth rib and the head of the second rib was also fractured. The right shoulder was restricted in external rotation and abduction motions.

Osteology and intervertebral disk morphology.

After completing the radiographic investigation, the bones were excised. As described previously, each bone was cleaned in preparation for measurement and study. The complete description of the morphological and pathological status was recorded for each subject (Appendix C).

Osteological measurements

The skeletal material was measured to describe the size, shape, amount of osteoarthritis and other skeletal pathologies. Fourteen dimensions of vertebral geometry were measured and twenty-three measurements of osteophyte development were made.

The bones investigated in this study were C_7, T_1, T_4, T_8, T_{12}, and L_1-L_5 from subjects #2-#9. Subject #1's skeleton was not included because his body was returned to the anatomy department before the osteological study was conducted.

Linear dimensions of vertebral geometry (Table 9) were measured according to the dimensions described by Singh & Bhasin, (Ref 57). However, angular dimensions of facet and spinous process orientations were made from 35 mm slides. Each slide was displayed on a rear-projection screen. A transparency with an orthogonal axis system lay on the screen to define axes tangent to anatomical landmarks. Positive angles represented counter-clockwise rotations.

The definitions of the measurements in Table 9 were:

Anterior height of vertebral body: anterior distance between superior and inferior endplates in the midsagittal plane (A, Figures 12a & b).

Middle height of vertebral body: middle distance between the superior and inferior endplates of the vertebral body in the midsagittal plane (B, Figure 12c).

Posterior height of vertebral body: posterior distance between the superior and inferior endplates of the vertebral body in the midsagittal plane (C, Figure 12c).

Superior sagittal diameter (anterior diameter): distance between the of the superior endplate in the midsagittal plane (D, Figures 12a & c).

Mid-sagittal diameter: distance between the anterior and posterior surfaces at mid-body in the midsagittal plane (E, Figure 12c).

Inferior sagittal diameter (posterior diameter): distance between the margins of the inferior endplate in the midsagittal plane (F, Figure 12c).

Superior transverse diameter: distance across the lateral margin of the superior endplate in the frontal plane (G, Figures 12a & b).

46

Middle transverse diameter: distance across mid-body in the frontal plane (H, Figure 12b).

Inferior transverse diameter: distance across the lateral margin of the inferior endplate in the frontal plane (I, Figure 12b).

Sagittal diameter of vertebral foramen: distance between the postero-superior margin of the body and the midpoint on the superior margin of the vertebral arch (J, Figure 12a).

Transverse diameter of vertebral foramen: distance between the most medial surfaces of the pedicles (K, Figure 12a).

Angle of superior facets: included angle between the posterior margin of the centrum and the superior facet. The centrum axis was tangent to the right and left pedicle-centrum margins. The facet axis was tangent to the most medial and lateral margins of the superior facets (L, Figure 12a).

Angle of spinous process: included angle between the spinous process and vertebral body in the sagittal plane. The spinous process axis bisected the superior and inferior surfaces. The vertebral body axis bisected the superior and inferior endplates (M, Figure 12c,).

Spinous process length: distance between the apex of the superior margin of vertebral canal and the most dorsal extent of the spinous process (N, Figure 12c).
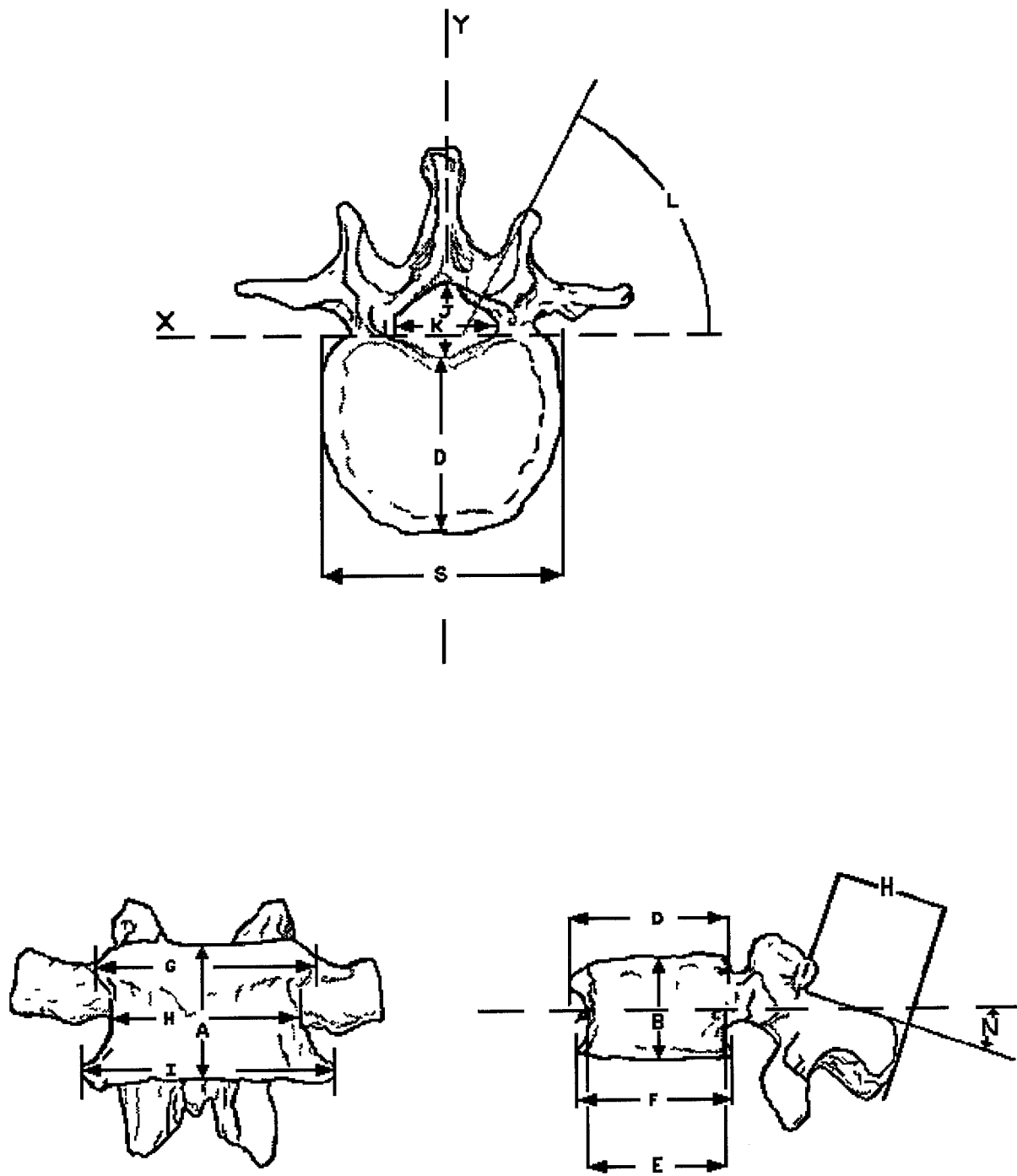
Figure 12. Osteometric dimensions in the vertebrae.

Table 9. Osteometric description of selected vertebrae.

	C7	T1	T4	T8	T12	L1	L2	L3	L4	L5	S1
Anterior Height of Vertebral Body (mm)											
Ave.	15.4	17.4	19.3	20.0	25.9	27.4	28.3	29.3	30.0	29.5	35.0
S.D.	1.3	1.3	1.2	1.9	2.1	1.7	1.8	1.5	0.9	1.6	3.3
N	8	8	8	8	8	8	8	8	8	8	8
Middle Height of Vertebral Body (mm)											
Ave.	12.4	15.0	16.7	19.0	23.4	24.1	24.4	24.0	23.5	21.4	
S.D.	1.3	1.1	1.3	1.3	2.3	1.4	1.6	1.4	2.2	2.4	
N	7	8	8	8	8	8	8	8	8	8	
Posterior Height of Vertebral Body (mm)											
Ave.	16.1	18.7	20.4	21.5	28.3	29.0	24.5	24.6	28.4	24.4	28.9
S.D.	1.1	1.7	1.3	1.6	2.1	2.2	2.0	3.1	2.6	2.3	3.4
N	8	8	8	8	8	8	8	8	8	8	8
Superior Sagittal Diameter of Vertebral Body (mm)											
Ave.	17.7	17.7	23.0	29.7	33.1	33.6	34.4	36.3	36.5	36.3	24.0
S.D.	1.7	1.3	1.9	1.5	2.0	2.8	2.4	2.8	3.3	2.8	2.6
N	7	8	8	8	8	8	8	8	8	8	8
Middle Sagittal Diameter of Vertebral Body (mm)											
Ave.	16.4	16.6	22.4	28.7	28.7	29.7	30.7	32.5	33.0	32.9	25.3
S.D.	1.3	1.3	2.0	1.8	2.1	2.2	2.1	2.8	3.1	3.0	2.3
N	8	8	8	8	8	8	8	8	8	8	8
Inferior Sagittal Diameter of Vertebral Body (mm)											
Ave.	17.4	18.6	24.9	31.4	33.0	34.0	35.4	36.4	36.9	35.4	22.5
S.D.	1.4	1.8	1.0	1.8	2.7	2.5	2.6	3.0	2.9	3.2	2.9
N	8	8	8	8	8	8	8	8	8	8	8
Superior Transverse Diameter of Vertebral Body (mm)											
Ave.	30.7	29.9	28.7	34.0	44.9	48.1	49.7	52.3	54.0	55.7	54.1
S.D.	2.3	2.5	2.1	1.9	2.1	3.3	3.7	4.6	4.8	4.3	3.1
N	8	8	8	8	8	8	8	8	8	8	8

49

Table 9. (cont.)

	C_7	T_1	T_4	T_8	T_{12}	L_1	L_2	L_3	L_4	L_5	S_1
Middle Transverse Diameter of Vertebral Body (mm)											
Ave.	25.9	27.9	25.7	31.0	38.3	40.4	41.7	43.3	44.1	45.9	25.9
S.D.	3.0	4.6	2.5	1.3	2.4	3.3	4.3	4.5	4.5	6.1	3.2
N	8	8	8	8	8	8	8	8	8	8	8
Inferior Transverse Diameter of Vertebral Body (mm)											
Ave.	29.7	31.7	30.3	36.1	48.6	49.9	52.7	54.7	55.7	54.5	33.0
S.D.	2.1	2.1	1.5	1.8	3.1	3.8	4.5	4.2	4.1	2.7	3.1
N	8	8	8	8	8	8	8	8	8	8	8
Sagittal Diameter of Spinal Canal (mm)											
Ave.	15.7	16.6	18.3	18.3	19.1	18.3	18.4	18.4	19.3	18.9	
S.D.	1.3	1.2	1.3	1.2	1.6	1.5	2.3	3.0	2.9	4.0	
N	8	8	8	8	8	8	8	8	8	7	
Transverse Diameter of Spinal Canal (mm)											
Ave.	25.4	22.3	17.5	17.4	22.5	23.1	23.6	23.6	23.9	27.4	33.0
S.D.	1.2	1.3	1.2	1.3	1.8	1.0	1.4	1.6	1.6	2.5	3.9
N	8	8	8	8	8	8	8	8	8	8	8
Angle of Spinous Process (degrees)											
Ave.	32.6°	35.9°	48.7°	55.5°	9.6°	13.3°	10.6°	15.0°	18.4°	29.1°	
S.D.	8.6	8.8	9.3	3.7	6.2	7.6	7.9	9.0	10.6	15.0	
N	8	8	8	8	8	8	8	8	8	8	
Spinous Process Length (mm)											
Ave.	34.9	37.5	41.0	43.9	29.3	34.7	37.4	38.3	36.4	30.9	
S.D.	3.8	3.3	3.3	3.3	1.9	3.0	3.2	2.4	3.6	2.5	
N	7	8	8	8	8	8	8	8	8	7	
Angle of Superior Facets: Left (degrees)											
Ave.	-9.1°	-19.7°	-19.3°	-21.0°	23.9°	66.7°	65.6°	58.1°	45.7°	42.7°	
S.D.	15.1	18.3	4.0	3.9	30.2	4.1	5.1	6.4	9.4	11.6	
N	7	8	8	8	8	8	8	8	8	8	
Angle of Superior Facets: Right (degrees)											
Ave.	-10.3°	-12.6°	-21.0°	-21.5°	9.4°	63.6°	61.6°	57.7°	47.6°	40.5°	
S.D.	12.4	12.0	5.9	2.8	21.5	6.7	5.0	4.7	8.7	12.2	
N	7	8	8	8	8	8	8	8	8	8	

Osteological observations.

The development of osteophytes was measured on the vertebral body, facets, arch and dorsal spinous process of the thoracic and lumbar vertebrae. Measurements were made from the vertebral margin to the end of osteophyte development. Osteophytes were measured with sliding calipers.

Osteophytic lipping of vertebral body margins was described for the inferior and superior surfaces that we divided into eight equal sections (I-VIII). Section I began at the left posterior margin (Figure 13). We correlated superior and inferior descriptions as shown in the following figure. Each superior surface section was directly above a corresponding inferior surface section.
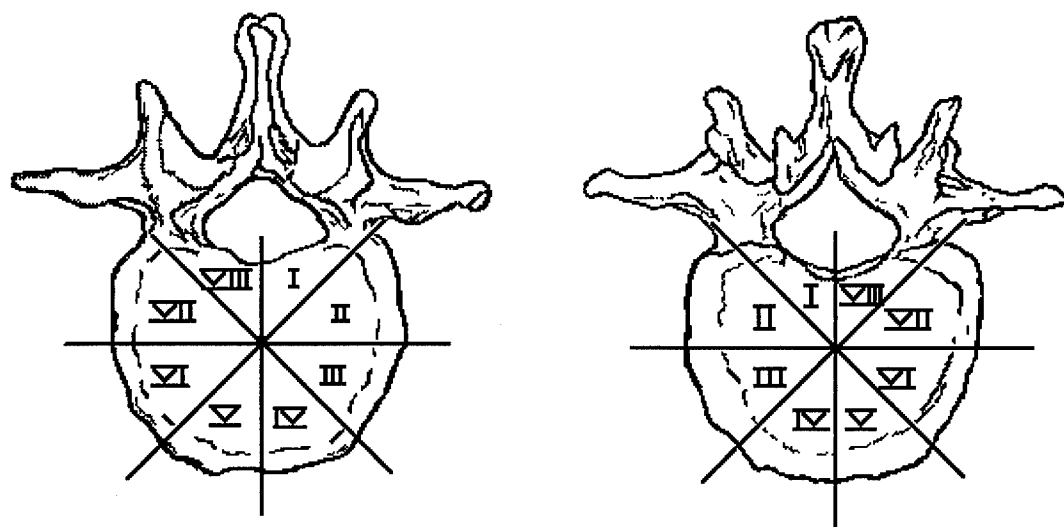
Figure 13. Division of vertebral body into 8 sections for assessment of osteophyte development.

In the thoracic region, subjects #2, 3, 6 and 8 had their most severe development of osteophytes on T8, T9 and T10. T9/T10

51

in subject #6 were ankylosed. In the lumbar region, subjects #3, 4 and 5 had their most severe development on L3, L4 and L5.

The largest growth from the vertebral arch measured extraosseous developments in the region of the ligamentum flavum. Subjects #5 and 8 had the most severe extraosseous growths in the lower thorax from T8 to T11.

The growth of osteophytes around the facets were most frequently found on the medial side of the superior facets and the pedicle-lamina border. Subjects #3, 5 and 8 had numerous osteophytes around the facets of the lower thorax. Subjects #5 and #8 also had severe osteophyte growth in the lower lumbar around the facets of L4, L5, and S1.

Similar to the assessment of extraosseous growth in the arch, the largest ossification of the supraspinous ligament was measured. In subjects #2, 5, 6 and 8, the ossification had developed inferiorly in the middle of the thorax, typically from T3 to T8. Subject #2 also had some mild ossification of the supraspinous ligament on L4 and L5.

The average lengths of osteophytes (Table 10) included all subjects who had an osteophyte. Thus, if the subject had no osteophytes, he was not used in the computation. For the vertebral body lengths, the average represented the combination of all eight regions. The posterior element length combined all seven boney regions. We treated the absence of an osteophyte in the same manner as in the vertebral body calculations. The posterior elements described the spinous process, right and left superior surfaces of the vertebral arch, the right and left superior facets, and the right and left inferior facets. Sliding calipers were used for these measurements.

Frequency of development (Table 10) was the percentage of total observations. There were 8 subjects and 8 regions of possible osteophyte growth for a total of 64 identifiable regions on the vertebral bodies. The frequency in the posterior elements was computed for 8 subjects and 7 boney regions of possible osteophyte development for 56 identifiable regions.

Table 10. Length (mm) and frequency (%) of osteophytes on the vertebrae.

	C_7	T_1	T_4	T_8	T_{12}	L_1	L_2	L_3	L_4	L_5	S_1
Superior Endplate											
Length (mm)	2.8	1.9	1.6	2.4	2.6	3.0	2.3	3.0	3.0	2.7	2.1
Freq. (%)	37.5	25.0	26.6	40.6	37.5	40.6	43.8	62.5	65.6	56.3	53.1
Inferior Endplate											
Length (mm)	1.4	1.7	1.6	3.0	2.2	1.6	2.1	2.5	2.3	2.0	
Freq. (%)	17.2	10.9	28.1	37.5	34.4	45.3	53.1	57.8	53.1	50.0	
Posterior Elements											
Length (mm)	3.7	3.2	5.8	6.7	5.8	4.4	3.0	2.8	3.6	3.7	3.9
Freq. (%)	25.0	32.0	53.6	50.0	53.6	58.9	69.6	51.8	57.1	50.0	30.3

The freqrency of osteophytes in the lumbar was greater than in the thorax (Table 10). The superior endplates in the lumbar region had longer and more osteophytes than the inferior endplates. Most osteophytes were in the middle to lower thorax from T4 to T12, but the longest was in the lumbar region.

Disc morphology

The degeneration of the disk at the time of excision had been evaluated according to a methodology developed by Nachemson (Ref 48). To illustrate groups in this sample, photographs were made of four vertebral specimens. In Group 1 (Figure 14), the margins between the gelatinous nucleus pulposus and layers of the annulus fibrosis were well defined. There were no observable ruptures or lesions present in the disc. In Group 2 (Figure 15), the margins between the nucleus pulposus and annulus fibrosis were not as well defined as in Group 1. As in Group 1, there were no apparent lesions. In Group 3 (Figure 16), the nucleus pulposus was very fibrotic and had lost its gelatinous nature.

Due to the degeneration in the disc, there were no clear margins existing between the annulus and the pulposus. There were no lesions in this specimen. The example of Group 4 (Figure 17) had large fissures that nearly obliterated the entire disc. Based on these criteria, all discs were graded (Table 11).

Table 11. Disk degeneration for all subjects.

Disc	\#1	\#2	\#3	\#4	\#5	\#6	\#7*	\#8	\#9
C6/7	2	2	1	3	3	2			1
C7/T	1	2	2	1	3	3	1	2	1
T1/2	1	2	1	1	3	3	1	2	1
T2/3	1	2	1	3	3	1	2		1
T3/4	1	2	1	1	3	3	1	2	1
T4/5	1	2	1	3	3	2	2		1
T5/6	1	2	1	3	3	2	2		1
T6/7	1	2	1	3	3	1	2		1
T7/8	1	2	2	1	3	3	3	2	1
T8/9	1	2	1	3	3	2	2		1
T9/10	2	1	3	3	3	2		1	
T10/11	2	1	3	3	3	2		1	
T11/12	2	1	1	3	3	3	2	1	
T12/L1	2	3	1	3	3	3	2	1	
L1/2	1	2	3	1	3	3	3	2	1
L2/3	1	2	3	1	3	3	2	2	1
L3/4	1	2	3	1	3	3	3	2	1
L4/5	1	2	3	1	3	3	3	2	1
L5/S1	2	3	1	3	3	3	2	1	

Degree of Degeneration by subject

* Videotape was used for the photographic record.
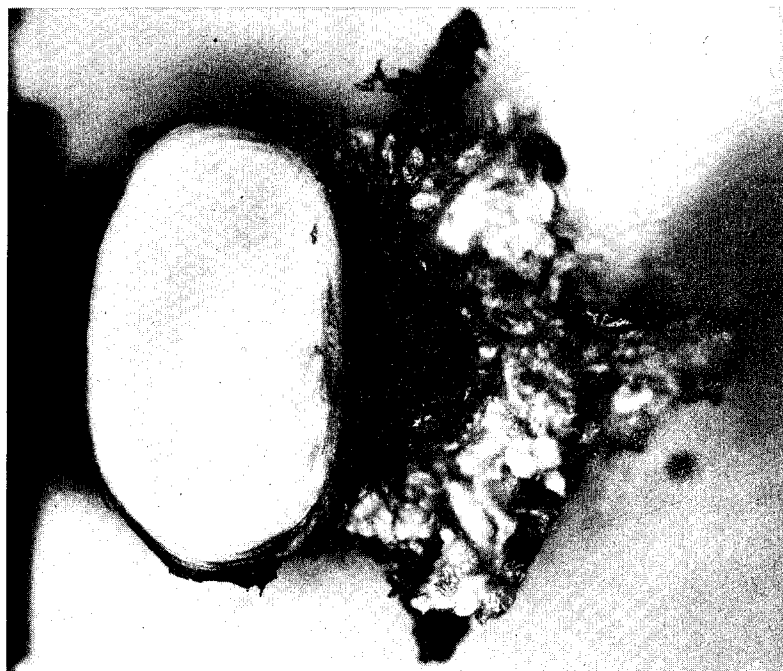
Figure 14. Group 1: subject #1, inferior surface of L4.

Figure 15. Group 2: subject #1, inferior surface of T12.
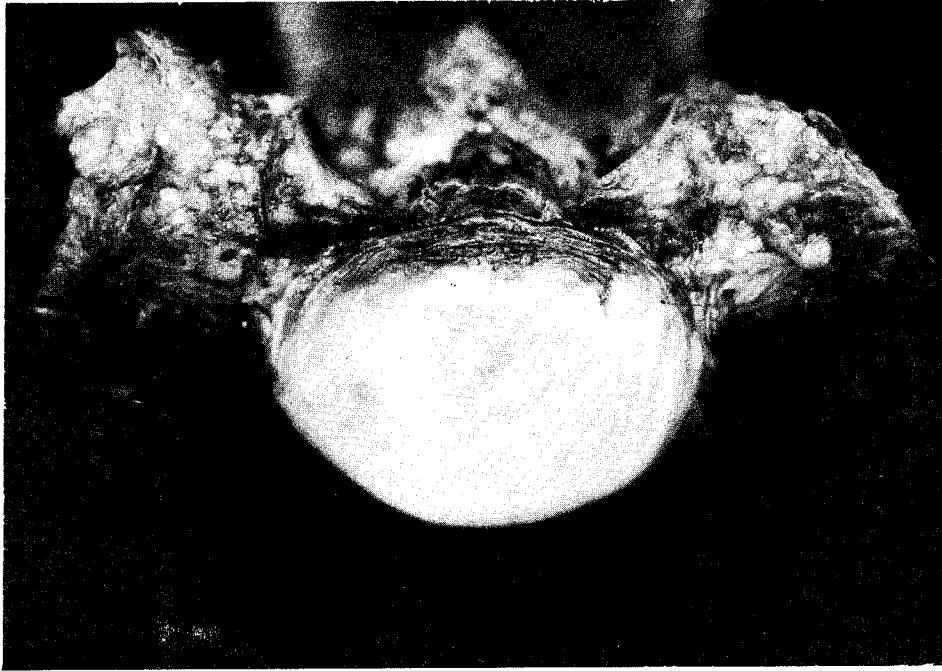
Figure 16. Group 3: subject #3, superior surface of S1.
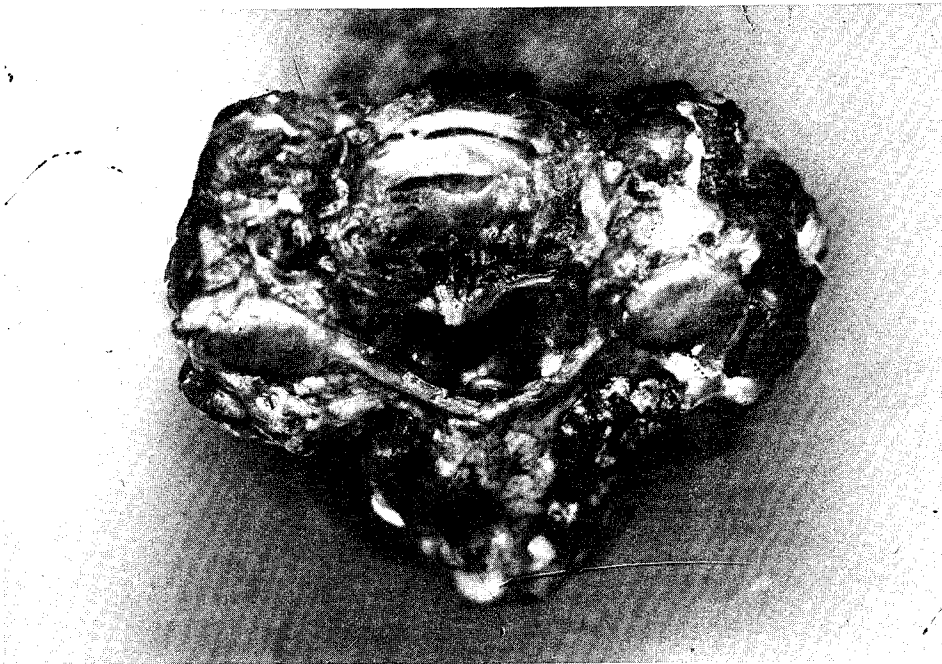
Figure 17. Group 4: subject #1, superior surface of C5.

RESULTS

Description of skeletal components

The skeletal pointmarks in Figures 18 and 19 were targeted and initially measured in the cadaver in the laboratory axis system. The data were then transformed into seat and local anatomical axes system. The three-dimensional coordinates that located the pointmarks shown in Figures 18 and 19 were in the seat axis system.

In Figure 18 the wireframe images depicted the anatomical pointmark of subject #4 in the sagittal plane. Each skeletal structure was defined by a geometrical shape. The sternum was depicted as a straight line from Suprasternale to the base of the sternal body in the mid-sagittal plane. A straight line from the sterno-clavicular to acromio-clavicular joints represented the clavicle. A triangle formed by the acromion process, inferior and superior angles of the scapula represented the scapula.

Each vertebrae was divided into two polygons: 1) anatomical pointmarks on the vertebral body and 2) anatomical pointmarks on the posterior elements of the vertebra. The vertebral body was defined by the most anterior and posterior pointmarks on the superior and inferior endplates. The pentahedron for the posterior elements was drawn through four pointmarks at the center of the facets and the most posterior point on the dorsal spinous process.

The bones of the pelvis were shown separately. The sacrum was represented by a line joining the most anterior (Promontorion) and posterior pointmarks on the sacral base. The right and left innominate bones were represented by pointmarks on the anterior superior iliac spine (ASIS), posterior superior iliac spine (PSIS), ischial tuberosity (ISCH), and pubic symphysis (PS) at symphysion. The hip joints (HP) were indicated by a cross (right) and circle (left).

57
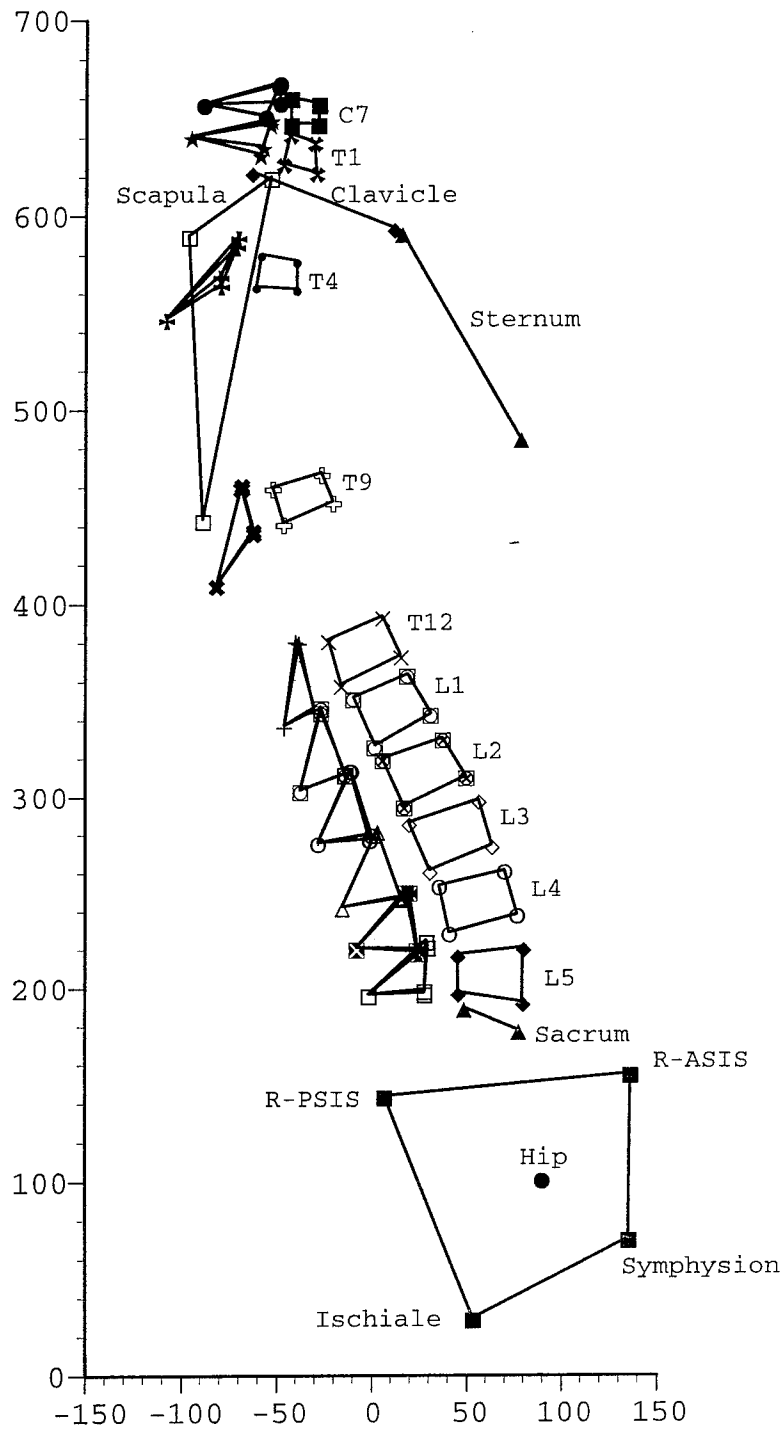
Figure 18. Wire frame image of the torso skeleton in the seat axis system projected into the sagittal plane.
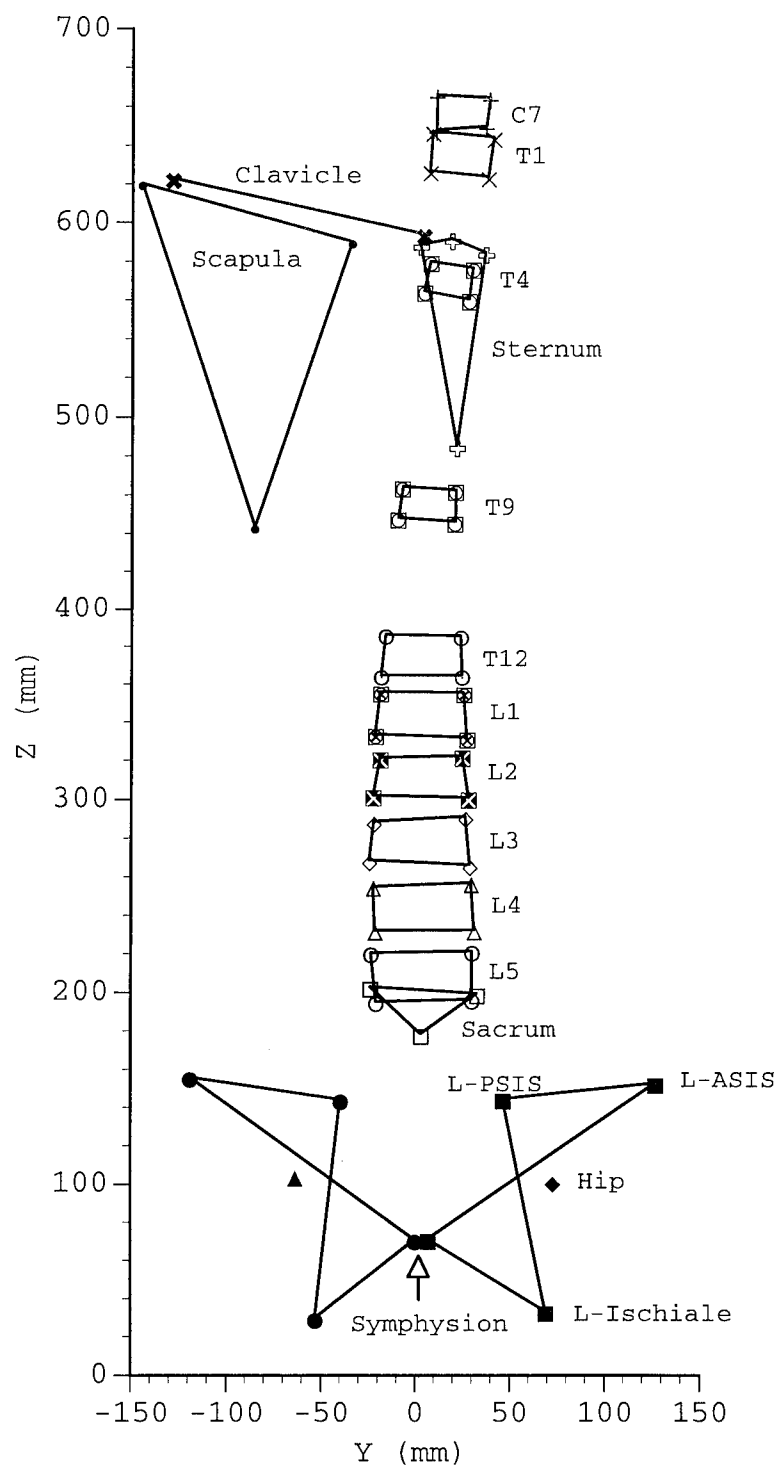
Figure 19. Wire frame image of the torso skeleton in the seat axis system projected into the frontal plane.

The same position of subject #4 in the frontal plane (Figure 19) showed the sternum, clavicle, scapula, and innominate bones with the same pointmarks used in Figure 18. In the vertebrae, the posterior elements were omitted. Four anatomical pointmarks on the lateral superior and inferior endplates represented the vertebral body. A triangle formed by Promontorion and two pointmarks at the center of the S1 facets represented the sacrum.

ERECT, NEUTRAL and SLUMP sitting positions.

Each subject was measured in postures representing ERECT, NEUTRAL and SLUMP sitting positions. The seated environment and experimental protocol were described in Section 2.0. Due to the difficulty of measuring the whole body in different seated position, small experimental variations were present in each subject's data.

In the ERECT positions, the primary difference between postures lay in the relative amount of lordotic curve in the lumbar region. A Plexiglas bar moved the lumbar vertebrae into a lordotic curve. The first measurement of this position began with the bar at a maximum position. The lumbar vertebra closest to the bar was identified by the two-dimensional locations of the bar and dorsal spine target on the vertebra (e.g. L03SPPCPMC). The x and z coordinates of the Bar in the seat axis system (Table 12) were calculated as a point midway between the most anterior, right and left lateral targets on the bar in seat position ERECT01. The closest vertebra to the bar mid-point in ERECT01 was typically L03, identified by subject number in Table 12. Subject #3 had L02 and subjects #6 and #7 had L04 closest to the bar.

ΔX and ΔZ of the Spine in Table 12 described the difference in coordinate location of the dorsal spine (Spine) and Bar mid-point in ERECT01. The displacement of BAR in Table 12 was

60

described by the magnitude of the vector from ERECT07 to ERECT01 positions.

Table 12. Locations and displacements (mm) of the bar and dorsal spine in the seat axis system for ERECT positions.

Subject-Bone	Bar		Spine		Displacement	
	X	Z	ΔX	ΔZ	BAR	Spine (%)
#1-L3	-66.6	257.2	36.6	-3.5	47.6	95.2
#2-L3	-66.6	257.2	38.3	-7.0	63.0	43.8
#3-L2	-66.6	257.2	39.9	-21.5	60.5	46.4
#4-L3	-48.7	236.7	6.2	-1.7	50.3	89.5
#5-L3	-47.3	236.2	31.4	-3.7	49.9	28.3
#6-L4	-48.0	236.5	56.2	-6.5	50.7	10.5
#7-L4	-47.9	236.6	49.1	4.4	48.6	33.7
#8-L3	-48.2	236.3	30.1	-4.0	49.9	43.2
#9-L3	-48.4	236.5	26.9	8.1	49.3	53.7
Average	-54.3	243.4	35.0	-3.9	52.2	49.4
St Dev	±9.3	±10.4	±14.2	±8.2	±5.5	±27.4

Since the bar was pushing the lumbar spine into a lordotic posture, it was expected that the distance between the bar and the dorsal spine remained constant. This distance between Bar and Spine described contact between the spinal column and bar. The average of Spine Δx in ERECT 01 was 35.0 mm. The average displacement of the bar (Table 12) perpendicular to the seat back was 52.2 mm. The movement of the vertebrae closest to the bar, however, was highly variable between subjects Yet the average displacement of the spine was 49.4% of the bar displacement.

Figure 20 showed the relationship between the spine identified in Table 12 and the Bar in all Erect positions. The displacements were calculated as the two-dimensional distances between measured positions. Each symbol on a subject's displacement in the figure represented a measurement position

from ERECT07, the initial position, to ERECT00, the final position.
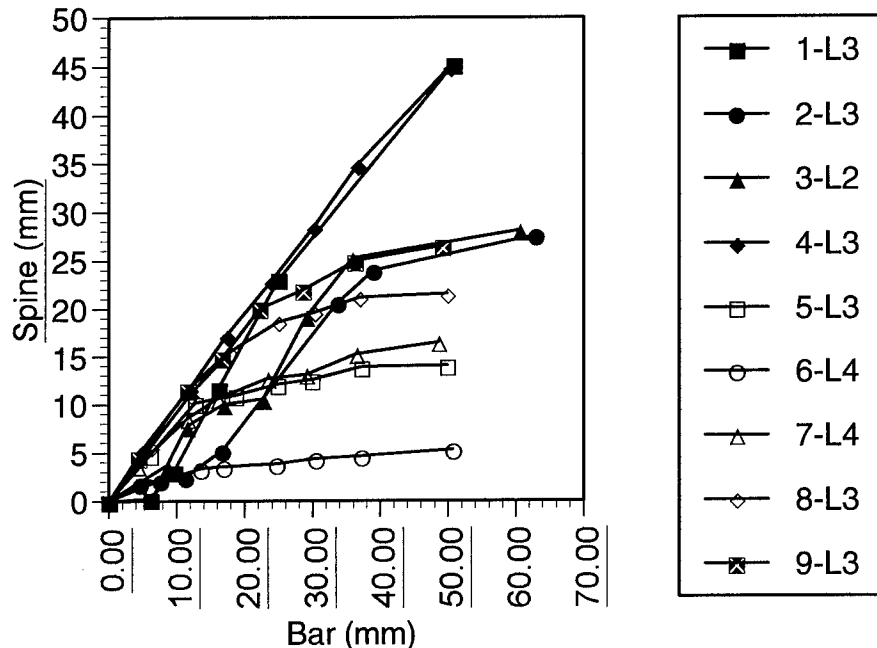
Figure 20. Translation (mm) of spine closest to bar as function of Bar translation.

In contrast to the procedure used in the ERECT positions, we used the position of the pelvis to identify comparable body positions in the SLUMP positions. The displacement of Ischiale, an anatomical landmark on the ischium, represented pelvic displacement. We selected this pointmark because the pelvic ischium contacted the seat. The x,z coordinates of ISCHIALE in the maximum ERECT position were calculated in the seat axis system (Table 13). The displacements (D) in the ERECT and SLUMP series were the magnitudes of the displacement vectors. In the ERECT series, the displacement was from ERECT07 to ERECT01. In the SLUMP series, the displacement was from SLUMP10 to maximum SLUMP. The location of Ischiale (Table 13), was slightly affected by the change of bar position.

Since the pelvis was held by a strap during the ERECT measurements, the displacement of Ischiale was primarily rotation. The initial angle of the pelvis was the angle between the horizontal x-axis and a line passing through the left anterior superior iliac spine and the pubic tubercle. The average pelvic angle at maximum ERECT was 102.1° (Table 13). The rotation of the pelvis in the ERECT and SLUMP positions was calculated by the dot product between the initial and final position vectors. These position vectors were defined by the relative locations of the left anterior superior iliac spine (HIPILILASM, 0910) and pubic tubercle (HIPPUBLAMC, 0950) pointmarks.

The pelvis was rotated rearward (i.e. a negative sign) from vertical an average of -6.4° in the ERECT series. The anterior superior iliac spines were not measured in subject #1. Thus, the motion of the pelvis in subject #1 used the right and left posterior superior iliac spines and right and left pubic tubercles.

Table 13. The initial locations (mm) and displacements of left Ischiale and the pelvis in the seat axis system for ERECT and SLUMP.

Subj. ID	ERECT X	ERECT Z	ISCHIALE ERECT D	SLUMP D	Initial Angle	PELVIS Rotations ERECT	SLUMP
#1	33.3	38.7	8.5	120.1	*	-7.0°	-37.7°
#2	45.6	22.8	13.5	159.1	102.1°	-8.5°	-47.0°
#3	28.0	29.9	11.8	114.6	103.9°	-5.9°	-34.7°
#4	56.9	35.0	3.4	102.2	108.0°	-8.3°	-43.6°
#5	32.6	38.9	3.2	117.4	94.9°	-5.0°	-33.3°
#6	21.1	37.1	1.9	66.8	90.5°	-1.5°	-12.8°
#7	37.1	43.1	5.2	142.0	100.0°	-5.1°	-41.4°
#8	52.9	29.8	2.5	127.3	103.0°	-5.9°	-32.5°
#9	42.1	34.3	11.5	152.9	114.5°	-10.0°	-37.0°
AVE	38.8	34.4	6.8	122.5	102.1°	-6.4°	-35.6°
SD	±11.6	±6.1	±4.5	±28.0	±7.4	±2.5	±9.8

63

The data in Table 14 for the average and standard deviation of three-dimensional coordinates for origins of the anatomical axes systems in the maximum ERECT and SLUMP positions were plotted (Figure 21). The most extreme positions for each subject were included in the averages for maximum ERECT and maximum SLUMP. The sample size varied between the pointmarks. There were six subjects for T08, eight for C07, T01, T04, T12 and L05, and nine for the remainder (See Appendix B).

Thus, comparable positions were identified following the data collection. Unique criteria to identify comparable postures in the ERECT and SLUMP positions were developed. Comparable positions were selected for further analysis. Thus, the parameters of torso geometry that described the torso linkage system from shoulder to hip were based on the analysis of comparable postures. For example, the locations of the shoulder and hip joints were calculated for comparable positions rather than for each measured position. Since different geometric parameters were used to select comparable ERECT and SLUMP positions, the description of comparable positions was separated into different subsections.
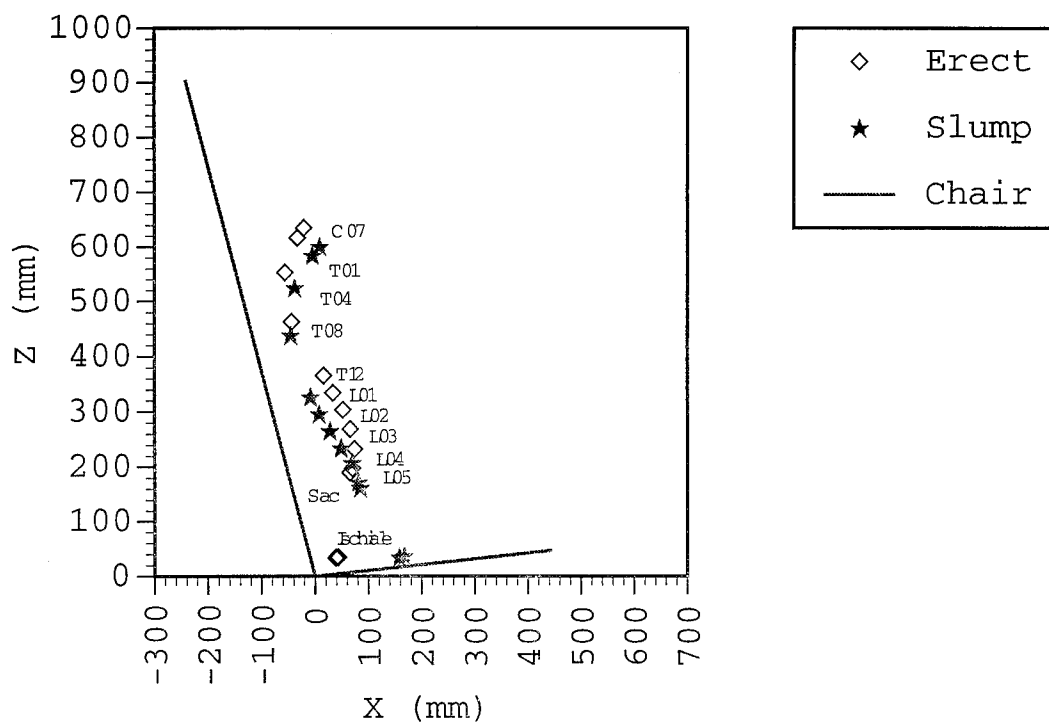
Figure 21. Two positions of the spinal column describing maximum ERECT and SLUMP positions.

Table 14. X, Y, Z coordinates (mm) in seat axis system for anatomical axis system origins and Ischiale pointmarks in maximum ERECT and SLUMP positions.

BONE	ERECT			SLUMP		
	X	Y	Z	X	Y	Z
C07	−20.8	18.9	635.9	9.2	13.8	600.7
	±30.3	±10.3	±25.9	±23.1	±9.0	±28.9
T01	−32.5	17.5	617.3	−4.6	12.9	584.6
	±26.0	±11.1	±24.2	±20.7	±8.3	±27.6
T04	−56.6	12.8	553.3	−38.2	5.5	525.5
	±18.9	±10.0	±18.0	±18.1	±10.6	±21.6
T08	−43.6	0.5	463.7	−45.0	−7.0	438.7
	±8.3	±7.2	±18.5	±15.6	±11.1	±21.7
T12	15.9	−2.3	366.7	−8.0	−15.5	326.9
	±7.9	±6.4	±9.8	±10.5	±8.5	±17.5
L01	33.5	−1.9	335.4	8.0	−12.8	296.1
	±6.6	±5.7	±10.7	±13.4	±12.9	±22.1
L02	52.1	−1.0	304.7	28.1	−12.0	266.4
	±4.7	±6.6	±11.1	±16.8	±11.6	±23.3
L03	65.8	−0.4	269.6	48.7	−11.1	234.7
	±4.9	±5.8	±11.2	±18.2	±13.4	±24.5
L04	73.8	0	233.3	69.4	−9.7	208.0
	±7.2	±5.2	±10.5	±18.4	±11.7	±22.3
L05	70.4	−2.9	198.5	81.6	−12.0	172.9
	±11.4	±4.6	±9.9	±17.1	±9.4	±23.6
SAC	65.2	−0.9	190.7	85.0	−10.4	162.4
	±12.8	±5.6	±7.8	±15.8	±9.3	±21.4
RISCH	43.2	−60.5	35.0	158.0	−66.4	35.1
	±12.7	±5.1	±5.0	±37.9	±9.7	±3.7
LISCH	38.8	63.3	34.3	167.7	57.7	37.4
	±11.6	±7.7	±6.1	±39.8	±11.2	±5.6

Selection of comparable ERECT positions.

Each subject was measured in 5-7 ERECT positions (Ref 51). ERECT07 began the ERECT series with the lumbar vertebrae in a maximum lordotic position.

The location of the bar controlled body position. Therefore, comparable positions were selected on the basis of equivalent bar locations. Since the seat back tilted rearward 15°, a 15° rotation of the x-coordinate in the XZ plane defined the perpendicular distance of the bar from the seat back. Thus,

$$x' = x \cos(\Theta) - z \sin(\Theta) \tag{47}$$

where x' was the perpendicular distance of the centroid to the seat back. x and z were the coordinates in the seat axis system. Θ was the 15° seat back rotation.

Equivalent perpendicular distances of the lumbar support from the seat back for each new posture were identified in Table 15. The alpha-numeric posture names in parentheses were abbreviations of the experimentally measured positions. For example, (E04) represented ERECT04 in position A. Differences in sample size for each new position resulted from this procedure.

Since the original laboratory names of measured positions in the ERECT series did not describe equivalent positions between subjects, the four comparable positions within the ERECT series were labeled A, B, C, and D. The average perpendicular distances, x', from the seat back for postures A, B, C and D were 47.0 ±0.9, 52.3 ±0.4, 59.1 ±1.0 and 64.5 ±0.8 mm respectively. These distances for the A, B, C and D postures were statistically different at the 0.001 level of significance as tested with a univariate repeated measures F-test (F = 3532.25). The results of this test were based on complete cases only, that is, subjects #4-#9. These subjects represented the total sample since differences in means between the A, B, C, and D samples in the F

67

test results in Table 14 and the samples with all subjects were 0.2, 0.1, 0.0 and 0.0 mm respectively.

Table 15. Distances (mm) of lumbar support centroid from seat back in comparable ERECT positions.

ID	A Position	x'	B Position	x'	C Position	x'	D Position	x'
#1	(E04)	46.7	(E05)	53.1				
#2	(E03)	48.0	(E04)	52.2	(E06)	57.3		
#3	(E04)	45.3	(E06)	52.6	(E07)	60.8		
#4	(E04)	47.1	(E05)	52.5	(E06)	59.5	(E07)	64.5
#5	(E04)	46.6	(E05)	52.6	(E06)	59.1	(E07)	65.3
#6	(E04)	48.6	(E05)	51.9	(E06)	59.6	(E07)	65.5
#7	(E04)	47.5	(E05)	51.9	(E06)	59.2	(E07)	63.5
#8	(E04)	46.6	(E05)	52.4	(E06)	58.1	(E07)	64.4
#9	(E04)	47.0	(E05)	52.0	(E06)	59.2	(E07)	63.7
Ave		47.0		52.3		59.1		64.5
SD		± 0.9		± 0.4		± 1.0		± 0.9

*Subject #5, (E04) coordinates of Plexiglas centroid estimated from interpolation of (E05) and (E03) locations.

The three-dimensional coordinates in the seat axis system for the origins of the anatomical axes systems and Ischiale pointmarks in four comparable ERECT positions were averaged (Table 16). The anatomical origins used the algorithm for the +y, -y, and +x pointmark locations (Section 3.3).

The ERECT-A, -B, -C, and -D positions in Table 15 had sample sizes of 9, 9, 8 and 6, respectively. Two (A & D) of the four positions were depicted in Figure 22.

68

Table 16. X, Y, Z coordinates (mm) in seat axis system for anatomical axis system origins and Ischiale pointmarks in four comparable ERECT positions.

Bone		ERECT-A			ERECT-B			ERECT-C			ERECT-D	
	X	Y	Z	X	Y	Z	X	Y	Z	X	Y	Z
C07	-16.0	18.7	636.2	-18.0	17.4	635.8	-18.8	16.5	635.6	-10.8	18.5	634.3
	±30.8	±10.1	±27.4	±30.1	± 9.0	±27.2	±31.0	± 8.7	±26.9	±28.2	±12.1	±28.4
T01	-28.1	17.5	617.8	-30.0	15.9	617.2	-30.8	15.3	617.0	-22.6	16.6	615.6
	±27.9	±10.6	±25.5	±27.1	± 9.7	±25.3	±27.7	± 9.4	±25.1	±23.4	±12.8	±26.2
T04	-56.5	12.8	555.1	-56.7	11.9	554.4	-52.9	10.6	551.7	-46.4	11.0	550.2
	±19.6	±10.9	±18.8	±18.6	±10.1	±18.8	±17.9	±10.3	±19.4	±16.0	±12.4	±20.9
T08	-47.4	0.9	464.4	-46.1	0.0	464.3	-42.6	2.0	462.2	-44.7	0.7	462.0
	± 5.8	± 8.8	±18.3	± 7.3	± 7.6	±18.4	± 6.4	± 6.9	±20.4	± 6.1	± 7.8	±25.5
T12	5.8	-2.7	364.9	9.1	-2.9	365.8	13.5	-0.8	363.4	12.4	-0.1	367.5
	± 9.1	± 6.2	± 9.8	±10.1	± 6.2	±10.1	± 9.1	± 4.3	±10.0	± 3.4	± 4.9	± 9.9
L01	22.9	-02.4	333.1	25.8	-02.7	333.9	31.1	-00.6	333.1	32.1	0.1	335.6
	± 8.4	± 5.5	±11.4	± 8.3	± 5.9	±11.1	± 6.9	± 3.9	±11.2	± 2.3	± 4.3	±12.3
L02	41.4	- 1.6	302.9	44.6	- 1.6	303.4	49.0	0.7	299.5	51.7	0.7	305.4
	± 8.2	± 6.6	±10.9	± 7.2	± 6.5	±11.1	± 5.9	± 3.8	± 6.8	± 3.9	± 3.6	±12.6
L03	55.9	- 1.3	268.3	58.9	- 0.8	268.6	62.7	0.6	267.3	67.2	1.5	270.8
	± 7.8	± 6.2	±11.1	± 6.3	± 5.9	±11.0	± 5.4	± 4.6	±10.7	± 5.6	± 5.1	±11.5
L04	65.0	- 0.2	232.5	67.5	0.2	232.7	70.6	1.6	231.3	76.6	2.6	234.3
	± 9.3	± 5.6	±10.2	± 7.6	± 5.5	±10.2	± 7.2	± 3.8	± 9.8	± 6.7	± 3.8	±10.3
L05	63.8	- 3.3	197.8	65.6	- 2.9	198.3	67.7	- 1.2	196.6	77.0	- 1.2	198.5
	10.7	± 4.5	± 9.8	± 9.9	± 4.7	± 9.5	±11.4	± 2.5	± 9.3	± 1.5	± 3.2	±10.9
SAC	57.2	- 1.5	190.2	59.2	- 1.5	190.4	61.6	0.8	189.2	69.7	1.0	190.9
	±13.5	± 5.7	± 7.6	±12.8	± 5.9	± 7.5	±12.6	± 4.1	± 8.4	±10.2	± 4.8	± 8.7
RISCH	44.6	-60.5	33.4	43.9	-60.4	33.8	44.9	-60.7	34.1	44.8	-60.4	36.4
	±12.8	± 5.2	± 4.4	±12.6	± 5.1	± 4.3	±12.6	± 5.5	± 4.7	±15.2	± 6.1	± 5.1
LISCH	40.1	63.4	32.8	39.8	63.4	33.0	40.0	64.7	33.1	40.4	66.8	36.5
	±14.4	± 7.5	± 5.5	±11.5	± 7.8	± 5.7	±12.2	± 7.1	± 6.0	±13.2	± 6.7	± 4.5

Figure 22. Two ERECT positions (A & D) in the seat axis system selected by comparable bar positions.

Selection of a comparable NEUTRAL position.

ERECT00 defined the upright posture of each subject when sitting with no lumbar support. Thus, the coordinates of this position represented NEUTRAL (Table 17).

The positions of the anatomical origins and Ischiale pointmarks were averaged for each axis. The standard deviation was reported in Table 17 immediately below the average. Sample size varied between the pointmarks because of variation in the identification of specific vertebrae previously described. There were six subjects for T08, eight for C07, T01, T04, T12 and L05, and nine for the remainder (See Appendix B).

The anatomical origins for the vertebrae were calculated as described in Section 3.3 using the algorithm for +y, -y, and +x pointmark locations. The anatomical origins and Ischiale pointmark were plotted in the sagittal (XZ) plane (Figure 23).
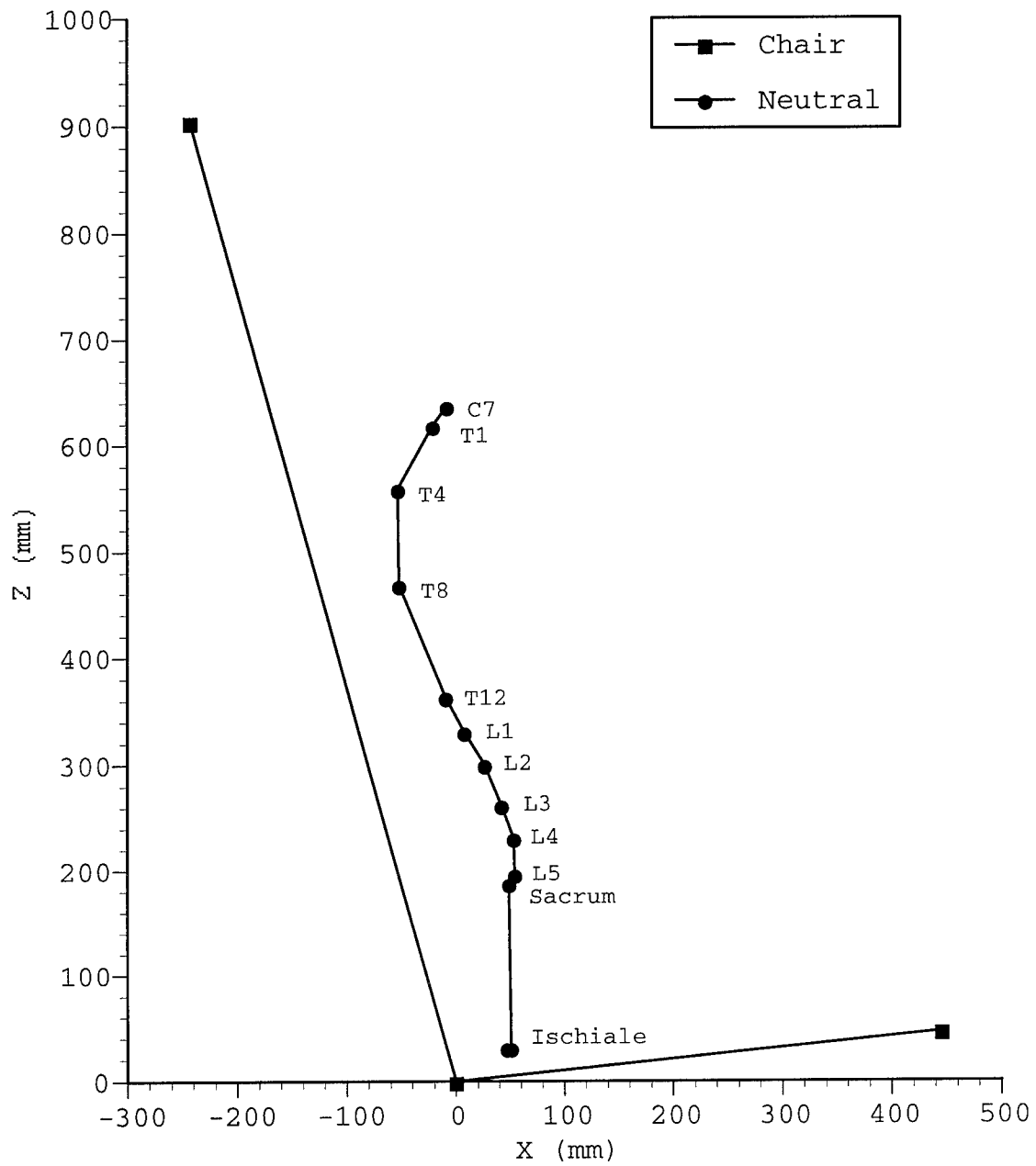
Figure 23. NEUTRAL position of the spinal column in seat axis system.

Table 17. X, Y, Z coordinates (mm) in seat axis system for anatomical axis system origins and Ischiale pointmarks in a comparable NEUTRAL position.

	X	Y	Z
C07	− 8.5 ±26.5	20.5 ±11.4	636.7 ±28.5
T01	−21.4 ±22.8	19.1 ±11.5	618.7 ±26.5
T04	−53.1 ±19.5	14.9 ±16.4	558.9 ±22.3
T08	−52.5 ± 5.1	2.0 ± 8.6	468.4 ±12.3
T12	− 9.7 ±11.2	− 4.4 ± 5.4	363.8 ±11.4
L01	7.3 ±12.7	− 5.0 ± 5.0	331.4 ±12.0
L02	26.3 ±15.3	− 3.9 ± 4.4	300.9 ±11.5
L03	41.7 ±16.1	− 3.1 ± 5.5	266.5 ±10.6
L04	52.7 ±16.2	− 1.6 ± 4.9	231.2 ± 9.5
L05	53.7 ±15.9	− 4.2 ± 3.2	196.7 ± 9.4
SAC	48.8 ±16.9	− 2.5 ± 5.2	187.8 ± 7.9
RISCH	50.8 ±13.3	−61.0 ± 5.4	31.5 ± 4.5
LISCH	46.8 ±12.8	63.0 ± 7.7	31.2 ± 5.4

Selection of comparable SLUMP positions.

Similar to the ERECT positions, the SLUMP series were
analyzed to identify comparable postures. The selection was
based on the position of left Ischiale pointmark in the XZ plane.
Ischiale was at the center of the lower rough surface of the
ischial tuberosity. This pointmark (Ref 53) represented the
pelvic surface that contacted the seat. In the present
investigation, the post-hoc analysis of Ischiale motion described
pelvic displacement.

Three comparable positions were identified on the basis of
the analysis of Ischiale locations in the XZ plane. These
positions maximized sample size and optimized comparable
anatomical geometry. These postures were SLUMP-M, SLUMP-N, and
SLUMP-O to distinguish them among the SLUMP10-17 positions (Table
18).

Table 18. X,Z coordinates (mm) in seat axis system for left Ischiale.

ID	SLUMP-M Position X, Z	SLUMP-N Position X, Z	SLUMP-O Position X, Z
21	(F14) 144.5, 37.6	(F15) 160.7, 38.8	(F16) 175.9, 40.3
22	(F13) 147.1, 32.2	(F14) 163.6, 35.3	(F15) 187.8, 40.1
23	(F14) 137.0, 25.9	(F15) 156.7, 29.5	---
24	(F15) 140.4, 32.5	(F16) 159.7, 33.3	---
25	(F16) 147.3, 34.1	---	---
27	(F15) 145.7, 37.9	---	(F16) 182.1, 43.1
28	(F14) 142.2, 31.3	(F15) 162.5, 31.0	(F16) 180.1, 33.5
29	(F14) 144.5, 31.9	(F15) 161.4, 33.8	(F16) 184.8, 38.2
Ave	143.6, 32.9	160.8, 33.6	182.1, 39.0
SD	± 3.5,± 3.8	± 2.4,± 3.3	± 4.5,± 3.6

The average x and z coordinates in the SRP axis system for
Ischiale in the NEUTRAL position were 46.9 ±12.8 mm and 31.0

±0.52 mm, respectively (Table 18). Ischiale moved an average distance in the XZ plane from first to last position of 122.5 ±28.0 mm (Table 13) in average increments of 19.3 ±0.40 mm. This displacement represented the movement of the pelvis from NEUTRAL to the last position in the SLUMP series. The average displacement for the left Ischiale pointmark x-coordinate from NEUTRAL to SLUMP-M was 96.9 mm. Since Ischiale in subject #6 moved 66.8 mm from SLUMP10 to maximum SLUMP (Table 13), subject #6 was not been included in the comparable SLUMP positions. The sample size varied between the pointmarks because of variation in identifying vertebrae as previously described in Table 2. Thus, there were five subjects for T08, seven for C07, T01, T04, T12 and L05, and eight for the remainder (See Appendix B).

Selecting comparable positions with the location of Ischiale reduced variation in the results. The standard deviation of the x-coordinates of LISCH in the maximum SLUMP position (Table 14) was ±39.8 compared to ±3.5, ±2.4, and ±4.5 for positions M, N, and O respectively (Table 19). Thus, there was a reduction in variation and a significant change in the relative position. The x-coordinates were closer to SRP because the positions were selected for comparable rather than most extreme position. The closest position (M) to SRP was an average of 143.6 (Table 19) and (O) the furthest from SRP, was 182.1 mm. The average displacement from NEUTRAL to SLUMP-M was 96.9 mm.

In addition to reducing the total displacement of the ischium, the use of SLUMP-M changed the location of the lumbar vertebrae. For example, the average of the maximum SLUMP position x-coordinate in Table 12 for L03 was 48.7 mm. When the subjects were grouped according to the location of left Ischiale, the average x-coordinates for L03 were 32.9, 31.2, and 43.5 mm for SLUMP-M,-N, and -O positions respectively (Table 19).

The origins of the anatomical axes systems for SLUMP-M, SLUMP-N, and SLUMP-O were plotted in the XZ plane of the seat axis system (Figure 24). The calculation of the anatomical

Table 19. X, Y, Z coordinates (mm) in seat axis system for the anatomical axis system origins and Ischiale pointmarks in three comparable SLUMP positions.

Bone	SLUMP-M			SLUMP-N			SLUMP-O		
	X	Y	Z	X	Y	Z	X	Y	Z
C07	9.3	18.4	609.3	3.9	8.8	607.7	7.9	6.3	610.0
	±25.1	±16.9	±31.1	±17.6	±11.8	±15.1	±15.8	±11.9	±18.6
T01	− 3.8	16.9	591.7	− 9.4	9.0	592.0	− 6.9	5.9	592.7
	±22.4	±16.0	±28.9	±17.2	±12.6	±15.8	±16.5	±11.1	±17.3
T04	−35.3	9.0	535.3	−40.8	2.5	535.3	−42.6	1.8	532.1
	±17.3	±11.0	±23.7	±13.2	± 6.7	±15.8	±14.7	± 7.7	±16.1
T08	−46.3	− 6.1	446.4	−48.0	−17.0	442.4	−45.7	−12.1	449.0
	± 5.5	±12.0	±23.9	± 6.3	± 4.1	±20.2	± 7.0	±12.0	± 9.8
T12	−16.4	−17.1	337.8	−15.4	−19.1	326.8	−10.3	−16.1	329.1
	± 8.4	± 8.2	±16.2	± 7.0	± 6.6	±13.4	± 9.7	±10.7	±15.7
L01	− 1.9	−11.0	304.1	− 3.2	−18.6	294.9	5.5	−19.5	297.8
	±13.2	±11.6	±15.8	±10.9	± 7.0	±11.8	±13.3	± 8.0	±15.9
L02	15.5	−11.1	273.3	13.2	−16.7	263.3	24.0	−18.9	266.9
	±16.1	±11.2	±16.4	±11.7	± 5.5	±11.7	±15.2	± 4.9	±17.7
L03	32.9	− 9.7	239.7	31.2	−15.4	229.7	43.5	−17.4	233.6
	±18.8	±12.9	±16.7	±13.5	± 4.0	±13.0	±16.8	± 4.6	±19.7
L04	51.1	− 8.4	207.7	51.1	−11.3	209.7	64.3	−15.5	201.1
	±19.5	±10.9	±16.0	±14.2	± 5.0	±14.1	±15.4	± 4.1	±19.3
L05	62.2	−10.7	175.6	63.3	−14.1	165.0	77.3	−17.7	169.4
	±22.0	± 8.4	±16.9	±18.6	± 5.4	±14.8	±19.3	± 3.5	±22.4
SAC	61.6	− 9.8	166.0	66.0	−13.2	157.0	80.4	−16.2	159.1
	±19.6	± 8.4	±15.0	±16.3	± 4.7	±13.4	±15.4	± 4.1	±18.9
RISCH	143.6	−64.2	31.9	167.4	−71.1	34.9	181.8	−72.4	37.5
	± 6.3	± 9.6	± 3.7	±14.7	± 4.0	± 3.7	± 9.1	± 3.0	± 2.8
LISCH	143.6	58.9	32.9	160.8	54.6	33.6	182.1	54.3	39.0
	± 3.5	± 9.3	± 3.8	± 2.4	± 9.6	± 3.3	± 4.5	±11.5	± 3.6

76

The origins of the anatomical axes systems for SLUMP-M,
SLUMP-N, and SLUMP-O were plotted in the XZ plane of the seat
axis system (Figure 24). The calculation of the anatomical
origins (See Section 3.3) used the +y, -y, and +x algorithm.
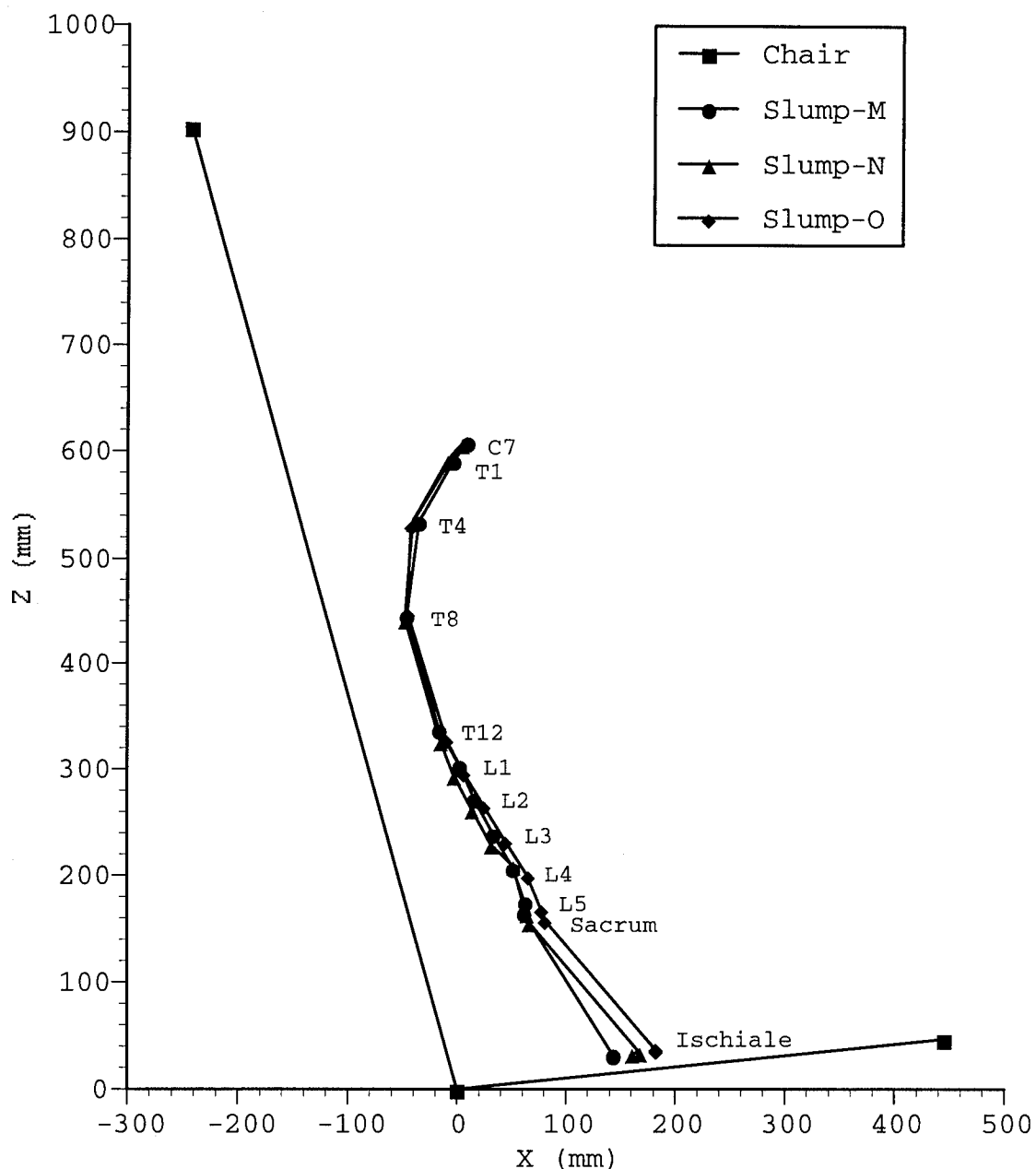
Figure 24. Three SLUMP positions in seat axis system selected by comparable locations of left Ischiale.

77

Anatomical axes' systems for the shoulder, thorax, and pelvis.

Local axes systems for the shoulder, thorax and pelvis were developed for ERECT-A, NEUTRAL, and SLUMP-M positions. The location of pointmarks for the definition of each axis system was based upon the average x, y and z coordinates of each pointmark in the subjects used for the sample. The average of the three pointmarks defined the local axis system for each body segment. Each position was analyzed separately.

Pelvis axis system.

The pelvis axis system was defined by four anatomical pointmarks that lay in the frontal plane. This axis system defined planes that approximated the orientation of the cardinal anatomical planes (Figure 25). The following four pointmarks were used: right anterior superior iliac spine (RASIS, 1010), left anterior superior iliac spine (LASIS, 0910), left pubic tubercle (LPT, 0950) and right pubic tubercle (RPT, 1050). The left and right pubic tubercle pointmarks were averaged to estimate the location of Symphysion. The average and standard deviation of the coordinates for all subjects were calculated in ERECT-A, NEUTRAL, and SLUMP-M (Table 20).

The pointmarks in Table 20 were defined in Reynolds, Leung & Kincaid (Ref 51). The pelvic axis system definition used the algorithm developed for pointmarks that lay in the directions of the +y (LASIS), -y (RASIS) and -z (Symphysion) anatomical axes (See Section 3.3). This pelvic axis system constructed the origin approximately midway on the y-axis that passed through RASIS and LASIS. Positive y was directed towards LASIS (Table 21). The positive z-axis was directed away from the Pubic Symphysis (Figure 24) through the origin. Positive x was normal to the plane formed by the three pointmarks, LASIS, RASIS, and Symphysion. The transformation matrix (TM) in Table 21 combined

78

rotation and translation of the coordinates in homogeneous form as a 4x4 matrix.

Table 20. X, Y, Z coordinates (mm) in seat axis system for anatomical pointmarks to define a pelvic axis system.

Point-mark	ERECT-A X	Y	Z	NEUTRAL X	Y	Z	SLUMP-M X	Y	Z
RASIS	135.4	-110.6	164.2	130.1	-111.5	168.0	142.9	-117.9	187.4
	± 6.0	±9.0	±10.7	± 8.6	± 8.9	±10.3	±19.0	±15.4	± 6.4
LASIS	125.7	121.9	162.8	120.9	121.1	166.8	134.2	112.7	188.7
	±10.5	± 9.9	± 8.6	±10.4	±10.0	± 8.8	±17.9	± 6.4	± 9.2
LPT	138.1	32.3	79.7	139.4	31.5	86.8	193.4	27.7	128.7
	± 9.4	± 7.4	± 9.6	± 7.5	± 7.9	±11.7	±12.1	±10.7	± 7.2
RPT	140.5	-21.9	79.1	141.7	-22.6	86.2	191.9	-27.5	126.1
	± 7.8	± 6.9	±11.8	± 5.9	± 7.2	±12.2	±11.9	±11.7	± 4.1

Figure 25. Pelvis axis system
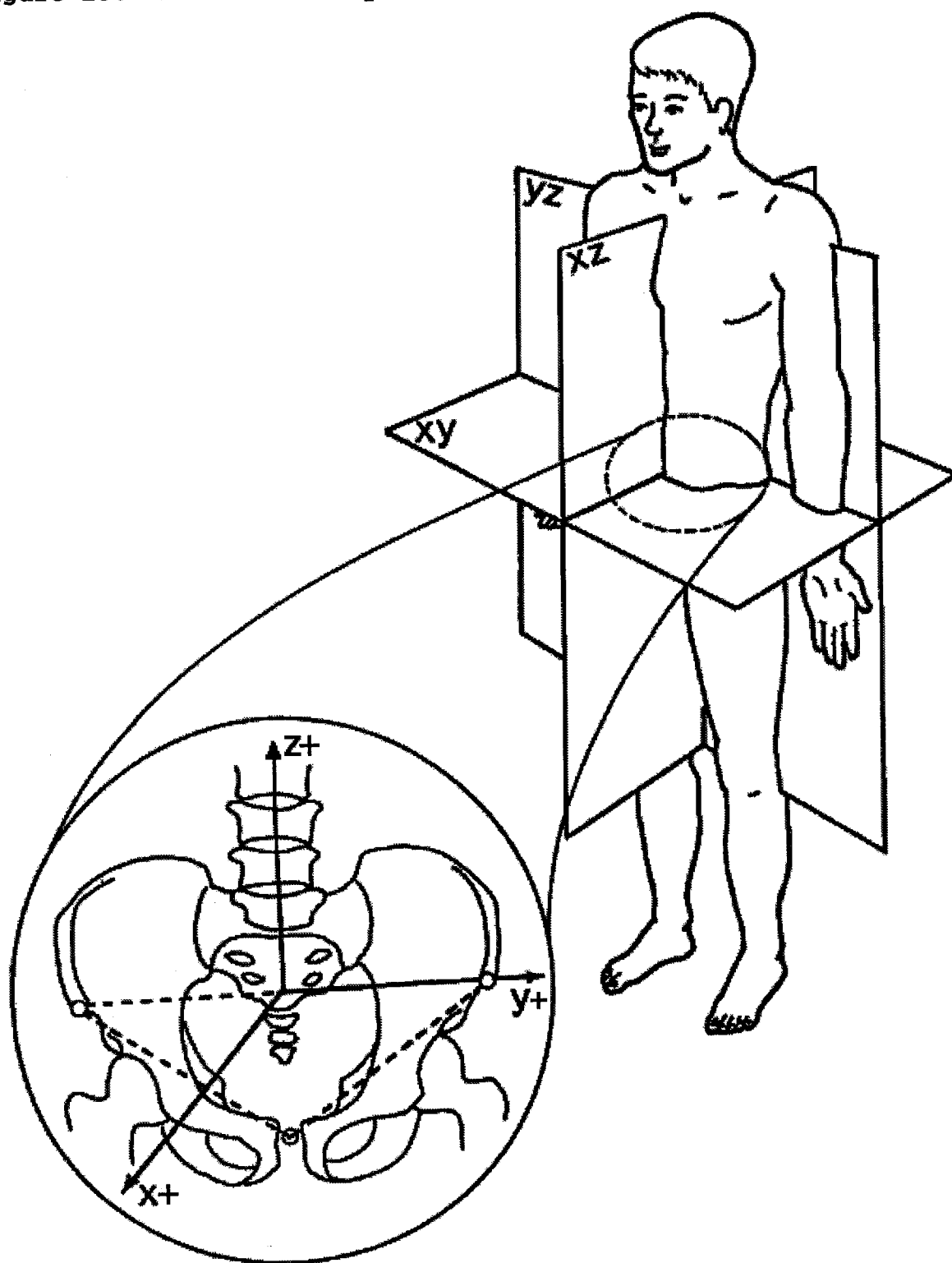
Table 21. **Pelvis axis system: origin (mm) and transformation matrix from seat axis system.**

ERECT A

Origin: $X_O = 130.6$ $Y_O = 5.3$ $Z_O = 163.5$

TM:

$$\begin{bmatrix} .994 & .042 & .103 & -146.860 \\ -.042 & .999 & -.006 & 1.070 \\ -.103 & .001 & .995 & -149.160 \\ .000 & .000 & .000 & 1.000 \end{bmatrix}$$

NEUTRAL

Origin: $X_O = 125.5$ $Y_O = 4.2$ $Z_O = 167.4$

TM:

$$\begin{bmatrix} .982 & .040 & .183 & -154.110 \\ -.040 & .999 & -.005 & 1.590 \\ .183 & -.002 & .983 & -141.560 \\ .000 & .000 & .000 & 1.000 \end{bmatrix}$$

SLUMP M

Origin: $X_O = 138.5$ $Y_O = -2.3$ $Z_O = 188.1$

TM:

$$\begin{bmatrix} .746 & -.024 & .666 & -228.48 \\ -.038 & .999 & .006 & 6.440 \\ -.665 & -.029 & .746 & -48.150 \\ .000 & .000 & .000 & 1.000 \end{bmatrix}$$

Thoracic Axis System.

The thoracic axis system was defined by three pointmarks: Suprasternale (Ref 51) and two pointmarks in the spinal column. The two pointmarks in the spinal column were selected by investigating the geometric relationships among T1, T4(T3), T8(T9), and T12(T11). Since the thoracic vertebrae and sternum included many joints, combinations of pointmarks were evaluated to identify the most rigid triad. The triad was selected by the magnitude of the perimeter of the triangle defined by the three pointmarks and the coefficient of variation (that is, the ratio of standard deviation to average) in the perimeter measurement.

Pointmarks identified initially to use in developing the axis system were as follows (See Ref 51 for code definition):

Vertebral Body	Spinous Process	Sternum
T01BODAVER (3111)	T01SPPCPMC (3190)	STEBODCAMC (3900)
T04BODAVER (2811)	T04SPPCPMC (2890)	
T08BODAVER (2411)	T08SPPCPMC (2490)	
T12BODAVER (2011)	T12SPPCPMC (2090)	

The TxxBODAVER (xx11) pointmark was calculated as the centroid of the following four pointmarks on each vertebral body:

TxxBODCASC (xx00)	TxxBODCPSC (xx00)
TxxBODCAIC (xx07)	TxxBOCCPIC (xx08)

These four pointmarks lay on the most anterior (CA in the above pointmark acronyms) and posterior (CP) projections (not including osteophyte developments) of the superior (SC) and inferior (IC) vertebral body surfaces.

For each triad, composed of two analogous thoracic vertebrae pointmarks (E.g., T01BODAVER AND T04BODAVER) and STEBODCACM, the perimeter of the triangle was calculated in each position. For example, subject #5 had a sample of 15 perimeters representing 7 ERECT, 2 NEUTRAL, and 6 SLUMP positions. The triads were ranked

for each subject based upon the smallest coefficient of variation for perimeter length. The coefficient of variation was independent of size and measured variation of all positions. The triad was selected by the largest perimeter and smallest coefficient of variation (Table 22).

As demonstrated in Table 22, the triad composed of T01, T12, and Suprasternale had the largest perimeter and second most stable geometry. The difference between the first and second rank in coefficients of variation was 0.001. As a result, the thoracic axis system was based upon the T01, T12, and Suprasternale pointmarks.

The coordinates (Table 23) were the average and standard deviation of the anatomical pointmarks of all subjects in ERECT-A, NEUTRAL, and SLUMP-M.

Table 22. Perimeters (mm) of anatomical pointmark triads for the thoracic axis system.

| Triad Group | Perimeter | | | Coefficient of Var. | |
	Ave.	SD	Rank	Ave.	Rank
3111-2811-3900	221	±25	12	0.011	4
3111-2411-3900	381	±21	10	0.037	6
3111-2011-3900	538	±42	5	0.011	4
2811-2411-3900	336	±19	11	0.040	8
2811-2011-3900	500	±39	6	0.011	4
2411-2011-3900	458	±36	8	0.039	7
3190-2890-3900	358	±33	9	0.006	1
3190-2490-3900	547	±24	4	0.029	5
3190-2090-3900	690	±36	1	0.007	2
2890-2490-3900	469	±42	7	0.029	2
2890-2090-3900	623	±36	2	0.008	5
2490-2090-3900	557	±27	3	0.029	3

The thoracic axis system definition used the algorithm developed for pointmarks that lay in the directions of the +x, -x, and -z anatomical axes (refer to Section 3.3). The origin of the thoracic axis system lay on the x axis defined by a line

connecting Suprasternale and T01 at the intersection of a perpendicular line passing through T12 (Figure 26). The thoracic axis system had +x from T01 through Suprasternale. +Z was perpendicular to the x axis, directed away from T12. +Y was the cross product of the x and z axes following the right hand rule. This coordinate system approximated the sagittal XZ plane, the frontal YZ plane and the horizontal or transverse xy plane (Table 24).

Table 23. X, Y, Z coordinates (mm) in seat axis system for anatomical pointmarks to define the thoracic axis system.

Pointmark	ERECT-A			NEUTRAL			SLUMP-M		
	X	Y	Z	X	Y	Z	X	Y	Z
3930	30.5	17.0	583.0	35.6	18.2	581.8	48.1	11.3	555.8
	±31.0	± 9.2	±26.1	±28.0	±12.2	±27.2	±28.0	±12.7	±28.4
3190	-77.6	14.9	635.0	-70.5	16.9	638.2	-51.8	16.1	613.5
	±32.8	±10.4	±22.9	±29.0	±13.2	±23.1	±27.7	±16.6	±24.8
2090	-40.9	- 2.5	338.5	-58.3	- 3.7	341.0	-66.4	-14.5	321.5
	±10.4	± 6.9	±11.0	±15.2	± 7.7	±11.8	±15.5	± 8.7	±14.3

Figure 26. Thoracic axis system, modified from Woodburne (Ref 72)
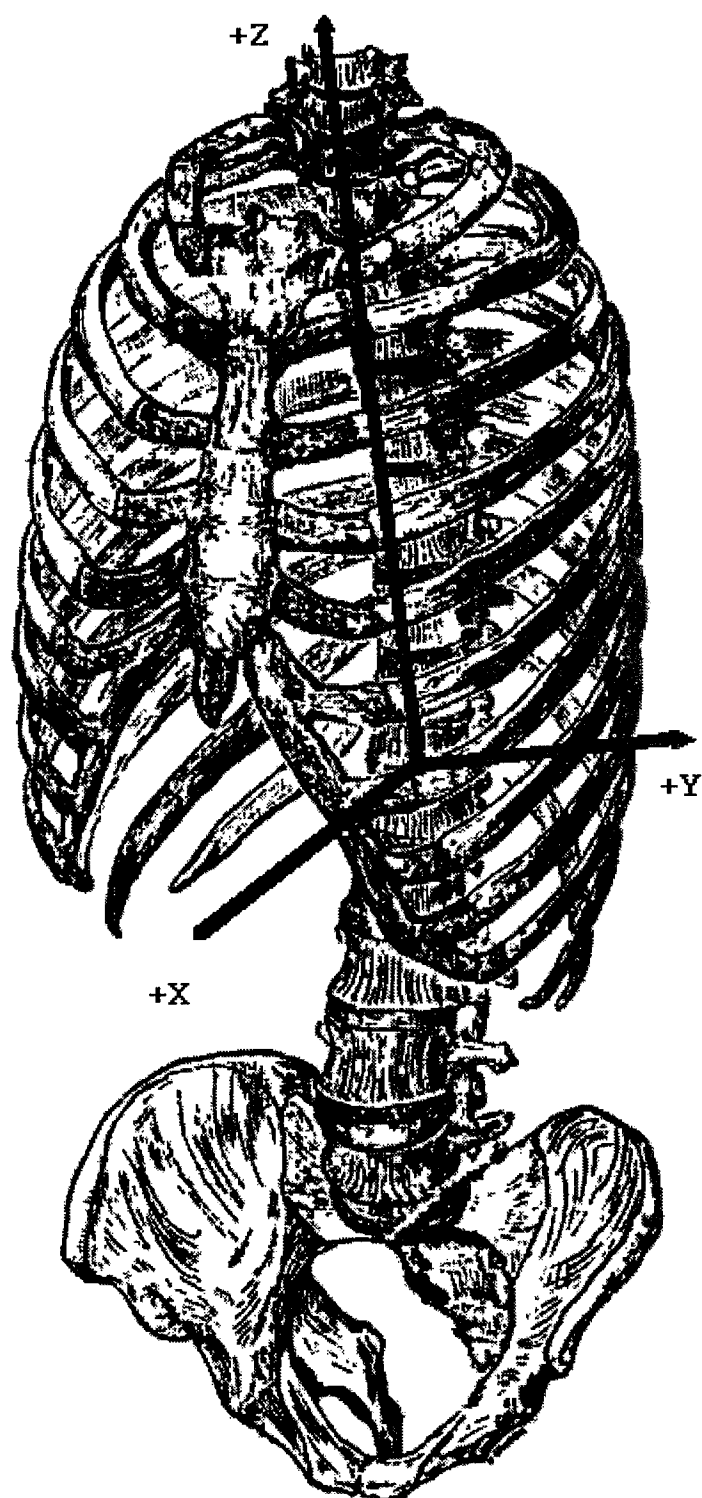
Table 24. Thoracic axis system: origin (mm) and transformation matrix from seat axis system.

ERECT A

Origin: $X_O = 67.7$ $Y_O = 17.7$ $Z_O = 565.1$

TM:

$$\begin{bmatrix} -.901 & -.017 & .433 & -183.590 \\ .050 & -.997 & .065 & -22.290 \\ .431 & .080 & .899 & -538.540 \\ .000 & .000 & .000 & 1.000 \end{bmatrix}$$

NEUTRAL

Origin: $X_O = 62.1$ $Y_O = 18.5$ $Z_O = 567.7$

TM:

$$\begin{bmatrix} -.883 & -.011 & .470 & -211.67 \\ .050 & -.996 & .071 & -25.040 \\ .467 & .086 & .880 & -530.130 \\ .000 & .000 & .000 & 1.000 \end{bmatrix}$$

SLUMPED M

Origin: $X_O = 64.5$ $Y_O = 10.6$ $Z_O = 546.3$

TM:

$$\begin{bmatrix} -.865 & .041 & .499 & -217.410 \\ .012 & -.995 & .104 & -46.850 \\ .501 & .096 & .860 & -513.300 \\ .000 & .000 & .000 & 1.000 \end{bmatrix}$$

86

Shoulder axis system

The three pointmarks used to define the shoulder axis system form a plane that approximated the plane of the scapular blade. The axis system was based upon the following right scapular pointmarks: Glenoid Fossa (SCAGLFRMMM 4340), Inferior Angle (SCAINARMIC 4350), and the Superior Angle (SCASUARMSC 4360). The average and standard deviation of anatomical pointmarks were calculated for all subjects who had comparable positions in ERECT-A, NEUTRAL, and SLUMP-M (Table 25).

Table 25. X, Y, Z coordinates (mm) in seat axis system for anatomical pointmarks to define the shoulder axis system.

Pointmark	ERECT-A			NEUTRAL			SLUMP-M		
	X	Y	Z	X	Y	Z	X	Y	Z
4340	-33.0	-136.5	577.9	- 26.6	-134.4	582.1	-11.1	-136.6	552.0
	±23.4	± 9.5	±13.1	± 19.5	± 8.4	±17.0	±21.4	± 14.9	±16.7
4350	-98.1	- 88.1	456.8	-102.3	- 89.0	465.2	-92.7	- 99.0	439.1
	±11.2	± 18.9	±20.8	± 11.1	± 20.9	±23.1	± 6.4	± 19.0	±16.3
4360	-73.9	- 60.9	608.4	- 66.3	- 58.9	614.9	-46.5	- 63.4	585.5
	±27.4	± 13.8	±16.7	± 22.8	± 11.1	±19.2	±26.0	± 20.6	±16.4

The axis system definition used an algorithm developed for pointmarks that lay in the directions of the +y, -y, and -z anatomical axes. The origin of the axis system was on the y axis. +Y was directed from the Glenoid Fossa through the Superior Angle. +Z was perpendicular to the y axis directed away from the Inferior Angle pointmark (Figure 27). +X was formed normal to the YZ plane by the cross product of the +y and +z axes, following the right hand rule (Table 25). This coordinate

system approximated the sagittal XZ plane, the frontal YZ plane
and the horizontal or transverse xy-plane.   The origin and
transformation matrices were calculated (Table 26).

**Figure 27.   Shoulder axis system, modified from Woodburne (Ref
72).**
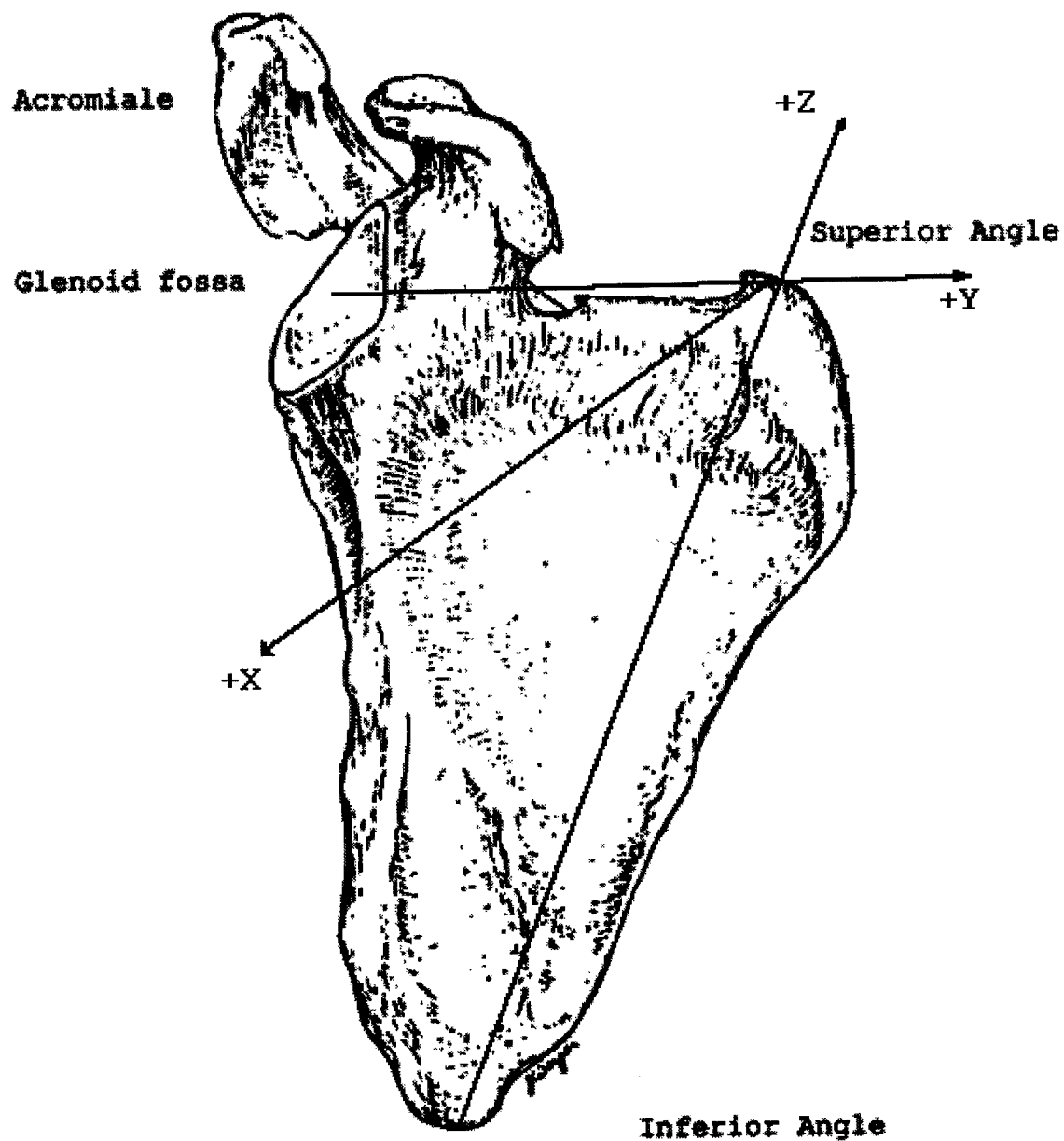
Table 26. Shoulder axis system: origin (mm) and transformation matrix from the seat axis system.

ERECT A

Origin: $X_O = -46.0$ $Y_O = -112.6$ $Z_O = 582.6$

TM:

$$\begin{bmatrix} .816 & .532 & -.225 & 229.810 \\ -.449 & .829 & .334 & -123.47 \\ .364 & -.171 & .915 & -540.330 \\ .000 & .000 & .000 & 1.000 \end{bmatrix}$$

NEUTRAL

Origin: $X_O = -39.0$ $Y_O = -110.9$ $Z_O = 592.3$

TM:

$$\begin{bmatrix} .785 & .543 & -.298 & 267.070 \\ -.435 & .826 & .358 & -137.590 \\ .440 & -.152 & .885 & -523.850 \\ .000 & .000 & .000 & 1.000 \end{bmatrix}$$

SLUMPED M

Origin: $X_O = -19.6$ $Y_O = -119.0$ $Z_O = 560.1$

TM:

$$\begin{bmatrix} .759 & .536 & -.370 & 285.660 \\ -.403 & .832 & .381 & -122.170 \\ .512 & -.140 & .848 & -481.340 \\ .000 & .000 & .000 & 1.000 \end{bmatrix}$$

Anatomical pointmarks in the pelvis axis system.

The most extensive set of three-dimensional data on the skeletal pelvis were collected in an investigation by Reynolds, Snow and Young (Ref 53). In this investigation, 123 anatomical pointmarks on 80 adult male pelves were measured in three-dimensional space. The pointmarks measured on the nine subjects in the current study were identified similarly to the 1981 pelvic study. However, the current study measured few pelvic pointmarks compared to the 1981 investigation.

The Reynolds et al (Ref 53) investigation reported data on the geometry of the hip joint, ischium, sacro-iliac joint, and iliac crest. Similar anatomical features were measured in the present investigation. In both investigations, a right-handed, orthogonal axis system was defined by three pointmarks: right anterior superior iliac spine, left anterior superior iliac spine, and symphysion. According to the algorithm described in Section 3.3, this axis system used the +y, -y, -z pointmark definition to identify axes lying approximately in the cardinal anatomical planes.

Acetabulion, Left Ischiale, and Left Posterior Superior Iliac Spine were measured in both investigations. The sampling protocol for 1982 study had been designed to describe the general population. Since data from the current sample lay within ±1.96 standard deviations of the CAMI-Pelvis study, it was reasonable to assume that this current sample was drawn from the same population as the 1982 sample.

There were several pointmarks in the pelvis that were of considerable importance in sitting and seat design. Primarily, the location of the hip joint center represented the pivot between thigh and pelvis. Ischiale represented the point of contact between the pelvis and seat surface. The posterior iliac spine represented the point of contact between the pelvis and the seat back surface.

90

The data in Table 27 were reported in the pelvis axis system defined in ERECT-A, Table 21. To compute the location of the pointmarks reported in Table 27, the inverse of the transformation matrix (Ref 45) for defining the pelvic axis system in the seat axis system was computed. The pointmarks were then transformed from the seat axis system location to the pelvic axis system location by:

$$[PM_A] \; = \; [TM_{AS}] \; [PM_S] \tag{44}$$

where **PM** was the pointmark in the anatomical and seat axes systems denoted by the subscripts A and S, respectively. **TM** was the inverse of the transformation matrix for ERECT-A in Table 21.

Table 27. Comparison of anatomical pointmark locations (mm) in the pelvic axis system between current sample and CAMI pelvic survey from Reynolds et al, (1982).

Pointmark	CAMI-Pelvis			MSU-Pelvis		
	X	Y	Z	X	Y	Z
L Hip Jt Ctr	-48	83	-65			
	± 5	± 5	± 7			
Acetabulion	- 56	62	-50	- 57	61	- 50
	± 4	± 6	± 8	± 7	± 9	± 4
L Ischiale	- 96	60	-118	-101	63	-121
	± 7	± 5	± 9	±11	± 7	± 5
L Inf Isch	- 76	39	-132			
	± 7	± 5	± 8			
L PSIS	-131	35	11	-130	37	13
	± 8	± 4	±15	±10	± 8	±15

The left hip joint center (L Hip Jt Ctr) in the CAMI-Pelvis data was defined by the center of a hemisphere that fits the acetabulum. This pointmark, at the center of the femoral head,

91

is the center of hip joint rotation in a ball-and-socket model. Acetabulion lay on the surface of the acetabulum in a line normal to the plane that best described the angular orientation of the acetabular rim with respect to the pelvic structure.

We considered the hip joint center to be coincident with the center of the sphere that best fit the acetabulum. The hip joint center was located by pointmarks HIPACELMMM (i.e. left) and HIPACERMMM (i.e. right) in the present study (Table 27).

The left inferior ischium (L Inf Isch) pointmark was measured in the CAMI-Pelvis data at the most anterior convergence of the medial and lateral margins of the ischial tuberosity. Left Ischiale was the highest point on the ischial tuberosity in a plane formed by the medial surface of the iliac blade and the pubic symphysis. Using simple trigonometric relationships, the data in Table 27 for the CAMI pelvis were transformed into the position of the pelvis in ERECT-A. The inferior ischium pointmark lay 17.1 and 15.8 mm above the seat surface in ERECT-A and NEUTRAL positions, respectively. In SLUMP-M, Ischiale lay 15.1 mm above the seat surface.

Left posterior superior iliac spine (L PSIS) was the most posterior point on the iliac crest from a plane formed by the anterior superior iliac spines and pubic symphysis. This pointmark on the pelvis contacted the seat back.

Shoulder joint complex in the thoracic axis system.

The shoulder joint complex was composed for four articulations: the sternoclavicular, acromioclavicular, scapulothoracic, and glenohumeral joints. The glenohumeral joint lay inferior to the Acromiale pointmark on the scapula (Ref 18). The center of rotation of the gleno-humeral joint was located at the center of the humeral head. The gleno-humeral joint simulated a ball and socket joint with the humeral head

simulating the ball, and the glenoid fossa and joint ligmants defining the socket.

In the present investigation, the positions of two pointmarks on the humeral epicondyles were used to calculate the centroid of the shoulder joint (See Section 3.4 for algorithm). Additional pointmarks, located on the acromion process, glenoid fossa and scapular blade, defined a shoulder axis system and anatomical geometry.

The upper arm, i.e. right humerus, was rarely visible on the ERECT series of films. As a result, the relationship between the upper arm and the scapula depended on two sets of measurements. The location of the shoulder joint was calculated in the SHOULDER positions. Typically, these films did not include the pelvis, lumbar, and complete thorax. The scapula, however, was present in ERECT and SHOULDER data and it defined the axis system for shoulder joint location. Thus, the center of shoulder motion was calculated first in the scapular axis system. Then with the transformation matrices given in Table 26, the position of this point was calculated in ERECT-A, NEUTRAL, and SLUMP-M positions (Table 30).

The shoulder joint center, in this investigation, lay at the centroid of a sphere of humeral motion (Section 3.4). Two pointmarks on the lateral (HUMLAERMML 4540) and medial (HUMMEERMMM 4530) epicondyles of the humerus were measured in nine positions. In this spherical model, pointmarks on the humerus were on spherical surfaces at a constant radii from the joint center in the scapular axis system.

To calculate the centroid of humeral motion, the effect of scapular motion was removed by transforming two humeral pointmarks into the scapular axis system. The shoulder joint center was, therefore, calculated for humerus movement in the scapula axis system (Table 28). This model of shoulder motion assumed a ball-and-socket gleno-humeral joint, and consequently the centroid was near the glenoid fossa pointmark (SCAGLFRMMM).

93

Table 28. X, Y, Z coordinates (mm) in shoulder axis system of the centroid and radius (R) of humeral movement (mm) for HUMMEERMMM (4530) and HUMLAERMML (4540) .

Subject ID	4530 x	y	z	R	4540 x	y	z	R
#1	-10.0	27.4	-13.5	353.9	3.8	4.2	- 8.1	325.4
#2	-18.3	75.9	-14.5	436.5	-19.3	72.9	-14.2	433.1
#3	- 7.3	43.6	-10.2	382.7	-7.6	39.9	- 7.8	372.3
#4	0.6	48.2	-10.1	359.8	-0.7	46.4	- 9.4	370.9
#5	- 7.7	16.0	- 1.8	336.4	-10.2	22.0	- 5.7	338.1
#6	- 7.4	70.5	-14.8	414.8	-7.7	99.1	-14.8	434.7
#7	1.7	35.2	-15.2	374.6	0.8	34.4	-15.0	378.4
#8	-2.0	23.7	-16.3	367.8	-3.9	21.3	-16.0	364.6
#9	-0.8	48.7	-14.0	391.0	-2.8	43.1	-14.1	387.6
Ave	- 5.7	43.2	-12.3	379.8	-5.3	42.6	-11.7	378.3
SD	± 6.3	± 20.3	± 4.5	±31.0	±6.9	±28.6	± 3.9	±37.0

The average radius for the total sample was 379.0 ±33.1 mm. However, subjects #2-9 had an acromion-radiale length 47 mm (Appendix A) shorter than the radius length model. The average radial length was 384 mm compared to the anthropometric link length of 337 ±11.9 mm.

The positions of the shoulder centroid and other anatomical pointmarks were located in the shoulder axis system. The average locations of the centroid for 4530 and 4540 and the scapular pointmarks in Table 25 were transformed into the shoulder axis system (Table 29). In addition, the location of Acromiale (SCAACPRAMC 4310) was in the shoulder axis system. Each pointmark was in the shoulder axis system defined for ERECT-A, NEUTRAL, and SLUMP-M. These three locations were averaged for Table 29.

Table 29. X, Y, Z coordinates (mm) in shoulder axis system for anatomical pointmarks.

	X	Y	Z
Average Centroid	- 5.5	42.9	- 12.0
Acromiale	- 0.1	-36.2	46.6
Glenoid fossa	0.1	-26.1	0.0
Inferior Angle	0.0	0.1	-143.1
Superior Angle	- 0.1	64.0	0.1

Anatomical geometry for seating.

Change in whole body center of gravity in the horizontal plane (XY) of the seat axis system.

The center of gravity was measured in the horizontal plane for subjects #4-9. The x- and y-coordinates of the center of gravity in the seat axis system were reported for ERECT A, NEUTRAL, and SLUMP M positions in Table 30.

From ERECT A to NEUTRAL, the center of gravity moved rearward 3.7 mm as the lumbar support was removed. When the body was moved from NEUTRAL to the SLUMP M position, the center of gravity moved forward 65.4mm. There was little change in the y axis indicating that the body was moved primarily in the sagittal (i.e. XZ) plane.

TABLE 30. X, Y coordinates (mm) in seat axis system for the center of gravity for maximum ERECT, NEUTRAL, and maximum SLUMP positions.

	ERECT		NEUTRAL		SLUMP	
	X	Y	X	Y	X	Y
Minimum	96.6	0.5	93.0	1.8	118.5	-0.4
Maximum	117.7	10.8	117.7	9.9	140.3	10.6
Average	104.5	7.9	103.9	6.7	127.1	5.8
SD	±7.5	±3.8	±8.8	±3.0	±8.9	±4.7

The average locations of the center of gravity, ischial
tuberosities, and Promontorion in ERECT A, NEUTRAL, and SLUMP M
were plotted (Figure 28). There was a tendency for the body to
be moved with a slight displacement in -y. Each subject had a
similar pattern of movement between anatomical pointmarks and the
center of gravity. Ischiale, representing the pelvic ischium,
moved more than the center of gravity. Furthermore, the center
of gravity changed from anterior‧to posterior of the ischium in
SLUMP.
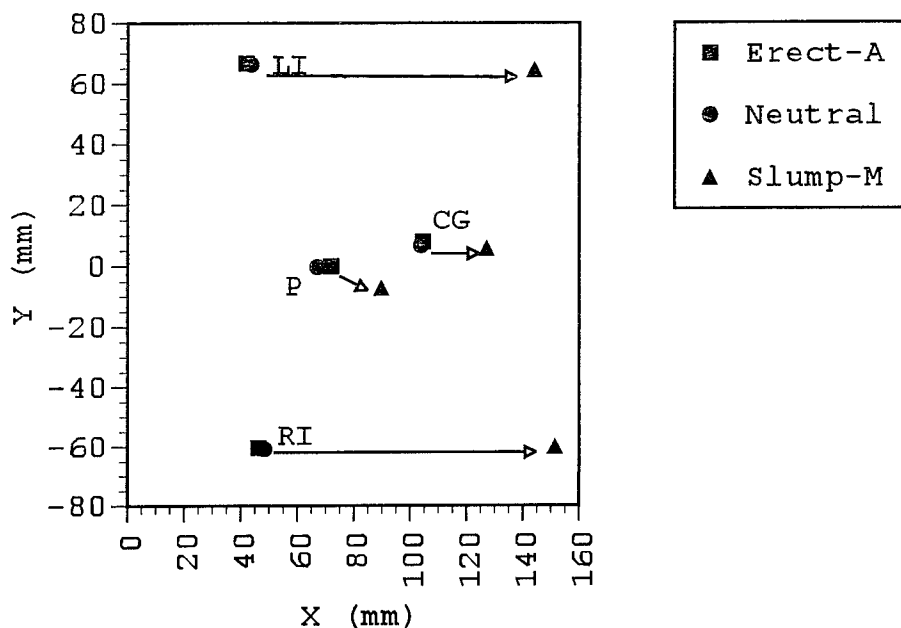
**Figure 28. Average Locations of right and left Ischiale (RI &
LI), Promontorion (P) and the center of gravity (CG) for all
subjects in ERECT-A, NEUTRAL, and SLUMP-M.**

Thoracic and lumbar curves in sitting.

Thoracic and lumbar curvatures were analyzed in the sagittal
plane of the body. The x and z coordinates of the anatomical

96

axis system origins in the seat axis system defined curves in ERECT, NEUTRAL, and SLUMP positions. In the thoracic region, C07, T01, T04, T08, and T12 were used except T09 in subjects #4 and #9, T03 in subject #7, and T11 in subject #5 (Table 2). In the lumbar region, T12, L01, L02, L03, L04, L05, and S1 were used for all subjects but #5 who had T11 targeted instead of T12.

The origin coordinate averages and standard deviations were in the seat axis system (Table 31). The centroid (x and z coordinates) of the sphere, radius of curvature, and the sum of squared errors (SSE) described the curvature of the thoracic and lumbar vertebrae. The thoracic and lumbar curves were reported for ERECT-A, NEUTRAL, and SLUMP-M only.

The SLUMP-M curve in the lumbar region was highly variable. The least squares fit of the curves converged in five subjects. One subject had a posterior convexity while the other four had anterior convexities. Subjects #2, 7, 8 and 9 had lumbar curves defined by an anterior convexity.

A univariate repeated measures F-test at the 0.05 level of significance was used to test for differences in the thoracic and lumbar curvature geometries. The thoracic and lumbar curves differed significantly in their centers and radii of curvature. The sums of squared errors were not significantly different. These statistical procedures were used for the sample composed of subjects with complete data. Thus, there were six subjects used in the univariate repeated measures tests.

Table 31. Back curvature: radius, sum of squares and X and Z coordinates (mm) in seat axis system of the center of thoracic and lumbar curves in ERECT, NEUTRAL, and SLUMP positions.

Posture	X	Z	Radius of Curvature	SSE
THORACIC CURVATURE				
ERECT A	193.7 ± 78.8	524.1 ± 42.9	250.1 ± 79.0	54.69 ±89.66
NEUTRAL	202.2 ± 90.5	505.1 ± 33.7	258.1 ± 90.0	44.05 ±59.84
SLUMP M	234.7 ± 93.7	458.5 ± 34.2	281.1 ± 94.5	55.24 ±85.35
LUMBAR CURVATURE				
ERECT A	-162.1 ± 71.3	208.9 ± 39.1	220.4 ± 74.3	54.5 ±34.5
NEUTRAL	-288.3 ±275.3	156.1 ±113.8	348.2 ±284.9	50.8 ±31.9
SLUMP M	-512.0 ±245.6	35.0 ± 53.1	589.5 ±226.7	54.8 ±59.0

Anatomical pointmark locations in seat axis system for ERECT, NEUTRAL, and SLUMP.

The three-dimensional locations of anatomical pointmarks in ERECT-A, NEUTRAL, SLUMP-M were calculated in the seat axis system (Table 32). Pointmarks were identified by their landmark or anatomical name and in the SAL code (Ref 50). SCASCJCALC, however, was the shoulder joint center as calculated by the algorithm presented in Section 5.4.2. The Average Centroid pointmark (Table 29) was transformed (Ref 45) into the seat axis system from the shoulder axis system by the inverse of the transformation matrices (Table 27). In addition, PUBSYM was Symphysion, calculated as the centroid of the right and left pubic tubercles (HIPPUBRAMC and HIPPUBLAMC). This centroid and the anterior superior iliac spines defined the anatomical axis system for the pelvis.

The ERECT-A, NEUTRAL, and SLUMP-M, positions of anatomical pointmarks in Table 32 were plotted (Figures 29, 30, and 31). The thoracic (T) and lumbar (L) curve centroids, as described in the preceding section, were also depicted for the ERECT-A and NEUTRAL positions. Only the thoracic centroid was shown in the SLUMP-M position.

Table 32. X, Y, Z coordinates (mm) in seat axis system for anatomical pointmarks in ERECT-A, NEUTRAL and SLUMP-M positions.

Pointmark	ERECT-A			NEUTRAL			SLUMP-M		
	x	y	z	x	y	z	x	y	z
STESUPCMSC	30.5	17.0	583.0	30.5	17.0	583.0	42.9	7.7	558.0
(Suprasternale)	±31.0	± 9.2	±26.1	±31.0	± 9.2	±26.1	±32.5	±13.5	±34.3
SCAACPRAMC	-22.3	-155.5	621.3	- 9.7	-151.0	625.8	15.9	-150.9	586.9
(Acromiale)	±29.2	± 9.2	±16.5	±24.2	± 10.9	±20.2	±30.5	± 14.1	±21.0
SCASCJCALC	-74.1	-78.1	592.3	-67.1	-76.3	598.6	-47.1	-84.5	567.9
(Shoulder Jt)									
C07SPPCMMC	-68.2	11.6	652.9	-59.1	15.4	655.5	-39.8	8.9	632.7
(Cervicale)	±40.0	±10.2	±27.7	±35.0	±13.3	±29.2	±39.6	±22.9	±36.7
T01SPPCMMC	-77.6	14.9	635.0	-70.5	16.9	638.2	-51.8	16.1	613.5
	±32.8	±10.4	±22.9	±29.0	±13.2	±23.1	±27.7	±16.6	±24.8
T12SPPCMMC	-40.9	- 2.5	338.5	-58.3	- 3.7	341.0	-66.4	-14.5	311.5
	±10.4	± 6.9	±11.0	±15.2	± 7.8	±11.7	±15.5	± 8.7	±14.3
SACSB1CASC	67.5	- 1.7	180.0	59.6	- 2.5	178.1	75.9	- 9.5	163.6
(Promontorion)	±12.1	± 5.6	±12.1	±17.0	± 5.9	±11.8	±22.3	± 7.6	±15.6
HIPILILPSM	- 4.5	36.7	162.7	-10.2	36.0	155.6	30.0	29.4	108.3
(PSIS-Lt.)	± 9.6	± 7.9	±14.7	± 8.5	± 7.9	±16.1	±15.1	± 8.1	±17.5
HIPILIRPSM	- 2.7	-41.1	163.0	- 8.9	42.0	155.8	29.7	-49.1	105.4
(PSIS-Rt.)	± 7.9	± 7.9	±13.9	± 6.3	± 8.0	±14.7	±16.8	±12.6	±15.4
HIPILILASM	125.7	121.9	162.8	125.7	121.9	162.8	134.2	112.7	188.7
(ASIS-Lt.)	±10.5	± 9.9	± 8.6	±10.5	± 9.9	± 8.6	±17.9	± 6.4	± 9.2
HIPILIRASM	135.4	-110.6	164.2	135.4	-110.6	164.7	142.9	-117.9	187.4
(ASIS-Rt.)	± 6.0	± 9.0	±10.7	± 6.0	± 9.0	±11.7	±19.0	± 15.4	± 6.4
PUBSYM	139.3	5.2	79.4	140.6	4.4	86.5	191.9	1.1	127.6
(Symphysion)	± 8.6	± 7.2	±10.7	± 6.7	± 7.5	±11.9	±12.0	±11.1	± 5.9
HIPACELMMM	76.7	65.4	107.7	75.7	64.6	108.9	127.2	58.9	114.4
(Acetabulion)	± 6.5	± 8.9	± 4.1	± 3.8	± 9.4	± 4.7	±11.0	± 9.7	± 0.52
HIPACERMMM	80.1	-61.4	106.7	79.0	-62.1	107.6	129.4	-67.8	112.1
(Acetabulion)	± 6.3	± 7.4	± 5.3	± 6.1	± 7.5	± 5.1	±12.9	±11.9	± 2.5
HIPISCLMIC	40.1	63.4	32.9	46.8	63.0	31.2	143.6	58.9	32.9
(Ischiale)	±11.3	± 7.5	± 5.5	±12.8	± 7.7	± 5.4	± 3.5	± 9.3	± 3.8
HIPISCRMIC	44.6	-60.5	33.4	50.8	-61.0	31.5	146.3	-64.2	31.9
(Ischiale)	±12.8	± 5.2	± 4.4	±13.2	± 5.4	± 4.5	± 6.3	± 9.6	± 3.7

Figure 29. Anatomical pointmarks and curve centroids (T = thoracic; L = lumbar) in the XZ plane for ERECT-A.
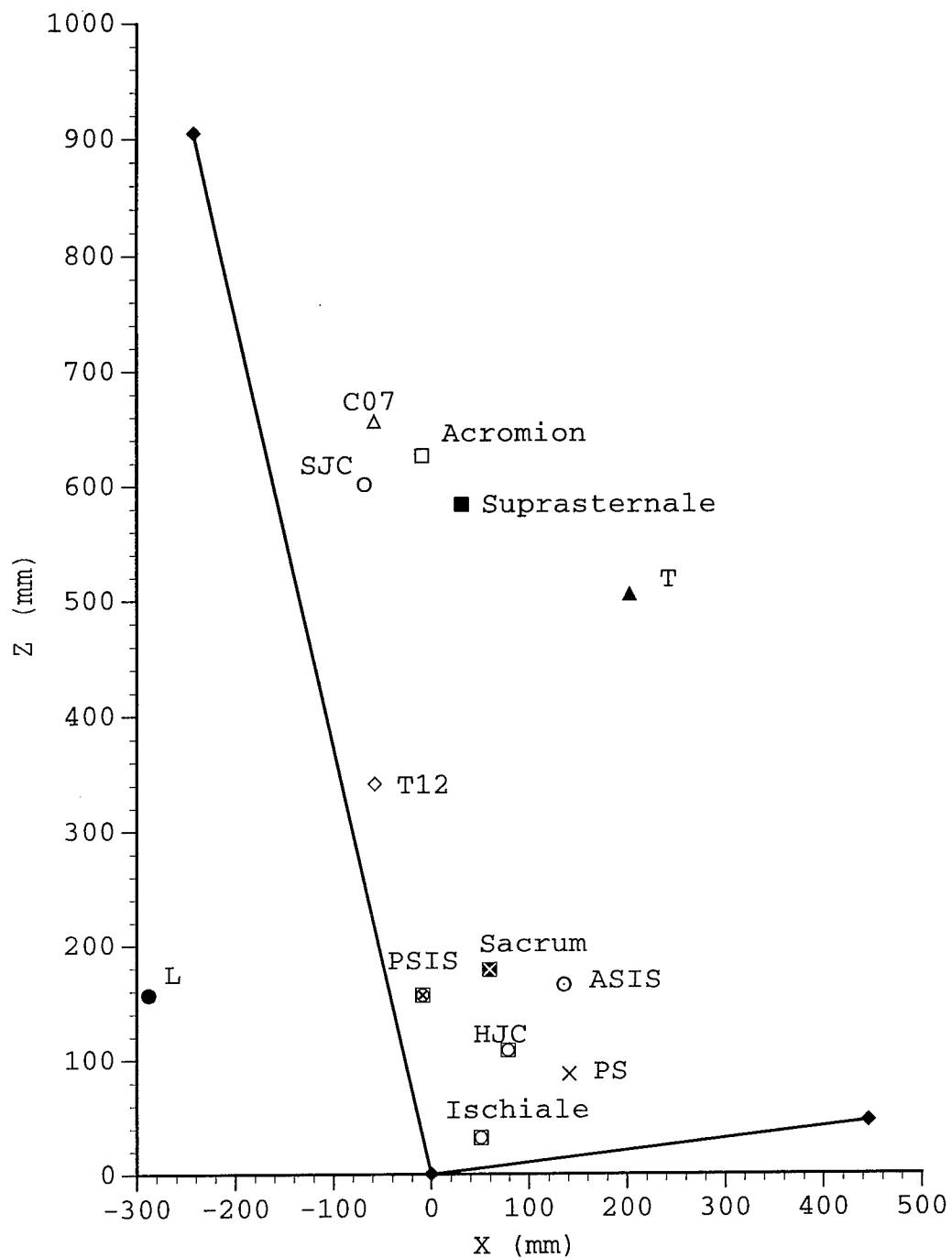
Figure 30. Anatomical pointmarks and curve centroids (T = thoracic; L = lumbar) in the XZ plane for NEUTRAL.

102
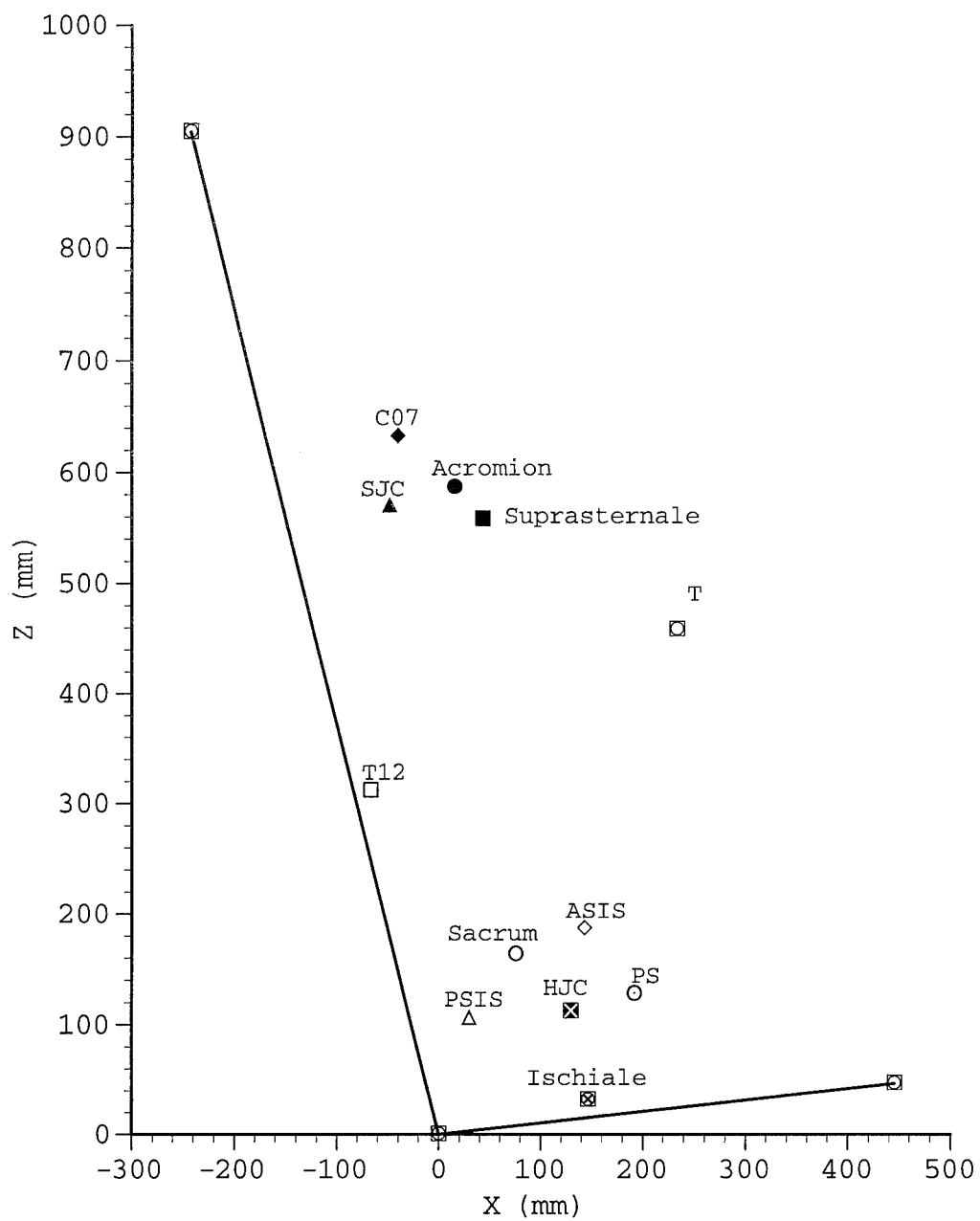
Figure 31. Anatomical pointmarks and curve centroid (T = thoracic) in the XZ plane for SLUMP-M.

103

Displacements of the thorax and pelvis from maximum ERECT to maximum SLUMP

The comparable seated postures ERECT-A, NEUTRAL, and SLUMP-M uniquely defined three relative positions of the torso. These postures, however, represented unique positions in a continuum of postures from maximum ERECT to maximum SLUMP. The displacement of the thorax relative to the pelvis from these maximum postures defined range of motion in the torso. Measurements of anatomical pointmarks and whole body center of gravity location showed that torso motion lay primarily in the mid-sagittal plane. Thus, we defined the range of motion in the torso between the thorax and pelvis by line segments projected in the mid-sagittal XZ-plane that represented the thorax and pelvis in ERECT and SLUMP postures.

For the thorax, an examination of the cross-product elements in the transformation matrices in Table 25 (Section 5.3.2) showed that the position of the thorax was defined primarily in the XZ plane. In the thorax, a position vector from T01 (T01SPPCPMC 3190) to Suprasternale (STESUPCMSC 3930) represented thoracic displacement in the sagittal plane.

The coordinates of T01SPPCPMC, direction cosines and magnitudes of the position vectors to Suprasternale were reported in the SRP axis system (Table 33) for maximum ERECT, ERECT-A, NEUTRAL, SLUMP-M, and maximum SLUMP. The T01 coordinates were reported in the SRP axis system. The direction cosines, α, β, and γ, in Table 33 described the angles that the position vector from T01 to Suprasternale made with the positive x, y, and z axes of the SRP axis system, respectively. The distance was the length of the line between the T01 and Suprasternale. The average, standard deviation and sample size were reported in Table 33. Subject #1 had no data for T01 and Subject #3 had no data for Suprasternale. Thus, the maximum sample size for the direction cosines and distance was 7. The sample size for SLUMP-

104

M and SLUMP-Max was reduced to 6 by the removal of subject #6 (See Section 5.2.3 for explanation).

Table 33. Thoracic segment position vector, T01→Suprasternale, in the SRP axis system.

| | | T01 | | | T01→Suprasternale | | | |
		x	y	z	α	β	γ	Distance
ERECT-Max	Ave	-77.7	15.1	637.1	.893	.029	-.416	125.5
	sd	±31.6	±10.7	±22.7	±.075	±.033	±.159	±5.2
	N	8	8	8	7	7	7	7
ERECT-A	Ave	-77.6	14.9	635.0	.875	.021	-.455	125.5
	sd	±32.8	±10.4	±22.9	±.079	±.031	±.152	±4.9
	N	8	8	8	7	7	7	7
NEUTRAL	Ave	-70.7	16.5	638.3	.865	.017	-.459	124.8
	sd	±29.2	±13.0	±23.0	±.087	±.029	±.194	±4.9
	N	8	8	8	7	7	7	7
SLUMP-M	Ave	-50.6	12.4	617.8	.844	.009	-.524	124.0
	sd	±30.1	±14.6	±24.1	±.065	±.019	±.103	±3.2
	N	7	7	7	6	6	6	6
SLUMP-Max	Ave	-50.1	8.6	600.0	.851	.009	-.513	123.9
	sd	±26.3	±11.3	±17.2	±.063	±.015	±.104	±3.6
	N	7	7	7	6	6	6	6

With torso flexion from maximum ERECT to maximum SLUMP, T01 moved downward 37mm and forward 27mm. There was, however, a 1.6mm reduction in distance between Suprasternale and the dorsal spine of T01. The average angular displacement of the thorax from maximum ERECT to maximum SLUMP was 13.2°.

For the pelvis, the transformation matrices in Table 22 (Section 5.3.1) showed that the position of the pelvis was primarily defined by an anatomical orientation in the sagittal plane. A position vector between two pointmarks, PSIS and ASIS, represented the pelvis. PSIS in Figure 32 was the average location between the right and left posterior superior iliac spines (HIPILIRPSM 1011 and HIPILILPSM 911), while ASIS was the

average of the right and left anterior superior iliac spines
(HIPILIRASM 1010 and HIPILILASM 910).

The PSIS coordinates in Table 34 were calculated in the SRP
axis system. The direction cosines, α, β, and γ, in Table 34
described the angles that the position vector from PSIS to ASIS
made with the positive x, y, and z axes of the SRP axis system,
respectively. The distance was the length of the line between
the two pointmarks in three-dimensional space.
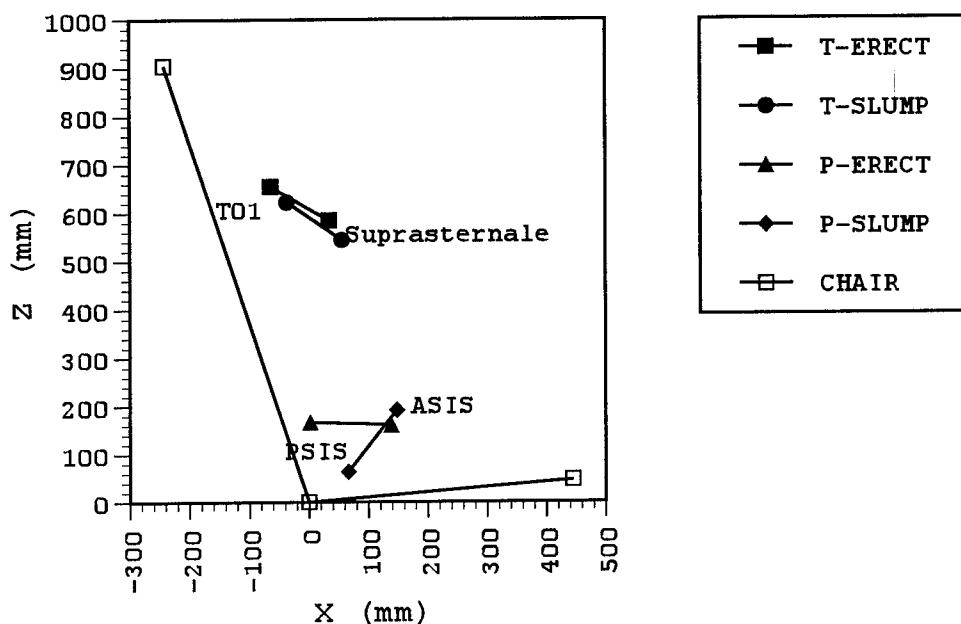
Figure 32. Line segments representing the thorax and pelvis in maximum ERECT and SLUMP positions.

The legend in Figure 32 identified the line segment in each
posture as T-ERECT for the thorax in the maximum ERECT posture
and T-SLUMP for the thorax in the maximum SLUMP posture. The
pelvis was identified by P-ERECT and P-SLUMP for the same
postures.

In Table 34, the position vectors for the various postures
were described by the average, standard deviation and sample
size. Subjects #7 and #9 had missing data on the right

106

innominate bone. For these latter two subjects, the data for the left innominate bone were considered symmetrical to the right innominate bone. Thus, the position vectors for the right and left were identical in the x and z coordinates. The sign was changed in the y coordinate.

The sample included all subjects for the PSIS pointmark in Table 34. Since the ASIS data were missing for subject #1, the sample for the direction cosines of the position vector from PSIS to ASIS was reduced to 8. A further reduction in the SLUMP data was made by the removal of data for subject #6 (See Section 5.2.3 for explanation).

Table 34. Pelvic segment position vector, PSIS→ASIS, in the SRP axis system.

Position			PSIS			PSIS→ASIS		
		x	y	z	α	β	γ	Distance
ERECT-Max	Ave	1.8	-1.9	167.1	.994	.051	-.036	136.8
	sd	±9.3	±5.5	±11.4	±.007	±.034	±.094	±7.9
	N	9	9	9	8	8	8	8
ERECT-A	Ave	-3.6	-2.7	162.9	.992	.053	.023	136.8
	sd	±8.6	±4.7	±14.2	±.008	±.032	±.117	±7.9
	N	9	9	9	8	8	8	8
NEUTRAL	Ave	-9.5	-3.0	155.7	.985	.048	.092	136.9
	sd	±7.3	±5.7	±15.3	±.013	±.027	±.145	±7.8
	N	9	9	9	8	8	8	8
SLUMP-M	Ave	30.0	-7.3	108.7	.789	.032	.606	135.9
	sd	±14.6	±8.2	±17.6	±.061	±.027	±.083	±8.6
	N	8	8	8	7	7	7	7
SLUMP-Max	Ave	54.3	-6.3	104.9	.704	.028	.695	136.1
	sd	±13.9	±9.0	±28.5	±.113	±.032	±.105	±10.1
	N	9	9	9	6	6	6	6

With torso flexion from maximum ERECT to maximum SLUMP, PSIS moved downward 62.2 mm and forward 52.5. There was no change in the distance between the pointmarks other than the effect of

107

changes in the sample making a difference in the sample average. When viewing the motion of the subject from the origin along the subject's positive y axis, the pelvis rotated counter-clockwise a total of 47.5°. Thus, the change from maximum ERECT to maximum SLUMP postures resulted in a rearward rotation of the pelvic iliac crest.

The position vectors representing the thorax and pelvis in Tables 33 and 34 were used to calculate the angle between these position vectors (Table 35). The dot product between the two position vectors calculated a Torso angle reported in Table 35. The Max and M-A columns under Displacement reported angular displacements. The Max column was the difference between maximum SLUMP and maximum ERECT. The M-A column reported the difference between SLUMP-M and ERECT-A.

Table 35. Torso angle between the Thorax, Pelvis for selected ERECT, NEUTRAL, and SLUMP positions.

| | ERECT | | NEUTRAL | SLUMP | | Displacement | |
	Max	A	M	M	Max	ΔMax	M-A
Ave	22.8°	28.7°	32.9°	68.7°	75.7°	52.0°	37.9°
St Dev	±12.6	±14.3	±16.2	±9.9	±10.5	±9.9	±8.6
N	7	7	7	6	6	6	6

The rotation in the XZ plane of the thoracic line segment was a small clockwise rotation of 14.7° while the rotation in the same plane of the pelvic line segment was a counter-clockwise rotation of 52.7°. The combination of these displacements about approximately parallel axes but in opposite directions produced an angular displacement of 60.5° between these line segments. The Torso angle reported in Table 35, however, was 52° because of differences in the sample between the two calculations representing the thorax and pelvis in ERECT and SLUMP positions. Thus, from maximum ERECT to maximum SLUMP, pelvis angle increased

nearly four times the amount that the thorax angle increased and motion of the pelvis was responsible for approximately 66% of the total motion within the torso for these seated postures.

Local vertebral displacements.

Angular orientation of each bone for ERECT-A, NEUTRAL and SLUMP-M positions.

The relative angular orientation of each bone in ERECT-A, NEUTRAL, and SLUMP-M was computed in the sagittal plane from anatomical pointmarks on the inferior surface of the vertebral body. The only exception was the sacrum where the anatomical pointmarks were located on the base which was the superior surface of the first sacral vertebrae.

For subjects #1-#3, the xyz coordinates of the anterior (e.g., L05BODCAIC 1407) and lateral (e.g., L05BODRMIL 1409 and L05BODLMIL 1410) pointmarks on the inferior surface of the vertebral body were used to calculate the angular orientation of each vertebrae. The xyz coordinates of the right and left lateral pointmarks on the inferior vertebral body surface were averaged to locate a pointmark in the middle of the vertebral body. For all other subjects, the xyz coordinates of the anterior and posterior pointmarks(e.g., L05BODCPIC - 1408) were used to defined a line segment in the sagittal plane that described flexion and extension positions in the spinal column. The xyz coordinates of the lateral pointmarks on the inferior surface were used to describe the out-of-plane positions in the spinal column for the measured flexion and extension positions.

For the angular orientation of the sacrum, Promontorion (SACBD1CASC 1100) and the posterior point on the first sacral vertebral body (SACBD1CPSC 1101) were used. The same line

109

segment definitions used for the vertebrae were used for the sacrum.

To describe the angular orientation of the right and left hip bones, anterior superior iliospinale (HIPILIRASM 1010 and HIPILILASM 0910) and the posterior superior iliospinale pointmarks (HIPILIRPSM 1011 and HIPILILPSM 0911) were used.

Table 36 reported the angular orientation of vertebrae and innominates in ERECT-A, NEUTRAL and SLUMP-M. The reported values were average positions for all subjects in each of the three comparable positions. The unit vectors in Table 36 showed that the angular orientation of the inferior surfaces lay primarily in the sagittal plane (XZ in the laboratory axis system). In addition, the greatest angle in the sagittal plane was relative to the z axis.

Table 37 illustrated the same type of data for a line segment defined in the frontal plane (YZ in the laboratory axis system). Unit vectors were computed relative to the seat axis system that defined the angular orientation of the vertebra in the frontal plane.

Table 36. Unit vectors describing the orientation of an anterior-posterior line segment on the inferior surface of each vertebrae listed under Bone.

Bone	Erect-A			Neutral			Slump-M		
	α	β	γ	α	β	γ	α	β	γ
C07	.817	.125	-.479	.810	.125	-.497	.793	.096	-.519
	±.12	±.18	±.23	±.12	±.17	±.22	±.15	±.17	±.24
T01	.853	.023	-.458	.837	.014	-.498	.807	-.007	-.536
	±.12	±.08	±.23	±.12	±.08	±.20	±.13	±.08	±.22
T04	.936	.035	-.119	.927	.041	-.190	.923	.014	-.226
	±.08	±.10	±.33	±.07	±.09	±.30	±.07	±.10	±.29
T08	.917	-.025	.366	.955	-.014	.266	.977	-.016	.165
	±.04	±.12	±.11	±.02	±.12	±.07	±.02	±.12	±.08
T12	.826	-.016	.553	.865	-.032	.489	.921	-.028	.377
	±.05	±.08	±.07	±.04	±.08	±.08	±.04	±.08	±.08
L01	.818	.032	.561	.838	.019	.533	.876	.037	.458
	±.06	±.07	±.09	±.06	±.07	±.09	±.07	±.08	±.12
L02	.869	.030	.469	.868	.023	.478	.871	.038	.467
	±.06	±.10	±.12	±.05	±.10	±.09	±.06	±.09	±.12
L03	.938	.019	.314	.925	.015	.353	.880	.036	.444
	±.03	±.11	±.10	±.04	±.11	±.09	±.06	±.13	±.10
L04	.980	.045	.132	.971	.042	.189	.898	.056	.418
	±.02	±.07	±.13	±.03	±.07	±.13	±.05	±.09	±.09
L05	.953	-.016	-.272	.973	-.012	-.196	.970	-.008	.211
	±.04	±.05	±.12	±.02	±.05	±.12	±.02	±.07	±.10
S1	.803	-.005	-.576	.849	-.001	-.505	.995	-.001	.022
	±.08	±.08	±.12	±.08	±.07	±.13	±.01	±.07	±.07

Table 37. Unit vectors describing the orientation of a lateral-to-lateral line segment on the inferior surface of each vertebrae listed under Bone.

Bone	Erect-A			Neutral			Slump-M		
	α	β	γ	α	β	γ	α	β	γ
C07	.087	−.989	−.058	.085	−.989	−.060	.056	−.991	−.048
	±.08	±.01	±.07	±.08	±.01	±.07	±.09	±.00	±.09
T01	.058	−.995	−.019	.054	−.995	−.014	.027	−.996	.018
	±.07	±.01	±.06	±.07	±.01	±.05	±.08	±.00	±.07
T04	.062	−.987	.123	.091	−.981	.151	.102	−.978	.166
	±.08	±.01	±.07	±.08	±.01	±.07	±.08	±.02	±.08
T08	−.022	−.992	.075	−.029	−.990	.085	−.020	−.991	.089
	±.06	±.01	±.08	±.06	±.01	±.09	±.07	±.01	±.07
T12	.001	−.996	.015	−.031	−.997	.033	−.025	−.996	.044
	±.08	±.01	±.05	±.08	±.01	±.06	±.09	±.01	±.06
L01	.041	−.994	.028	.021	−.994	.036	.031	−.994	.040
	±.09	±.01	±.04	±.10	±.01	±.04	±.10	±.01	±.05
L02	.050	−.992	−.001	.043	−.992	−.004	.054	−.991	.009
	±.12	±.01	±.04	±.12	±.01	±.04	±.11	±.01	±.07
L03	.039	−.996	−.002	.038	−.995	−.010	.055	−.991	.006
	±.08	±.00	±.04	±.08	±.00	±.05	±.10	±.01	±.08
L04	.055	−.995	.016	.056	−.994	.004	.066	−.992	.032
	±.06	±.01	±.06	±.07	±.01	±.07	±.07	±.01	±.09
L05	.027	−.996	−.006	.031	−.996	−.010	.033	−.996	.000
	±.07	±.00	±.06	±.07	±.00	±.06	±.09	±.01	±.04
S1	.008	−.997	.025	.007	−.997	.022	.005	−.997	.009
	±.06	±.00	±.05	±.06	±.00	±.05	±.07	±.00	±.04

Angular displacement of each bone for three positions from ERECT-A to SLUMP-M.

Since the position of the vertebrae was in the sagittal plane, angular displacements between motion segments were a planar calculation. The angular displacement calculations used the anterior-posterior line segment in the preceding section. However, only the x and z coordinates defined the line segment in two-dimensional space. To calculate the angle, the Arc tangent of the slope of the anterior pointmark to the posterior pointmark was

$$Angle = Arc\tan\left(\frac{(z_a - z_p)}{(x_a - x_p)}\right) \tag{50}$$

where x_a and z_a were the coordinates in the seat axis system for the anterior vertebral body pointmarks. The x_p and z_p coordinates represented the posterior pointmarks in the seat axis system.

Promontion (SACBD1CASC 1100) and the posterior point on the first sacral vertebral body (SACBD1CPSC 1101) represented the sacrum. In the pelvis, the average represented the right and left anterior superior iliospinale pointmarks (HIPILIRASM 1010 and HIPILILASM 0910) and likewise for the posterior superior iliospinale pointmarks (HIPILIRPSM 1011 and HIPILILPSM 0911).

Table 38 reported the total angular displacements between motion segments moving from ERECT-A to SLUMP-M positions. The angular displacement from ERECT-A to NEUTRAL, for example, was:

$$Angular\ displacement = (A_S - A_I)_N - (A_S - A_I)_A \tag{51}$$

where A_S and A_I represented the angular orientation of the superior and inferior bones of a motion segment in the spinal column as calculated in equation (50). Subscripts N and A indicated the NEUTRAL and ERECT-A positions, respectively. For

113

example, the superior and inferior bones in the C07/T01 motion segment were C07 and T01, respectively. Similarly for the motion from NEUTRAL to SLUMP-M, equation (46) calculated the angular displacement for SLUMP in Table 39. The total in Table 39 was the angular displacement from ERECT-A to SLUMP-M.

A negative angle represented flexion and a positive angle, extension. Thus, the motion of the torso from ERECT-A to SLUMP-M flexed the chest about the pelvis. The motion segments from T12/L01 to L05/S1 described this rotation. The motion of the segments in the chest and at the sacro-iliac joints (S1/RInn and S1/LInn) demonstrated more complexity.

The torso angle and each motion segment angle in the maximum ERECT position were set to zero and changes from these angles were computed for the regression analysis. The initial position in the analysis was the maximum ERECT position. The final angle was the maximum SLUMP position measured for each subject. The change in motion segment angle was regressed over the change in torso angle. Two columns of data per motion segment in Table 40 described the slope and the correlation coefficient.

The numbers in parentheses in Table 39 were the correlation coefficients that describe the goodness of fit between the change in motion segment and torso angles. The "r" values were high, except the L03/L04 and L04/L05 motion segments in subject #5. There were no values reported for motion segments involving L05 in subject #9.

The average of the maximum torso angles was 55.0° ±12.0. Each subject's torso angle was reported in column Torso A. of Table 40. The average of the slopes in Table 40 indicated approximately 1/6 to 1/5 of the motion between chest and pelvis was contributed by the motion segments in the lumbar spine.

TABLE 38. Angular displacements between motion segments from ERECT-A to SLUMP-M positions.

	TOTAL	ERECT-A to NEUTRAL	NEUTRAL to SLUMP-M
C07/T01	2.5° ± 2.3	1.2° ± 1.0	1.0° ± 1.2
T01/T04	2.4° ± 2.2	2.1° ± 3.8	− 0.7° ± 3.7
T04/T08	1.7° ± 2.2	0.1° ± 3.5	1.1° ± 3.7
T08/T12	−1.1° ± 3.9	− 1.3° ± 3.5	1.6° ± 2.7
T12/L01	− 3.9° ± 2.8	− 1.9° ± 3.0	− 1.6° ± 1.1
L01/L02	− 6.8° ± 2.2	− 2.6° ± 2.4	− 3.9° ± 2.8
L02/L03	− 8.0° ± 3.4	− 1.8° ± 2.5	− 6.0° ± 2.8
L03/L04	− 8.7° ± 3.0	− 1.0° ± 1.3	− 7.6° ± 2.4
L04/L05	−10.7° ± 4.3	− 0.9° ± 1.4	− 9.7° ± 3.5
L05/S1	− 8.1° ± 2.9	− 0.4° ± 3.3	− 7.6° ± 2.4
S1/RInn	0.9° ± 1.9	− 0.8° ± 1.6	1.4° ± 4.1
S1/LInn	− 0.9° ± 2.4	− 0.7° ± 2.0	0.5° ± 4.8

Table 39. Regression slopes between relative lumbar motion segments and torso angles.

ID	Torso A.	L1-L2	L2-L3	L3-L4	L4-L5	L5-S1
#1	66.3°	.15 (.94)	.19 (.95)	.14 (.97)	.23 (.95)	.25 (.95)
#2	69.4°	.15 (.95)	.15 (.96)	.16 (.98)	.14 (.97)	.15 (.95)
#3	66.8°	.23 (.93)	.20 (.99)	.16 (.97)	.21 (.98)	.05 (.87)
#4	54.5°	.13 (.90)	.14 (.95)	.16 (.93)	.11 (.85)	.13 (.95)
#5	34.5°	.43 (.87)	.23 (.96)	.10 (.73)	.18 (.47)	.16 (.90)
#7	47.4°	.15 (.97)	.12 (.93)	.13 (.94)	.22 (.93)	.35 (.93)
#8	52.9°	.19 (.91)	.17 (.98)	.12 (.92)	.18 (.90)	.11 (.69)
#9	48.1°	.22 (.94)	.20 (.97)	.28 (.98)	*.*	*.*
Ave	55.0°	.21	.17	.16	.18	.17
SD	±12.0	±.10	±.04	±.05	±.04	±.10

Linear displacement of the anatomical axis system origin for all postures.

The translations of bone origins from maximum ERECT to maximum SLUMP characterized the linear displacement in the seat (Table 40). Similarly, linear displacements were computed within motion segments (Table 41). The calculation of the bone origin translation within motion segments used vectoral subtraction as follows:

$$\text{Translation} = (X_S - X_I)_A - (X_S - X_I)_N \qquad (52)$$

where X_S and X_I were the x-coordinates in the seat axis system of the superior and inferior bones, respectively. Subscripts A and N were the ERECT-A and NEUTRAL positions, respectively. Each motion segment used similar equations to compute translations along the y and z axes.

First, the translations of the bone origins from ERECT-A to NEUTRAL and from NEUTRAL to SLUMP-M were calculated. The total translation was as the vectoral sum of the two motions. Tables 40 and 41 reported the average and standard deviation (±).

116

Translational motion in the sacro-iliac joint used analogous pointmarks on the joint surfaces of the sacrum (SACSIJRMML) and innominate bones (HIPSIJRMML and HIPSIJLMML) to compute the displacements reported in Table 42. The translations used equation (47) where the sacrum was the superior bone and the innominate was the inferior bone. The translations between ERECT-A and NEUTRAL and between NEUTRAL and SLUMP-M were calculated first. The Total in Table 42 was the vectoral sum of the two motions.

TABLE 40. Displacements (mm) of anatomical axis system origins from ERECT-A to SLUMP-M positions in the seat axis system.

	TOTAL			ERECT-A to NEUTRAL			NEUTRAL to SLUMP-M		
	X	Y	Z	X	Y	Z	X	Y	Z
C07	26.5	− 4.4	−29.6	12.3	1.6	0.9	17.7	− 6.7	−36.0
	±17.5	±16.6	±14.6	± 5.4	±10.5	± 3.5	±12.5	±23.5	±14.2
T01	24.5	− 3.8	−27.3	11.1	1.6	1.4	16.9	− 6.2	−34.1
	±16.6	±15.8	±14.0	± 4.6	±10.3	± 3.8	±12.5	±23.5	±14.7
T04	18.3	− 6.9	−25.8	3.5	2.1	5.6	14.9	− 9.3	−33.4
	± 9.9	±14.6	± 9.5	± 2.6	± 9.2	± 5.4	± 8.5	±20.7	±14.1
T08	− 1.5	− 6.3	−20.5	− 7.6	1.4	4.0	6.4	− 7.8	−25.4
	± 4.9	±12.4	±14.6	± 7.5	± 5.2	± 5.1	± 4.7	±17.3	±18.2
T12	−24.3	−11.9	−37.8	−25.6	− 2.1	2.9	1.7	−11.1	−36.9
	±15.7	± 7.6	±14.9	±13.5	± 3.0	± 2.8	± 6.1	± 8.2	±16.4
L01	−26.6	−11.2	−37.6	−26.3	− 3.1	− 4.0	0.7	− 7.8	−35.3
	±16.1	±10.2	±13.8	± 2.1	± 2.6	±15.5	± 7.7	± 9.6	±17.1
L02	−25.3	−11.4	−36.9	−25.8	− 2.9	− 3.7	1.9	− 8.2	−34.5
	±17.2	± 9.5	±16.7	±13.5	± 2.1	± 2.7	± 9.4	± 9.2	±17.5
L03	−18.9	−11.0	−33.7	−24.1	− 2.7	− 3.1	7.0	− 8.0	−31.9
	±16.8	± 9.2	±17.4	±12.9	± 1.9	± 2.8	±10.7	± 8.8	±17.9
L04	− 6.4	−10.3	−24.4	−21.1	− 2.0	− 2.2	16.7	− 8.1	−23.2
	±15.5	± 8.7	±16.4	±11.9	± 1.8	± 2.4	±12.0	± 7.9	±17.3
L05	9.8	− 9.0	−25.3	−16.8	− 1.3	− 1.8	28.0	− 7.8	−23.8
	±13.1	± 8.4	±18.0	±11.2	± 2.1	± 2.3	±10.6	± 7.4	±17.5
SAC	17.2	− 9.7	−27.5	−16.4	− 1.6	− 2.9	36.2	− 8.0	−25.4
	±12.4	± 6.7	±17.8	± 9.7	± 2.3	± 2.7	±13.9	± 6.1	±17.5
RInn	49.2	− 6.8	3.5	− 7.0	− 1.0	0.4	54.7	−15.2	2.0
	±15.7	± 9.6	±23.1	± 5.0	± 1.2	± 4.7	±15.7	± 8.5	±19.5
LInn	56.3	− 7.4	− 0.9	− 6.1	− 0.9	0.6	65.4	− 6.5	− 1.6
	±13.9	± 7.6	±24.4	± 4.8	± 1.0	± 3.8	±16.3	± 7.4	±22.2

TABLE 41. Translations (mm) between motion segments in the seat axis system from ERECT-A to SLUMP-M positions.

	TOTAL			ERECT-A to NEUTRAL			NEUTRAL to SLUMP-M		
	X	Y	Z	X	Y	Z	X	Y	Z
C07/T01	1.4	0.6	− 1.1	0.8	0.2	− 0.4	0.6	0.5	− 0.6
	± 0.9	± 1.6	± 1.3	± 0.6	± 0.8	± 0.9	± 0.9	± 0.9	± 0.6
T01/T04	8.8	1.9	− 4.5	4.6	0.4	− 1.1	3.5	1.4	− 3.3
	± 7.3	± 4.7	± 1.4	± 3.7	± 1.2	± 2.0	± 5.3	± 4.7	± 1.8
T04/T08	22.3	2.1	1.7	10.1	3.1	1.1	9.9	− 1.6	0.2
	±11.1	± 6.8	± 4.9	± 8.1	± 3.0	± 2.8	± 6.3	± 7.6	± 2.3
T08/T12	−24.4	− 3.4	12.0	11.8	0.9	5.7	14.8	− 4.6	5.0
	±13.7	± 5.4	± 6.1	±10.3	± 4.1	± 5.5	± 7.3	± 8.7	± 2.1
T12/L01	4.6	0.4	1.8	1.7	1.3	0.7	2.7	−1.1	− 1.1
	± 3.3	± 1.3	± 0.5	± 2.8	± 2.1	± 1.3	± 2.3	± 3.1	± 1.5
L01/L02	0.8	0.0	0.1	− 0.5	− 0.4	0.2	1.2	0.5	0.5
	± 1.3	± 2.0	± 1.9	± 1.9	± 1.2	± 0.9	± 2.5	± 1.3	± 1.3
L02/L03	− 3.3	− 1.0	− 1.0	− 0.9	− 0.7	− 0.1	− 2.2	− 0.3	− 0.8
	± 1.7	± 1.1	± 1.9	± 2.0	± 1.1	± 1.1	± 1.4	± 1.5	± 1.4
L03/L04	− 9.4	− 0.5	− 3.5	− 1.9	− 0.1	− 0.5	− 7.3	0.0	− 3.0
	± 2.1	± 1.2	± 1.4	± 2.0	± 0.9	± 0.6	± 1.7	± 1.3	± 1.6
L04/L05	−14.0	− 0.8	− 1.9	− 2.5	− 0.5	0.0	−11.1	− 0.2	− 1.9
	± 2.7	± 1.0	± 2.3	± 2.3	± 0.4	± 0.8	± 1.0	± 1.3	± 1.7
L05/S1	− 4.8	0.2	1.3	− 1.7	0.0	1.0	− 2.9	0.2	0.3
	± 3.1	± 1.8	± 1.8	±2.0	± 0.5	± 2.1	± 4.7	± 1.9	± 1.8
S1/RInn	−33.2	− 0.8	−19.8	− 4.0	− 0.1	− 2.8	−26.4	− 0.7	−16.2
	±15.9	± 2.6	±15.5	± 9.5	± 0.8	± 4.1	±11.4	± 2.8	±10.8
S1/LInn	−34.4	− 2.5	−22.5	− 5.6	− 0.2	− 2.8	−28.3	− 2.2	−19.4
	±11.9	± 3.3	±13.7	± 8.4	± 1.3	± 4.0	± 9.4	± 3.1	±10.5

Table 42. Translations (mm) in the seat axis system in the sacro-iliac joints.

	TOTAL			ERECT-A to NEUTRAL			NEUTRAL to SLUMP-M		
	X	Y	Z	X	Y	Z	X	Y	Z
Right SI Jt.	2.6	-0.5	-0.7	0.2	-0.1	0.8	3.6	-0.4	0.4
	±6.9	±0.8	±4.0	±3.3	±0.7	±2.2	±9.3	±1.3	±2.5
Left SI Jt.	2.9	0.3	1.1	0.0	0.1	0.4	2.9	0.1	0.5
	±3.8	±2.5	±1.8	±1.2	±1.1	±2.3	±4.3	±2.6	±2.1

120

DISCUSSION

Sitting positions, anatomical geometry and torso segments.

Erect, slumped, and side bent postures describe different seated positions. These descriptions form our typical postural vocabulary. However, they do not define the location or orientation of skeletal structures that transmit forces in these postures. The present investigation measured the three-dimensional locations of bones in the torso in ERECT, NEUTRAL, and SLUMP sitting positions.

Rigid body models are used in the definition of the location and orientation of skeletal structures in seated postures. Normally, adjacent body segments comprise links that are motion-segments. This approach is applied quite logically in the appendicular skeleton but the torso presents a different set of conditions. Ergonomic and biomechanical models have frequently simplified the torso into a few rigid body segments, such as head, neck, thorax and pelvis. This approach reduces the complexity of the twenty-three motion segments in the spinal column to a simpler model. It assumes that motions in the thoracic motion segments, such as seen between the eighth and ninth thoracic vertebrae, are negligible.

The representation of the torso must determine acceptable criteria for rigid body divisions into body segments. For example, if a rigid body segment, composed of a mass from joint center to adjacent joint center, is the fundamental unit of mechanical geometry, the chest as a rigid body segment may need redefinition. The chest has a complex linkage system represented by the vertebral motion segments. Anatomically, the motion segments in the thoracic vertebra have three "joints": an intervertebral disc and two apophyseal joints at the facets. Their motions in the sagittal plane, however, reduces to motion about an axis passing through the intervertebral disc.

121

The present investigation described the position of individual pointmarks in the spinal column and pelvis. The displacements between motion segments did not support a mechanical linkage system composed of large rigid body models representing unique positions if, the intervertebral motions in the thorax are of consequence in the design.

Skeletal components of the shoulder are the humerus, clavicle and scapula. These bones are joined at the gleno-humeral and acromio-clavicular joints. The shoulder is joined to the thorax at the scapulo-thoracic and sterno-clavicular joints. Targets on the right humerus, scapula, clavicle and sternum were measured. However, only the gleno-humeral joint was analyzed.

The thorax is composed of 12 vertebrae, 12 rib pairs and a sternum. If the rib and sternum connections are not considered, there are 35 motion-segments in the thorax. These motion-segments are 11 vertebra-vertebra and 24 rib-vertebra pairs. However, only the sternum, T1, T4, T8, and T12 were measured in the present study. In this investigation, thoracic motion-segments did not incorporate all 35 natural motion segments. For example, T1 and T4 formed a motion-segment in this study. This motion-segment included the T1/T2, T2/T3 and T3/T4 motion segments.

There are four motion-segments in the abdomen body segment. They are L1/L2, L2/L3, L3/L4, and L4/L5. L1 forms a motion-segment with T12. L5 forms a motion-segment with the sacrum. T12/L1 and L5/S1 are therefore considered as transitional motion-segments between the thorax, abdomen, and pelvis body segments.

The motion-segments in the pelvis are formed between two innominate bones, the sacrum and coccyx. The sacrum and coccyx are unique anatomical structures because they are fused spinal vertebrae. However, they complete the anatomical pelvis and transmit forces between the spinal column and pelvis through the sacroiliac joint and associated soft tissues. In the present investigation, the sacrum and coccyx were considered part of the

pelvis, although motions in lumbo-sacral and sacro-iliac joints were measured.

The positions of seated human posture are highly variable. Variation in sitting position comes from physical constraints of the environment, differences in anatomical geometry and willful behavior of the subject. The definition of anatomical geometry can serve as a major building block in the accurate simulation of the human torso. Geometry of the sitting environment constrains possible seated positions. The neuro-muscular system, utilizing both conscious and unconscious behaviors, controls the relative location of the rigid skeletal structures within these two constraints. An active neuro-muscular system and a subject's participation in the determination of the measured sitting position are important in any investigation of human posture. However, physical constraints and anatomical geometry are independent of the subject's active participation.

Åkerblom (Ref 2) pointed out that the Weber brothers in 1836 investigated the relative importance of joint ligaments in "locking of the joints" (p. 16) in erect standing. Thus, different roles between active and passive tissues have been recognized for many years. Their respective function in the maintenance and control of body positions also has long been recognized.

Seated postures are limited in large part by the physical properties of the musculo-skeletal system and geometry of the seat. The present investigation measured the locations of anatomical pointmarks in various sitting positions determined experimentally by the seat and anatomical geometry. The locations of bones and mass segments in different sitting positions were defined by the positions of comparable pointmarks on each bone. Thus, the position and orientation of the chest and pelvis were defined by anatomical axes systems.

The definition of these anatomical axes systems facilitates the measurement and description of the hip and shoulder joints. The location of the hip and shoulder joint centers in different

123

sitting positions assumes that these joints are suitably modeled as ball-and-socket joints.

Visual examination of the hip joint shows a large capsule described as a socket. The head of the femur very nearly approximates a ball. Figures 28-30 illustrate the locations of the hip joint center (HJC), the anterior superior iliac spine (ASIS), and pubic symphysis (PS). In ERECT-A, NEUTRAL, and SLUMP, the HJC is posterior to these anatomical pointmarks. It is anterior to Ischiale in ERECT-A and NEUTRAL.

The shoulder joint is not defined by skeletal structure as well as the hip joint in the pelvis. The shoulder depends in large part on soft tissue for its integrity. Thus, the measurement of the location of the shoulder joint requires more than fitting the socket with a hemisphere and calculating the location of its centroid in an anatomical axis system. The shoulder joint is inferior to Acromion, but superior to Suprasternale. In the present model, it is posterior to Acromion.

The sitting positions reported in Table 32 were selected because ERECT-A had a lumbar support at approximately the same location investigated by Andersson, et al (Ref 5) in living people. That is, Andersson investigated the geometry of the lumbar spine and pelvis with a lumbar support at -20, 0, +20 and +40 mm from the seat back. We measured ERECT-A position with the lumbar support at +47 mm (Table 16) and NEUTRAL with zero lumbar support. ERECT-A and SLUMP-M also were based on the largest sample sizes in their series.

A calculation of lumbar angle, computed similar to Andersson et al's (Ref 6) Total Lumbar Angle, revealed large differences from ERECT-D to SLUMP-O (Table 34). Total lumbar angle between L1 and the Sacrum was calculated by Andersson et al between lines representing the superior vertebral endplate of L1 and the endplate of the sacral base. The wedged shape of the L1 vertebral body made the present results approximately 5° larger than Andersson et al's results.

124

The locations of Ischiale and the sacrum (SAC) showed a large change in the direction and magnitude of the moment acting on the sacro-iliac joint. In the ERECT-A position, Ischiale was posterior to the sacrum. In the SLUMP-M position, Ischiale was anterior to the sacrum. Thus, the loads acting on the sacro-iliac joint were very different in the two positions.

Lastly, the curvature of the back in sitting postures describes the relative amount of stress on the soft tissues, including the intervertebral disk. The present investigation described the thoracic and lumbar curves in the sagittal plane.

Posture as a function of passive tissues.

The current investigation of posture in unembalmed cadavers assumes that the positions of the skeletal system are constrained primarily by skeletal morphology, joint capsular ligaments, and fascia. The effects of muscles and tendons in cadavers act through their myofascial sheaths and consequently respond as passive tissues. Comparable positions between subjects were selected on the basis of comparable pointmark measurements and seat geometry.

After selecting comparable body positions, the three-dimensional coordinate data were very consistent. Variation in subjects could be attributed to body size and temperature.

The effect of body size was not controlled, either experimentally or analytically. Thus, there was some variation, particularly in the location of the anatomical pointmarks, that was attributable to body size differences.

Internal temperature of the body was inconsistent between subjects. The effect of temperature upon the visco-elastic tissues of the body is well known. Subjects #1-3 remained in the radiographic laboratory until all data in the experimental series had been collected. Typically, the series of sitting postures from maximum ERECT to maximum SLUMP required a period of 8-10

hours to complete. For subjects #4-9, however, the body was refrigerated for 10-14 hours when a laboratory procedure extended to 6 hours.

As a result, the change in protocol between subjects #3 and #4 reduced the amount of time in which the body was available for experimental measurements probably reduced the maximum internal body temperature. If the temperature was significantly affected in this manner, the total amount of motion between thorax and pelvis was probably reduced. There was a decrease in torso angle reported in Table 36 that might be explained by this change in protocol.

There were no controls nor animal studies to determine the differences between living and dead tissues responses in sitting positions. Differences in torso angle might be attributed to variation as expected in a sample or a systematic change due to the probable reduction in maximum internal temperature.

Spinal geometry was highly dependent upon the passive structures of bone and ligament. Internally consistent data, however, were based on anatomical pointmarks, a very accurate roentgen stereophotogrammetry system, and carefully selected body positions for analysis.

Vertebral motion segments.

Motion in the vertebral motion segments was analyzed for sagittal plane movements of the torso, i.e. forward and backward bending. Bakke (Ref 8), Tanz (Ref 66), and Pearcy, Portek, and Shepherd (Ref 42) conducted radiographic investigations of lumbar motion in living subjects during forward and backward bending. Their results on living subjects described larger ranges of motion in the lumbar spine than measured in these unembalmed cadavers. Differences between living and cadaveric subjects were expected. In general, the differences were small and the average of the current sample fell within the range of the living

subjects. As mentioned previously, this decrease in lumbar motion segment range of motion might be attributable to core temperature, rigor mortis, and physical constraints of the seat and radiographic procedure.

The present investigation measured the spinal column from C07 to the pelvis and calculated motions between segments. Patterns of movement could be identified for each bone and motion segment in the spinal column. The pattern of movement could be described by both the direction of motion and the magnitude of motion.

In general, there were two distinct patterns. First, the upper thorax from C7 through T4 moved anteriorly from the maximum ERECT to the maximum SLUMP position. The motion was largest from NEUTRAL to SLUMP, but it was positive in the x direction throughout the change in posture. Second, from T8 through the pelvis, motion from maximum ERECT to NEUTRAL was rearward, or negative on the x axis, and forward from NEUTRAL to maximum SLUMP. Two regions of movement were related to change in seated posture.

When rotations and translations in the local motion segments from ERECT to NEUTRAL and NEUTRAL to SLUMP were examined, similar patterns were seen. There was little difference in the angular displacement when changing from ERECT to NEUTRAL, but the largest change occurred when moving from NEUTRAL to SLUMP. In this last change of position, the pelvis was moved forward but rotated rearward. Thus, the change of angular position in the lumbar and lower thoracic vertebrae were determined in large part by the location of the pelvis.

When the displacements were examined from maximum ERECT to NEUTRAL, the magnitude and direction of the displacements were different. Table 37 showed that the displacements in the x axis are small, ranging from -6.1 mm for the right hip to -26.3 mm for the first lumbar vertebra (L01). There was a pattern of movement in the displacements as the largest displacements occurred in the lumbar vertebrae in a rearward direction while the upper thoracic

127

vertebrae moved forward. In Table 37, the displacements from NEUTRAL to SLUMP changed the pattern to a forward movement for all bones in the spinal column and a downward movement of the body.

Translations in the thoracic motion segments were not representative of the results between motion segments defined by two adjacent bones. The motion segments, T01/T04, T04/T08, and T08/T12 were anomalous because they represented the combined motions of several motion segments. Thus, the large translations, for example -24.4 mm within T08/T12 and 22.3 mm within T04/T08, were unique to the definition of thoracic motion segments in this investigation.

In the lumbar motion segments, the largest linear displacement was within the L04/L05 motion segment. It was a -x displacement of L04 from L05. The next largest translation occurred within the L03/L04 motion segment in the x direction. Along the z axis, where a negative sign indicated that the superior bone moved downward towards the inferior bone of the motion segment, the L03/L04 motion segment had the largest translation. In general, the translations in the lumbar motion segments along the y-axis were no greater than a millimeter.

Of particular interest, however, were the sacro-iliac joints represented by S1/RInn and S1/LInn motion segments. In Table 38, the translation was reported between points defined by the origin of the respective axes systems in the three bones. The motion between these points was magnified by their distance from the axis of rotation. That is, the origin of the pelvic axis system lay on a line passing through the anterior and posterior superior iliac spines. The origin of the sacrum axis system lay at the base of the sacrum. A more representative pointmark for translation in the sacro-iliac joint was at the intersection of the inferior and superior poles of the sacro-iliac joint. On the sacrum, these pointmarks were SACIJLMML (1150) and SACIJRMML (1140). On the innominate, these pointmarks were HIPSIJLMML

128

(0970) and HIPSIJRMML (1070). Utilizing equation 47, the translations in the sacro-iliac joints were computed (Table 43).

The pelvis controls lumbar curvature (Ref 52, 2, 28). A lordotic lumbar spine is produced by an upright, forwardly rotated pelvis. The converse, a rearward rotated pelvis, produces a kyphotic lumbar spine. These data described this observation in three-dimensional space. The previously noted pattern of movement in the thorax indicated that the thorax was part of this coupling behavior. That is, the lumbar motion segments in the human body were controlled by the location of the pelvis and thorax.

Thorax and pelvis as rigid bodies.

The thorax and pelvis are considered rigid bodies in mass distribution (Ref 36) and seating (Ref 30) models of the human body. The reduction of the torso to two segments simplifies the linkage system immeasurably. For example, a rigid thorax and pelvis rotates around two parallel axes. For flexion and extension, then the mechanical linkage in the lumbar spine is reduced to a linear function like torso angle. Thus, changes in the torso from ERECT to SLUMP positions can be reduced from a positive thoracic rotation and a negative pelvic rotation to a single angle.

In this model of a rigid thorax and pelvis, the lumbar linkage system depends on the positions of the thorax and pelvis. Theoretically, by controlling the locations of the thorax and pelvis, the configuration of the lumbar spine can be determined.

In the present investigation, the assumption of rigidity in the thorax and pelvis was examined. Results of the triad of pointmarks in the thorax selected axis system definition suggested that Suprasternale, T01, and T12 described a rigid body. However, when local motions between thoracic vertebrae were examined, the rigidity of the thorax was questionable.

129

There are 1° to 2° rotations but 8 to 24 mm translations (Tables 39 and 42) between motion segments analyzed in the thorax. In addition, the thoracic radius of curvature (Table 31) increased 12% from ERECT-A to SLUMP-M. In the lumbar, the corresponding change was 167%. Reference to the three SLUMP curves in Figure 23 suggested that a rigid thoracic model may fit better in the upper than lower thorax.

The pelvis, in contrast to the thorax, has fewer joints to be considered. However, if there is motion in the sacro-iliac joints and pubic symphysis, the assumption of a rigid pelvis is violated. The sacro-iliac joint has been investigated recently by Lavignolle et al (Ref 33), Scholten et al (Ref 55), and Sturesson, et al (Ref 64). These investigations demonstrated movements in the sacro-iliac joint. In addition, Drerup and Hierholzer (Ref 20) found that the pelvis is not rigid due to torsional rotations of the innominate bones when the sacro-iliac joint is loaded asymmetrically. In the present investigation, however, the seated center of gravity lay midway between the ischial tuberosities. Thus, the loading of the sacro-iliac joint was symmetrical in the sagittal plane, and the motions in the sacro-iliac joint were symmetrical. Motion in the pubic symphysis was negligible. Thus, the sacro-iliac joint moved because of symmetrical spinal loads.

There was greater angular displacement of the sacrum than in either the right or left innominates in the ERECT positions (Table 34). The data were unclear in the SLUMP positions because of the large difference in sample size between the right and left innominates. The assumption of a rigid pelvis for a pelvic axis system might be compromised in side-bending because of asymmetrical loading of the sacro-iliac joints.

Shoulder and hip as ball-and-socket joints.

The model of the shoulder used in this investigation was a better _in-vivo_ model than _in-situ_ model. In the present investigation, the shoulder joint, i.e. the gleno-humeral joint, is held in position by passive soft tissue. As a result, the geometry of the shoulder joint center is highly responsive to load since there are no neuro-muscular constraints.

Experimentally, the load acting on the shoulder joint was larger at the initial and final measurement positions. The load was not measured, but the arm was weighted by gravity and the cuff in the initial position. In the final position, the limit of pull on the arm was determined by the weight of the body. Consequently, the spherical surface might have had a greater radius of curvature in the initial and final positions than the remainder of the arm measurements.

Unlike the shoulder, the pelvis has a rigid skeletal structure that determines the shape and load-bearing quality of the hip joint. A previous three-dimensional study was used to determine the location of the hip joint center. Although the femoral head does not have perfect sphericity (Ref 14), fitting the acetabulum with an optimally-sized hemisphere defines a reasonable approximation of the centroid of the femoral head. The investigation of pelvic geometry, (Ref 53), utilized hemispheres that were available for the current investigation. Thus, the location of the hip joint center was represented by the center of a ball-and-socket joint.

Spinal curvature.

The s-shaped curvature of the spinal column and problems of back pain have long been attributed to the erect standing posture of modern man (Ref 24). Reynolds and Lovett (Ref 52) pointed out the importance of pelvic orientation on lumbar curvature. Keegan

(Ref 29) recorded lumbar curvature in various postures. However, one of the most interesting questions in recent years has been directed at the change of curvature from standing to sitting. The present investigation calculated the location of the center and radius of curvature in the lumbar and thoracic regions of the spinal column.

An initial goal for this research was to define an initial body position for mathematical models of seated posture. Investigators have studied this problem in the standing position since Braune and Fischer's "normal stellung" in 1892 (Ref 12). Subsequently, physicians and scientists have assumed "normal stellung" is the best posture for the human body. Hellebrandt and Franseen (Ref 24) argued against this assumption, but designers have continued to believe there is a best spinal posture. This belief has led to the widespread assumption that lumbar-supported seats are the best. This is based, primarily, upon data from Nachemson and Elfström (Ref 38) that demonstrate reduced intervertebral pressures in the erect standing posture. Many designers based specifications on the belief that people should sit with a spinal curvature like the curvature in their erect standing posture. This investigation has developed a set of curves that can be used to test this assumption.

Biomechanical research investigations study spinal motion segments and load transmission across the facets and through the disc because of the association between mechanical function of the spinal motion segments and low back pain (Ref 22, 1). The mechanical properties of anatomical structures in the spinal column have been well investigated. However, the properties of the in vitro spinal motion segment also must be understood within the context of the total spinal column. The objective in this investigation was, therefore, to develop a set of accurate data describing spinal geometry in seated positions. Thus, the effects of spinal position and body segment orientation on load transmission and injury to the spine can be more accurately simulated with mathematical models.

132

The use of roentgen-stereophotogrammetry for three-dimensional anthropometry.

Various research groups in the United States and Europe have made impressive progress by applying roentgen stereophotogrammetry to the study of human skeletal position and mobility. The most widely used three-dimensional radiographic technique in the United States is the orthogonal technique developed by Brown (Ref 13). In Brown's technique, vertebral position and motion are studied using anatomical landmarks identified on antero-posterior and lateral roentgenograms. This procedure uses skeletal morphology to identify film targets.

Rab and Chao (Ref 46) compared the accuracy of untargeted landmark measurements from Brown's orthogonal method with caliper measurements on dissected material. The accuracy of the inter-landmark distances is 3.5-4.0 mm. Stokes et al (Ref 62) used the same method with nine anatomical landmarks per vertebra. Stokes et al calculated a standard error of 1.4-2.7 mm for facet joint motion and 1.53 mm for disc motion. More recently, Pearcy et al (Ref 42) developed an x-ray measurement system. He used anatomical landmarks capable of measuring translations with rms error less than ± 2 mm and rotations with less than $\pm 1.5°$ rms error.

The roentgen stereophotogrammetric technique has been developed extensively at the University of Lund in Sweden by Selvik and co-workers (Ref 57). Selvik uses small tantalum balls implanted (Ref 7) for measurement targets. Inter-target distances with Selvik's methodology have an rms error of approximately 0.1 mm. Other investigators (Ref 69, 68, 21) report a roentgen stereophotogrammetric accuracy with small balls of 0.1-0.4 mm.

Roentgen stereophotogrammetry in the SAL (Ref 50) digitizes tungsten-carbide balls as targets. In a typical SAL experiment, such as measuring lumbar spine motion, the errors in distance measurements range from 0.1 to 0.4 mm (Tables 3 and 4). When

data were compared between different experiments, the errors in three-dimensional coordinate accuracy were slightly greater in the x direction, but similar in the y and z directions (Table 5). However, the effects of these systematic errors partially cancel when the inter-target distances were calculated.

When data were transformed from the laboratory to the seat axis system, the effect of these errors was reduced. The SRP origin in the laboratory axis system had approximately the same magnitude in the x direction as the pointmarks on the bones. In summary, the accuracy of inter-target distances in the SAL was similar to other laboratory investigations.

Physical condition of the subjects

In the present investigation, the intact, unembalmed cadaver was the subject of study. The use of unembalmed cadavers presented unusual problems because rigor mortis restrains joint mobility and body segment position. To eliminate the effects of rigor mortis in each subject, all major joints were passively moved through their ranges of motion in the cardinal planes of motion. For example, the torso was flexed from a supine position until the back, neck and head were in a maximum kyphotic posture. As a result of this passive musculo-skeletal exercise, the subject was flexible and difficult to control.

Following the initial conditioning of each subject, a physician performed a musculo-skeletal physical examination. Since the study was conducted to identify specific posture positions for mathematical models of spinal geometry, a physical examination described the condition of the body. The results surprised the physicians because they found similar palpatory results to those observed in living patients. Although several physicians participated in the project, most cadavers were examined by one physician. As he became more experienced, the data became more exhaustive. However, in the reports of Section

134

4.2, there were some unique observations in the lumbar vertebrae. The description of alternating prominent transverse processes or tissue texture abnormalities is difficult to explain and is related to a clinical model the physician uses.

In general, however, the results of the examinations described typical musculo-skeletal systems for the age and sex of the sample. No asymmetries in the palpatory examinations were found that were not observed in asymptomatic males of comparable age in the general population. When the physical examination, osteology, and disc degeneration results were combined, the highest frequency and most severe findings were observed in the oldest subject, #5. A linear relationship between severity of musculo-skeletal problems and age was observed. Subjects #6 and 8, the second and third oldest at 77 and 70 years of age, had either significant disc degeneration (3 on a 4 point scale) or significant osteoarthritis. Subjects #1-4, and #7 had no remarkable musculo-skeletal problems. Subject #9 died from head injuries suffered in an automobile accident and had a spondylolisthesis at L05. Thus, this sample appeared to be a reasonable representation of a wide cross-section of the general, non-institutionalized adult male population.

A note of caution in interpreting the results of the physicians was needed, however. Since the cadavers could not respond to applied loads, the observations were based on what he felt in the cadaver. Furthermore, these observations must be interpreted solely for passive tissues, i.e. fascia, tendons, ligaments and bones. In addition, the remaining effects of rigor mortis in each cadaver were unknown. Most, if not all, of the rigor mortis present initially in the subjects was removed during the radiographic measurements. This opinion, however, was not based upon scientific measurements.

Osteometrics and the general nature of the skeletal system.

Previous studies of spinal vertebral morphology concentrated on specific aspects of morphology such as vertebral dimensions in the sagittal plane (Ref 26, 39) and the morphometrics of pedicles, facets and vertebral canals (Ref 73, 17, 3). Berry, et al. (Ref 11) extensively measured the entire vertebra, but pathology-affected vertebrae were not included in the study. Conversely, other researchers usually considered only pathologies and age changes in the vertebral column (Ref 65, 54, 34). The purpose of the measurements in the present study was to characterize the general patho-anatomical status of the vertebrae in the sample.

Osteometrics. The height of the vertebral body gradually increased from C7 to L3 in anterior, middle and posterior heights. The largest increases occured between T8 and T12 and again at the level of L5-S1. Decreases in body height were noted from L3-L5 in the posterior and middle dimensions while a gradual increase continued in the anterior direction. Posterior height was 1 mm greater than anterior height from C7-L3.

Sagittal diameters displayed an increase from C7 to L5 with the largest increase occurring between T1 and T5. Here, an average increase of 12 mm was observed for all dimensions (superior, middle, posterior). A rapid decrease in diameter occurred from L5 to S1 in all three dimensions. Superior and inferior dimensions were virtually the same (within 0.5 mm) from C7-L5.

The transverse diameter increased from C7 to L5 with the most rapid increase occurring between T4 and T12 (average increase 17 mm). Middle and inferior transverse diameters exhibited reductions in size for S1.

The sagittal diameter of the spinal canal remained constant. From C7 to T4 the dimension increased 2.6 mm, but remained constant (± 1 mm) from T4 to S1. The data for the transverse diameter of the spinal canal were less constant than in the

136

sagittal direction. From C7 to T4 the transverse diameter decreased 7.9 mm, remained steady at T8, then increased 15.6 mm to S1. From T8 to L4 a slight increase of 6.5 mm occurred, but L4 to S1 increased 8.1 mm.

Spinous process length increased from C7 to T8. From T8 to T12, length decreased 15 mm. This trend then reversed; increasing to the level of L3 and again decreasing from L3 to L5. The angle of the spinous process data displayed nearly opposite results to those of spinous process length. From C7 to T8 spinous process angle decreased approximately 17° before an increase of 45° was observed between T8 and T12. From T12 to L5 a more gradual decrease in angle occurred.

The superior facet angles ranged from -25.5° to 66.7°. From C7 to T8 the superior facet angle had a slight medial inclination of -9.7° and rotated gradually to -21.3°. At T12 a marked increase was observed as the average angle rose to 16.6°. L1 demonstrated an equally large increase with the average angle being 65.2°. Lumbar vertebrae averaged a decrease in facet angle of 4.7° from the inferior vertebrae of each motion segment pair.

Extraosseous development. Osteophytic lipping was most extensive on the anterior halves of affected vertebrae (sections III-VII). Lumbar vertebrae had the most osteophytes. L3 and L4 had the most and the longest osteophytes. The cervical vertebrae, represented by C7, were next in frequency and severity. They were affected primarily on the superior surface. The inferior surface of C7 displayed only minimal osteophytes and was surpassed in frequency and size by the thoracic region. The most significant development of osteophytes in the thoracic region occurred at T8. In sections V and VI the mean length of osteophytes increased abruptly, making these growths some of the largest in the spine. Overall, osteophytes on the superior surface were an average 30% longer than those on the inferior surface.

Osteophyte development on the articular facets displayed a similar pattern to that of osteophytic lipping on vertebral

137

bodies. Superior facets had larger osteophytes than those on
inferior facets. However, in this instance the average
difference was only 8%. An exception was present in the thoracic
region where inferior facets contained osteophytes that were 21%
larger than those of the superior surface. The lumbar facets had
the largest osteophytes. Cervical facets had the second largest
spicules while those on the thoracic facets were 54% and 41%
smaller than lumbar and cervical facet osteophytes respectively.

Ossification in the region of the ligamenta flava
demonstrated an interesting pattern that had not been discussed
in previous patterns of extraosseous growth. The unique aspect
of these osteophytes was that the thoracic vertebrae were
affected much more frequently by larger bone spicules than any
other region of the skeletal spine (77% and 61% larger than those
of lumbar and cervical regions, respectively). As with previous
observations, the pathologies on the superior portion of the bone
were significantly more severe than their counterparts on the
inferior side.

Thoracic vertebrae were also more affected by ossification
of the anterior longitudinal ligament than either cervical or
lumbar vertebrae. In the thoracic vertebrae, 16 of 32 displayed
some ossification of the anterior longitudinal ligament. Three
thoracic vertebrae had complete ossification of the ligament
(i.e. ossified ligament ran the length of the vertebral body).
Of seven C7's only one was partially ossified.

CONCLUSION

In conclusion, the present investigation measured the positions and motions of the torso body segments and local motion segments in three-dimensional space. The nine unembalmed cadavers exhibited less total motion than other researchers observed. However, differences between age and body posture and between _in vivo_ and _in situ_ measurements, made the results difficult to compare. In general, joint motions were less in sitting positions than in standing positions. These subjects had motion characteristics that were within the range described by White and Panjabi (Ref 71).

Predictable movement patterns were associated with torso flexion. The translation within the local motion segments was clearly coupled with the rotation of the vertebral bodies when the seated position was flexed. Furthermore, there were also motions representative of compressive and lateral shear forces acting on the flexed spinal column.

Of particular interest to seat design was the observation that the center of gravity changed its position relative to the ischial tuberosities. In the ERECT position, the center of gravity was clearly acting to rotate the pelvis forward thereby helping create a lordotic lumbar spine. However, in the SLUMP position, the center of gravity shifted rearward producing a moment on the pelvis that flattened the lumbar spine if no muscle activity in, for example, the iliopsoas muscle stabilized it.

In summary, the present investigation established a new set of three-dimensional anthropometric positions that could be used in mathematical modeling of the load transmission through the seated spine to increase our understanding of spinal kinematics.

REFERENCES

1. Adams, M. A. and Hutton, W. C., 1985, "The effect of posture on the lumbar spine," J. Bone & Joint Surg., 67-B(4):625-629.

2. Åkerblom, B., 1948, Standing and Sitting Posture with Special Reference to the Construction of Chairs (Translated by Ann Synge), Stockholm, A. B. Nordiska Bokhandeln.

3. Amonoo-Kuofi, H. S., 1985, "The sagittal diameter of the lumbar vertebral canal in normal adult Nigerians," J. Anat., 14:69-78.

4. Anderson, J. A. D. and Sweetman, B. J., 1975, "A combined flexi-rule/hydrogoniometer for measurement of lumbar spine and its sagittal movement.," Rheum. & Rehab. 14:173-179.

5..Andersson, B. J. G., Örtengren, R., Nachemson, A., and Elfström, G., 1974, "Lumbar disk pressure and myoelectric back muscle activity during sitting. I. Studies on an Experimental Chair," Scand J. Rehab Med 6:104-114.

6. Andersson, G. B. J., Murphy R. W.,Örtengren R., and Nachemson A. L., 1979, "The influence of backrest inclination and lumbar support on lumbar lordosis," Spine 4(1):52-58.

7. Aronson, A. S., Holst, L., and Selvik, G., 1974, "An instrument for insertion of radiopaque bone markers," Radiol. 113,733-734.

8. Bakke, S., 1931, "Röntgenologische Beobachtungen über die Bewegungen der Wirbelsäule", Acta Radiol., Suppl. 13, 75p.

9. Belytschko, T., Schwer, L., and Schultz, A. B., 1976, "A model for analytic investigation of three-dimensional head-spine dynamics," AMRL-TR-76-10, Aerospace Medical Research Laboratory, Wright-Patterson Air Force Base, Ohio.

10. Bendix, T., 1987, "Adjustment of the seated workplace - with special reference to heights and inclination of seat and table," Laegeforeningens Forlag, Kobenhavns Universitet.

11. Berry, J. L., Moran, J. M., Berg, W. S., Steffee, A. D., 1987, "A morphometric study of human lumbar and selected thoracic vertebrae," Spine 12:362-367.

12. Braune, W. and Fischer, O., 1892, "Bestimmung der Tragheitsmomente des menschlichen Korpers and seiner Glieder," Abh. d. Math. Phys. Cl. d. K. Sachs. Gesell. d. Wiss. 18(8):409-492.

13. Brown, R. H., Burstein, A. H., Nash, C. L., and Schodk, C. C., 1976, "Spinal analysis using a three-dimensional radiographic technique," <u>J. Biomech.</u> 9,355-365.

14. Clarke, E. C., Fiske, C. and Amstutz, H. C., 1979, "Spherometer measurements of human hip-joint geometry," <u>Med & Biol Eng & Comput.</u> 17:155-160.

15. Clauser, C. E., McConville, J. T., and Young, J. W., 1969, "Weight, Volume, and Center of Mass of Segments of the Human Body," AMRL-TR-69-70, Aerospace Medical Research Laboratory, Wright-Patterson Air Force Base, Ohio.

16. Chubb, R. M., Detrick, W. R., and Shannon, R. H., 1965, "Compression fractures of the spine during USAF ejections," <u>Aerosp. Med</u>. 36:968-972.

17. Davis, P. R., 1959, "The medial inclination of the human thoracic intervertebral articular facets," <u>J. Anat.</u> 93:68-74.

18. Dempster, W. T., 1955, "Space requirements of the seated operator," WADC-TR-55-159, Wright Air Development Center, Ohio.

19. Dempster, W. T., Sherr, L. A., and Priest, J. G., 1964 "Conversion scales for estimating humeral and femoral lengths and the lengths of functional segments in the limbs of american caucasoid males," <u>Human Biology</u>, 36(3):246-262.

20. Drerup, B. and Hierholzer, E., 1987, "Movement of the human pelvis and displacement of related anatomical landmarks on the body surface," <u>J Biomech.</u> 20(10):971-977.

21. Fraser, C. S. and Abdullah, Q. A., 1981, "Simplified mathematical model for applications of analytical x-ray photogrammetry in orthopaedics," <u>Photogram. Eng. & Remote Sensing</u> 47(5),641-646.

22. Gracovetsky, S. and Farfan, H., 1986, "The Optimum Spine," <u>Spine</u> 11(6):543-573.

23. Green, D. L., Bahnuik, E., Liebelt, R. A., Fender, E., and Mirkow, P., 1983, "Biplane radiographic measurements of reversible displacement (including clinical loosening) and migration of total joint replacements," <u>J. Bone & Jt. Surg.</u> 65-A(8),1134-1144.

24. Hellebrandt, F. A. and Franseen, E. B., 1943, "Physiological study of vertical stance of man," <u>Phsiol. Rev.</u> 23:200-255.

25. Henzel, J., 1966, "The human spinal column and upward ejection acceleration," AMRL-TR-66-233, Aerospace Medical Research Laboratory, Wright-Patterson Air Force Base, Ohio.

26. Katz, P. R., Reynolds, H. M., Foust, D. R., Baum, J. K., 1975, "Midsagittal dimensions of cervical vertebral bodies," <u>Am. J. Phys. Anthrop.</u> 43:319-326.

27. Kazarian, L. E., 1978, "Identification and classification of vertebral fractures following emergency capsule egress from military aircraft," <u>Aviat. Sp. & Environ. Med.</u> 49:150-157.

28. Kärrholm, J., Hansson, L. I., Laurin, S., and Selvik, G., 1983, "Post-traumatic growth disturbance of the ankle treated by the Langenskiold procedure," <u>Acta Orthop. Scand.</u> 54,721-729.

29. Keegan, J. J., 1953, "Alterations of the lumbar curve related to posture and seating," <u>J Bone & Jt Surg</u> 35A(3):589-603.

30. Kohara, J. and Sugie, T., 1972, 'Development of biomechanical manikins for measuring seat comfort," SAE 720006, Society of Automotive Engineers, New York.

31. Kohara, J., S. Ucheida, and H. Uemo, 1979, "<u>Architecture, Interior and Human Factors Engineering,</u>" [In Japanese] Tokyo, Kashima Publ. Co.

32. Kratky, V., 1975, "Analytical x-ray photogrammetry in scoliosis," <u>Photogram.</u> 31,195-210.

33. Lavignolle, B., Vital, J. M., Senegas, J., Destandau, J., Toson, B., Bouyx, P., Morlier, P., Delorme, G., and Calabet, A., 1983, "An approach to the functional anatomy of the sacroiliac joints in vivo," <u>Anat. Clin.</u> 5:169-176.

34. Malmivaara, A., Videman, T., Kuosma, E., Troup, J. D. G., 1987, "Facet joint orientation, facet and costovertebral joint osteoarthrosis, disc degeneration, vertebral body osteophytosis, and Schmorl's nodes in the thoracolumbar junctional region of cadaveric spines," <u>Spine</u> 12:458-463.

35. Marcus, J. H., 1980, "The accuracy of screw axis analysis using position data from anatomical motion studies," M.S. Thesis, Department of Mechanical Engineering, Michigan State University.

36. McConvillle, J. T., Churchill, T. D., Kaleps, I., Clauser, C. E., Cuzzi, J., 1980, "Anthropometric relationships of body and body segment moments of inertia," AFAMRL-TR-80-119, Air Force Aerospace Medical Research Laboratory, Wright-Patterson Air Force Base, Ohio.

37. Mohr, G. D., Brinkley, J. W., Kazarian, L. E. and Millard, W. W., 1969, "Variations of spinal alignment in egress systems and their effect," <u>Aerosp. Med.</u> 39:983-988.

142

38. Nachemson, A. and Elfström, G., 1970, "Intravital dynamic pressure measurements in lumbar discs," Scand J Rehab Med Suppl 1, 104 pp.

39. Nissan, M., Gilad, I., 1986, "Dimensions of human lumbar vertebrae in the sagittal plane," J. Biomech 19:753-758.

40. Olsson, T. H., Selvik, G., and Willner, S., 1977, "Mobility in the lumbosacral spine after fusion studied with the aid of roentgen stereophotogrammetry," Clin. Orthop. & Rel. Res. 129,181-190.

41. Panjabi, M. M., Brand, Jr., R. A., and White III, A. A., 1976, "Three-dimensional flexibility and stiffness properties of the human thoracic spine," J. Biomech. 9:185-192.

42. Pearcy, M., Portek, I., and Shepherd, J., 1984, "Three-Dimensional X-Ray Analysis of Normal Movement in the Lumbar Spine," Spine 9(3),294-297.

43. Plesha, M. and Belytschko, T., 1981, "Analysis of vertebral stress distribution and ejection-related injury mechanisms," AMRL-TR-80-67, Aerospace Medical Research Laboratory, Wright-Patterson Air Force Base, Ohio.

44. Pope, M. H., Wilder, D. G., Matteri, R. E., and Frymoyer, J. W., 1977, "Experimental measurements of vertebral motion under load," Orthop. Clin. of N. Amer. 8(1):155-166.

45. Press, W. H., Flannery, B. P., Tejkolsky, S. A., and Vetterling, W. T., 1989, Numerical Recipes: The Art of Scientific Computing, Cambridge University Press, New York.

46. Rab, G. T. and Chao, E. Y., 1977, "Verification of roentgenographic landmarks in the lumbar spine," Spine 2(4),287-293.

47. Rebiffé, R., 1980, "General reflections on the postural comfort of the driver and passengers; consequences on seat design," pp 240-248. In: Oborne, D.H. and Levis, J.A. (eds); Human Factors in Transport Research, Vol. 2, Academic Press, London.

48. Reynolds, H. M., Hallgren, R., and Marcus, J., 1982, "Systems Anthropometry: Development of a stereoradiographic measurement system," J. Biomech. 15(4),229-233.

49. Reynolds, H. M., Hubbard, R. P., Freeman, J. R., and Marcus, J., 1979, "A Foundation for Systems Anthropometry, Phase III," Annual Report, Contract F49620-78-C-0012, Air Force Office of Scientific Research (NL), Bolling AFB, DC 20332.

50. Reynolds, H. M. and Leung, S. C., 1983, "A Foundation for Systems Anthropometry: Lumbar/Pelvic Kinematics," AFAMRL-TR-83-016, Aerospace Medical Research Laboratory, Wright-Patterson Air Force Base, Ohio.

51. Reynolds, H. M., Leung, S. C., and Kincaid II, V., 1985, "The Position and Mobility of the Shoulder, Spinal Column, and Pelvis in Seated Subjects," AFAMRL-TR-84-060, Aerospace Medical Research Laboratory, Wright-Patterson Air Force Base, Ohio.

52. Reynolds, E. and Lovett, R., 1909, "A method of determining the position of the centre of gravity in its relation to certain landmarks in the erect position," Am J Physiol 24:286-293.

53. Reynolds, H. M., Snow, C. C., and Young, J., 1981, "Spatial Geometry of the Human Pelvis," AAC-119-81-5, Civil Aeromedical Insitute, Federal Aviation Administration, Oklahoma.

54. Saluja, G., Fitzpatrick, K., Bruce, M., Cross, J., 1986, "Schmorl's nodes (intravertebral herniations of intervertebral disc tissue) in two historic British populations," J. Anat. 145:87-96.

55. Scholten, P. J. M., Schultz, A. B., Luchies, C. W., and Miller, J. A. A., 1988, "Motions and loads within the human pelvis: A biomechanical model study," J. Orthop. Res. 6(6):840-850.

56. Selvik, G., 1974, "A roentgen stereophotogrammetric method for the study of the kinematics of the skeletal system," Thesis, University of Lund, Sweden.

57. Selvik, G., Alberius, P., and Aronson, A. S., 1983, "A roentgen stereo-photogrammetric system," Acta Rad. Diag. 24(4),343-352.

58. Singh, I. and Bhasin, M. H., 1968, "Anthropometry," Bharti Bhawan, Dehli, India.

59. Snyder, R. G., Chaffin, D. B., and Schutz, R. K., 1972, "Link system of the human torso," AMRL-TR-71-88, Aerospace Medical Research Laboratory, Wright-Patterson Air Force Base, Ohio.

60. Staffel, F., 1884, "Zur Hygiene des Sitzens," Zbl. f. allg. Gesundheitspflege, Vol. 3, pp 403-421.

61. Staffel, F., 1889, "Die menschlichen Haltungstypen und ihre Beziehungen zu Rückgratsverkrümmungen," Wiesbaden.

62. Stokes, I. A. F., Wilder, D. G., Frymoyer, J. W., and Pope, M. H., 1981, "Assessment of Patients with Low-Back Pain by

144

Biplanar Radiographic Measurement of Intervertebral Motion,"
Spine 6(3),233-240.

63. Strasser, H., 1913, "Lehrbuch der Muskel- und
Gelenkmechanik, Vol. 2, Chapter VI: Die Rumpfhaltungen, pp 244-
320, Berlin.

64. Sturesson, B., Selvik, G., and UdÅn, A., 1989, "Movements of
the sacroiliac joints: A roentgen stereophotogrammetric
analysis," Spine 14(2):162-165.

65. Swedborg, I., 1974, "Degenerative changes of the human spine
- a study on dried macerated skeletons," Karolinska Hospital and
University of Stockholm, Stockholm, Sweden.

66. Tanz, S. S., 1953, "Motion of the lumbar spine - a
roentgenologic study," J Roentgen. 69(3):399-412.

67. Terry, R. J., 1940, "On measuring and photographing the
cadaver," Am J Phys Anthropol, 26:433-447.

68. Thurson, A. J. and Harris, J. D., 1983, "Normal kinematics
of the lumbar spine and pelvis," Spine 8(2):199-205.

69. Veress, S. A., Lippert III, F. G., Takamoto, T., 1977, "An
analytical approach to x-ray photogrammetry," Photogram. Eng. &
Remote Sensing 43(12),1503-1510.

70. Veress, S. A., Lippert, F. G., Hou, M. C. Y., Takamoto, T.,
1979, "Patellar tracking patterns measurement by analytical x-ray
photogrammetry," J. Biomech. 12,639-650.

71. White III, A. A. and Panjabi, M. M., 1978, Clinical
Biomechanics of the Spine, J. B. Lippincott Co., Philadelphia.

72. Woodburne, R. T., 1973, Essentials of Human Anatomy, Fifth
Edition,,Oxford University Press, New York.

73. Zindrick, M., Wiltse, L. L., Doornik, A., Widell, E. H.,
Knight, G. H., Patwardhan, A. G., Thomas, J. C., Rothman, S. L.
Fields, B. T., 1987, "Analysis of the morphometric
characteristics of the thoracic and lumbar pedicles," Spine
12:160-166.

Appendix A

Cadaver Anthropometry by Subject

Body Wt. in kg, all other dimensions in mm.

Cadaver	21	22	23	24	25	26	27	28	29
Body Wt.	61.45	67.25	65.40	45.75	52.00	61.00	83.35	58.55	65.40
Head-to-									
Heel L	1,731	1,837	1,765	1,708	1,633	1,747	1,779	1,767	1,781
R	1,738	1,829	1,771	1,707	1,636	1,747	1,776	1,780	1,772
Aver.	1,735	1,833	1,768	1,708	1,635	1,747	1,778	1,774	1,777
Troch L	856			867	787	842	849	820	860
R	866			850	792	840	846	815	859
Aver.	861			859	790	841	848	818	860
Pubic Symph	851			863	813	871	861	838	882
Supra-sternale	331			333	299	326	326	324	354
Suprasternale-									
Symph	520	571	526	530	514	545	535	514	528
Bispin B.		257	231	249	214	268	221	235	213
Acromion-									
Radiale R		353	326	327	328	330	335	355	345
Radiale-									
Stylion R				237	242	276	276	283	272
Seated Height				930	818	912	937	905	931

Appendix B

Inventory of Positions Measured per Subject by Bone.

ERECT

Bone	Subject								
	21	22	23	24	25	26	27	28	29
Sternum	6	8	--	8	8	8	8	8	8
Clavicle	1	8	8	8	8	8	8	8	8
Scapula	6	8	8	8	8	8	8	8	8
Humerus	--	--	--	--	--	--	--	--	--
C07	--	8	8	8	8	8	8	8	8
T01	--	8	8	8	8	8	8	8	8
T03	--	--	--	--	--	--	8	--	--
T04	6	8	8	8	8	8	--	8	8
T08	6	8	8	--	8	8	8	--	--
T09	--	--	--	8	--	--	--	--	9
T11	--	--	--	--	8	--	--	--	--
T12	6	8	8	8	--	8	8	8	8
L01	6	8	8	8	8	8	8	8	8
L02	6	8	8	8	8	8	8	8	8
L03	6	8	8	8	8	8	8	8	8
L04	6	8	8	8	8	8	8	8	8
L05	6	8	8	8	8	8	8	8	--
SAC	6	8	8	8	8	8	8	8	8
RHIP	6	8	8	8	8	8	8	8	8
LHIP	6	8	8	8	8	8	8	8	8

SLUMP

Bone	Subject								
	21	22	23	24	25	26	27	28	29
Sternum	7	8	--	7	7	7	7	7	8
Clavicle	2	8	6	7	7	7	7	7	8
Scapula	7	2	4	7	--	7	--	7	8
Humerus	--	--	--	--	--	--	--	--	--
C07	--	8	6	7	7	7	7	7	8
T01	--	8	6	7	7	7	7	7	8
T03	--	--	--	--	--	--	7	--	--
T04	7	8	6	7	7	7	--	7	8
T08	7	8	6	--	7	7	7	--	--
T09	--	--	--	7	--	--	--	--	8
T11	--	--	--	--	7	--	--	--	--
T12	7	8	6	7	--	7	7	7	8
L01	7	8	6	7	7	7	7	7	8
L02	7	8	6	7	7	7	7	7	8
L03	7	8	6	7	7	7	7	7	8
L04	7	8	6	7	7	7	7	7	8
L05	7	8	6	7	7	7	7	7	--
SAC	7	8	6	7	7	7	7	7	8
RHIP	6	7	6	7	7	7	7	7	--
LHIP	7	8	6	7	7	7	7	7	7

SHOULDER

Bone	Subject								
	21	22	23	24	25	26	27	28	29
Sternum	10	7	--	13	10	12	11	11	11
Clavicle	9	7	7	13	10	12	11	11	11
Scapula	10	7	8	13	10	12	10	11	11
Humerus	9	6	7	13	9	11	9	11	10
C07	--	7	5	7	7	10	7	8	8
T01	9	7	8	12	10	12	10	8	9
T03	--	--	--	--	--	--	11		
T04	10	7	8	13	10	12	--	11	9
T08	8	7	8	--	10	10	11	11	--
T09	--	--	--	13	--	--	--	--	11
T11	--	--	--	--	10	--	--	--	--
T12	6	3	8	5	--	5	5	5	6
L01	5	2	7	5	5	4	3	4	4
L02	5	1	6	4	3	2	2	3	4
L03	5	1	6	2	3	2	2	2	4
L04	--	1	4	2	2	1	1	1	4
L05	--	1	4	2	2	1	1	1	--
SAC	--	1	3	1	2	1	1	--	--
RHIP	--	1	4	1	2	1	--	1	--
LHIP	--	1	3	1	1	1	1	--	--

Appendix C

Physical and Osteological Examinations of each Subject

Subject #1

PHYSICAL EXAMINATION:

The left leg was 15 mm shorter than the right leg in the prone position, but this difference decreased to 10 mm in the supine position. The left hip resisted internal rotation. The left transverse process of the fifth lumbar vertebra was prominant. In contrast, L03 and L04 had prominant right transverse processes.

OSTEOLOGICAL EXAMINATION:

The bones of specimen #1 were not available for examination as explained above.

Subject #2

PHYSICAL EXAMINATION:

The medial malleoli were equal in the prone position but a 15 mm difference was observed in the supine position with the right leg shorter than the left. The subject's right sacroiliac articulation felt restricted. The right anterior superior iliac spine was more anterior than the left. The predominant findings for tissue texture abnormalities in the back were mainly on the right side. The right scapulo-humeral joints were hypermobile.

OSTEOLOGICAL EXAMINATION:

Vertebral Body Pathology:

150

Osteophytes--the most significant amount of lipping occured in the lumbar region with some isolated growths in the thoracic region. While lipping was present on both superior and inferior surfaces of all lumbar vertebrae, it was most prevalent on the anterior margins of the superior surfaces. Where the osteophytes grew superiorly, lipping was largest on L5 and gradually decreased in an ascending manner. T8 and T9 exhibited severe lipping, however the osteophytes were isolated on the right lateral margins. T9 had a small osteophyte growing downward from the inferior surface as well as a large osteophyte growing up from the superior surface. T8 had a large osteophyte growing laterally from the inferior surface as if to buttress the superior growth of T9. Slight lipping occurred on nearly all vertebral bodies but this appeared insufficient to limit mobility of the spinal column.

Vertebral endplates--lesions were on the following articular surfaces:

T8: two small erosions exposed cancellous bone on the inferior endplate. They originated near the center and radiated laterally toward the right margin.

T9: inferior endplates had general compression with a 14 mm node on the posterior half exposing cancellous bone.

L4: inferior endplates had an 11 mm long erosion on the posterior margin surrounded by reactive bone deposits.

Posterior Element Pathology:

Facets--No significant osteophytic growth was observed in Specimen #22. However, the T11/T12 motion segment was asymmetrical. The left facet had a lumbar orientation and the right facet was thoracic in shape.

Vertebral arch--Moderate extraosseous development occurred in the region of the ligamentum flava in vertebrae T3-T11. The primary site was on the superior margin of the lamina and grew along the medial margins of the superior articular facets. Ossification was slightly more prevalent along the right superior

151

articular facet. Slight ossification on the inferior margin of the lamina was seen only on T9-T11.

Subject #3

PHYSICAL EXAMINATION:

In the supine position, the left leg was shorter than the right by 15 mm. The right leg had greater internal rotation than the left. In straight leg raising, however, the right leg moved 85° and the left leg 115°. Both legs had marked muscle atrophy.

In the prone position, the subject appeared to have very little natural lumbar curvature. Motion in the lumbar vertebrae felt restricted when moving to the left. Soft tissues over the left sacroiliac joint and the right lumbar felt tight. With the subject in the prone position, increased areas of soft tissue density were palpated in the left scapula and thoraco-lumbar areas.

OSTEOLOGICAL EXAMINATION:

Vertebral Body Pathology:

Osteophytes--Significant lipping was limited to T8-T9. T8 & T9 were severely affected by large osteophytes that grew towards each other but did not fuse. The growth on T9 originated from the right side of the anterior margin (superior surface) and grew superiorly. For T8 the lipping grew towards T9 from the right side of the anterior margin (inferior surface). The lumbar vertebrae, L3/L4, exhibited moderate lipping on the antero-lateral margins of superior surfaces. C5-C7 were also severely affected but no ankylosis was present.

Vertebral endplates--A single Schmorl's Node was identified on T12. The pathology originated near the center of the body and expanded toward the posterior margin of the superior surface. The lesion had eroded quite deeply. However, considerable erosion of the inferior endplates was present. The motion

152

segment L3/L4 had much reactive bone growth on the opposing vertebral endplates.

Posterior Element Patholgoy:

Facets--Two significant abnormalities were noted on the facets. The inferior margin of the right superior articular facet (T4) exhibited considerable vertical and slightly superior lipping, creating a hinge-like structure. The corresponding inferior articular face (T3) showed a vertically rounded build-up of bone along its inferior margin, forming a pseudoarthrosis with T4. A second abnormality was located between L4-L5. There were extraosseous growths similar to those described between T3-T4. The growth on the inferior facets extended beyond the inferior margin of the facet and onto the lamina for both right and left sides.

Vertebral arch--Vertebrae T2-T12 displayed considerable extraosseous development in the ligamentum flava. Significant boney growth was present on the superior margin of the lamina (a similar pattern was described for subject #2). The most common site of inferior margin ossification was just superior to the inferior facets. At this location, new bone growth was broad tabular and of varying length. Significant ossification also was present between the inferior facets, approximately at the level of their midpoint. These slender spicule-like growths formed to either side of midline. The most severe growth occurred at T2-T4 and T6-T7 with the largest on T6, then T3.

Subject #4

PHYSICAL EXAMINATION:

Deep tissue tension was palpated over the right sacroiliac joint. The spine had prominent tissue tension at T1 on the

right. Less prominent tension was felt on the right side of T2-4 and on the left side of T6-9.

OSTEOLOGICAL EXAMINATION:

Vertebral Body Pathology:

Osteophytes--Slight to moderate lipping was observed in the vertebrae. S1 contained a large osteophyte on its right anterior margin of the superior surface that was associated with a small amount of lipping on L5. Osteophytes in the lumbar region were slight to moderate.

Vertebral endplate--No significant abnormalities were observed.

Posterior Element Pathology:

Facets--No significant abnormalities were observed.

Vertebral arch--Moderate to heavy extraosseous development in the ligamentum flava was on the superior lamina surface of vertebrae T1 - L2. Moderate to heavy ossification on the inferior lamina surface occurred from T6 - T12. Overall, the most severe area was between T6 and T7. Normal movement between T6-T12 was probably reduced.

Subject #5

PHYSICAL EXAMINATION:

There was considerable muscle atrophy in the lower extremities. The left leg was approximately 3-5 mm shorter than the right leg in either prone or supine positions. A marked increase in tissue density was felt on the right side. Transverse processes of L5 and L4 were prominent on the right, L3 on the left, L2 on the right and L1 on the left. No evidence of

154

scoliosis but marked kyphosis was present. There was much
tension in the paravertebral tissues and palpable malalignment of
the lower thoracic vertebrae from T7 to T12.

In the shoulder, there was a marked palpable restriction
involving the acromio-clavicular joint and shoulder girdle on the
right. Muscles in the upper thorax were atrophied. Internal
rotation of each shoulder indicated that the posterior shoulder
tissues on the right were restricted. Similar findings of the
glenohumeral attachments were observed when the shoulder was
externally rotated. The right arm was more developed than the
left.

OSTEOLOGICAL EXAMINATION:

Vertebral Body Pathology:

Osteophytes--Extensive osteoarthritis was observed
throughout the axial skeleton. Significant lipping was present
on C5-C6 and from T6 to S1. Most osteophytes developed on the
right anterior-lateral margins of both inferior and superior
surfaces. The inferior surfaces had the largest osteophytes.
The most serve lipping in the lumbar vertebrae occurred at L3 and
L4. No ankylosis in the spinal column was observed.

Vertebral endplates--A single node was observed cutting
through the midline of the inferior surface of the body of T8.

Posterior Element Pathology:

Facets--Nearly every facet in this specimen had some
evidence of osteoarthritis. Three regions existed where the
facets were most severely affected; each region expressed a
different type of osteophytic lipping. From C5 to T1, large
osteophytes grew on the posterior surfaces of the articular
processes and on all margins. From T3 to T7, lipping on the
inferior margins of the inferior facets were associated with
hinge-like lipping on the inferior margin of the superior facets.

155

These lesions were smaller and more localized than those of the other two regions. From T12 to S1, lipping was developed on all margins. The posterior margins were affected the most. Pathology was most severe between L4/L5 and L5/S1.

Vertebral arch--Moderate to heavy extraosseous development on the superior lamina margin was observed from T1 - L2. T3, T10, and T11 were the worst. T8 and T9 showed significant ossification of the inferior portion of ligamentum flava. Ossification would probably produce loss of mobility between T9 and T10.

Subject #6

PHYSICAL EXAMINATION:

The subject was very flexible. There were three scars on the anterior surface of the torso: midline sternal scar ($\approx$250 mm), midline suprapubic scar ($\approx$125 mm), and a left inguinal scar ($\approx$120 mm).

In the supine position, the left leg was shorter than the right by approximately 15 mm. In the prone position, this difference disappeared. The straight leg raising was approximately equal, 110° - 115° on both sides. The subject had symmetrical hip function and good low back flexibility.

In the prone position, a classic right thoracolumbar scoliosis was evident from T8 to L1, with its apex at T8. There was an increase of the AP diameter of the chest with marked kyphosis.

The sacrum appeared to have soft tissue symmetry. L5 transverse process was prominant on the left with motion on the left and restriction on the right. L2-L4 on the right side were restricted in sidebending.

The subject had a pacemaker that affected right shoulder motion. The arms abducted and externally rotated on the left but the left side was hypermobile. A marked restriction was felt at

the posterior and inferior right teres attachments. Full elbow
extension above the head was not possible. The shoulders were
restricted by postero-medial displacment of the scapula.

OSTEOLOGICAL EXAMINATION:

Vertebral Body Pathology:

Osteophytes--Lipping from none to slight was observed on the
antero-lateral margins of both superior and inferior surfaces of
all vertebrae. Most lipping occurred at T12 and L1 where
osteophytes grew towards each other. On T9 a single, large
osteophyte (located just right of the midline on the anterior
margin) united with a small growth on T10. No ankylosis occurred
anywhere else in the axial skeleton.

Vertebral endplates--No nodes or any significant boney
erosion in the endplates from C6-T5 were observed.

- T8: inferior endplate had two very small erosions near the
  midpoint of body.
- T12: inferior endplate had a deep compression with no
  exposure of cancellous bone in the left posterior
  quadrant.
- L2: same as T12.
- L3: inferior endplate had a deep compression in the right
  posterior quadrant.
- L4: same as T12.
- L5: inferior endplate had deep compressions in right and
  left posterior quadrants.

Posterior Element Pathology:

Facets--None to slight lipping was observed on the articular
facets.

Vertebral arch--Moderate to heavy extraosseous development
in the region of the ligamentum flava (superior portion) was
present from T4 to T12. T6 and T8-T11 exhibited the most
ossification. Only moderate ossification of the inferior portion

157

was present on T8-T11. Loss of mobility due to ossification might have been present between T9-T10-T11.

Subject #7

PHYSICAL EXAMINATION:

With the subject supine, there were seven scars visible primarily in the abdominal region. One scar was at the internal right sternocleidomastoid and several were bilateral inguinal scars.

The left hip internally rotated less than one-half the right hip with the legs extended. External hip rotation was about 50% less on the right from the left. However, circumferential muscle symmetry was bilaterally equal throughout the lower extremity. The left leg was 3-6 mm longer than the right. There was no valgus or varus deformity evident at the knees. Straight leg raising measured 112° on the right, and 117° on the left. In the prone position, the leg length discrepancy was approximately 3-5 mm. There was no evidence of muscle asymmetry but a marked restriction of left knee flexion. The right hip also appeared to move easier in internal and external rotation than the left.

The sacrotuberous ligaments were very tight on the left. Thus, the sacrum was rotated right. L5 and the lumbodorsal fasciae were tight and resisted motion to the right. A pattern of hard and soft texture of the soft tissues alternated from L4 to T12. L1-L4 resisted left rotation and right sidebending. In general, the back appeared to have tight left sacroiliac, right lumbar, and left shoulder joints.

In the examination of the shoulder in the supine position, abduction of the humerus showed marked tightness. However, there was less total abduction in the left shoulder than in the right. In raising the arms completely above the head, the restriction on

158

the left was clearly felt in the posterior scapulo-humeral function.

OSTEOLOGICAL EXAMINATION:

Vertebral Body Pathology:

Osteophytes--Slight lipping was observed on the vertebral bodies. The bodies of C6-C7 had been surgically fused. A strip of bone from the anterior crest of the right ilium had been grafted on the left anterior margin of the vertebral body. The right side of C6-C7 was fused by the union of two large osteophytes.

Vertebral endplates--nodes were observed at the following locations:

  T12: superior surface had a shallow, 7 mm long node near the center. An amorphous erosion was on the anterior margin.

  L3: superior surface had a 4 mm round node, posterior to the center.

Posterior Element Pathology:

Facets--Osteophytes were poorly developed. In the thoracic region (T2 to T10), characteristic hinge-like structures were formed from osteophytic lipping. Lipping in the lumbar region (T12-L5) reflected the same pattern as previous specimens, i.e. general bone build-up along the margins. Moderate to heavy lipping was present on joints T5-T6 and T6-T7.

Vertebral arch--Significant extraosseous development along the superior margin was present in vertebrae T1 to L2 with most occuring from T8 to T12. Significant inferior ossification occurred on T2 and T5-T12. From the degree of ossification, mobility was probably restricted from T5-T12.

PHYSICAL EXAMINATION:

Scars were noted in the right antecubital fossa. Two puncture scars were between the left fifth and sixth ribs. A scar traversed the abdomen for 200 mm from xyphoid to left symphysis pubis. There were one proximal and one medial scars on the knee. There was no evidence of gross boney asymmetry anywhere on the body in the supine position.

In the supine position, there was no evidence of coxa vara or coxa valga. The straight leg raising was symmetrical to 75°. The right leg was approximately 10 mm longer than the left and the left hip had more internal and external rotation than the right. The leg length discrepancy was also present in the prone position although slightly less than in the supine position. There was significant muscle atrophy of the hip extensors.

In the prone position, there was clear evidence of a prominent thoracic kyphosis typically found in chronic obstructive lung disease. A significant scoliosis was observed convex to the right from the upper lumbar to approximately T8-9. This scoliosis was accompanied by marked kyphotic changes involving the upper thoracic spine.

The lumbar springing test was positive with dramatic backward bending of the sacral base. L1, L2, L3, L4, L5 had prominent transverse processes on alternating sides.

Shoulder abduction with humeral internal rotation indicated a motion restriction on the right side. The right humerus was restricted in external rotation. The left humerus had normal to hypermobile external rotation. The scapulas abducted and externally rotated over the costal cage with greater mobility in the left.

OSTEOLOGICAL EXAMINATION:

Vertebral Body Pathology:

Osteophytic lipping--The most severe lipping was observed in this subject. Severe or heavy lipping was present on C6 and T7-T10. All other vertebrae demonstrated moderate lipping. The growth on C6 encompassed the entire anterior margin of the inferior surface and grew towards the superior margin of C7. The lipping on T7-T10 was characterized by very large growths on the right side of the anterior margin and extended along the right anterior-lateral margin. These growths developed in the same direction as their origin. Inferior margins lipped downward and superior surface growths lipped upward. T9-T10 were ankylosed.

Vertebral endplates--This subject was affected by numerous, severe nodes.

C7:   superior endplates had much erosion along the right margin and center.

T8:   inferior endplates had a very deep and wide node.

T8:   superior endplates had a small node in posterior half.

T9:   superior endplates had reactive bone on posterior half.

T12: inferior endplates had a large lesion with reactive bone deposits on posterior half.

T12: superior endplates was porous.

L1:   superior endplates had a 7 mm in diameter, very deep node on the left side of posterior half.

L1:   inferior endplates had a large node with reactive bone on posterior margin.

L2:   superior endplates had a small, circular, shallow node with reactive bone on left posterior half.

L2:   inferior endplates had a 7 mm, oval-shaped, shallow node, posterior and left of body center.

L3:   inferior endplates had a very deep, 10 mm, oval-shaped lesion on the left side of the posterior half.

Posterior Element Pathology:

Facets--Osteophytic development in the cervical and thoracic vertebrae was minimal. Greater degeneration was in the lumbar vertebrae, with slight to moderate development on the margins, primarily, posterior of T12-L4. L4/L5 and L5/S1 motion segments had moderate osteophytes that radiated from all margins of the left facets. The posterior margins were the worst.

Vertebral arch--Significant extraosseous development along the superior margins were observed on T2-T12 and L2. The most severe ossification occurred on T8-T11. The ossification of T3-T6 might have been associated with reduced mobility. For the inferior portion only slight ossification was observed on T8-T11.

Subject #9

PHYSICAL EXAMINATION:

Subject was mesomorphic with multiple contusions and abrasions primarily at the cranio-facial, right arm, right neck, right pelvis and right hemithorax. The knees had asymmetry in the collateral ligaments. The left side was more lax than the right. There was, however, no musculo-skeletal deformity in these joints.

In the spine, the right sacroiliac sulcus had increased palpatory depth indicating tension in the left sacral tuberous ligament. The left transverse process of L5 and right contralateral prominence at L4 were prominent. Sites of paravertebral soft tissue tension were found at T8 on the right, T5 or T6 on the left, and T3 on the left. In the radiographic exam, a fracture of the 5th rib in the midline and the head of the second rib were observed.

There was significant tension in the right shoulder with restriction to external rotation and abduction. The scapula on

162

the right had much less range of abduction motion than on the left. However, the right upper arm had significant trauma--abrasion and lacerations. The shoulder girdle was bilaterally symmetrical. Despite some rigor remaining at time of examination, the ranges of motion in the shoulder, elbow, wrist, hip and ankle joints were bilaterally equal.

OSTEOLOGICAL EXAMINATION:

Vertebral Body Pathology:

Osteophytes--No significant osteophytic lipping occurred on any of the vertebral bodies. The compact boney rim around the margins of all vertebrae bodies was not completely developed.

Vertebral endplates--Nothing remarkable.

Posterior Element Pathology:

Facets--Nothing remarkable.

Vertebral arch--Slight to moderate extraosseous development along the superior rim of the arch was present on vertebrae T1-S1. The amount of ossification was very small. A spondylolisthesis of L5 and incomplete closure of the sacral roof were observed. The sacral roof was completely closed only over S2 and partially at S3.